Biogeosciences, 20, 3943–3979, 2023
https://doi.org/10.5194/bg-20-3943-2023

Biogeosciences Open Access EGU

Deciphering the origin of dubiofossils from the Pennsylvanian of the Paraná Basin, Brazil

João Pedro Saldanha[1], Joice Cagliari[1], Rodrigo Scalise Horodyski[1], Lucas Del Mouro[2], and Mírian Liza Alves Forancelli Pacheco[3]

[1]Programa de Pós-Graduação em Geologia, Universidade do Vale do Rio dos Sinos, São Leopoldo, RS, 93022-750, Brazil
[2]Instituto de Geociências, Universidade de São Paulo, São Paulo, SP, 05508-080, Brazil
[3]Departamento de Biologia, Universidade Federal de São Carlos – Campus Sorocaba, Sorocaba, SP, 18052-780, Brazil

Correspondence: João Pedro Saldanha (saldanhajpedro@gmail.com)

Received: 15 March 2023 – Discussion started: 17 May 2023
Revised: 19 July 2023 – Accepted: 29 August 2023 – Published: 27 September 2023

Abstract. Minerals are the fundamental record of abiotic processes over time, while biominerals are one of the most common records of life due to their easy preservation and abundance. However, distinguishing between biominerals and abiotic minerals is challenging due to the superimposition and repetition of geologic processes and the interference of ubiquitous and diverse life on Earth's surface and crust. Mineral dubiofossils, being potential outcomes of both abiotic and biotic environments, emerge as valuable entities that can contribute significantly to the understanding of this issue, facilitating the testing and refinement of biogenicity criteria. The aim of this contribution is to decipher the origin and history of branched mineralized structures that were previously considered mineral dubiofossils from the Pennsylvanian of the Paraná Basin, Brazil. While this material has different forms and refers to biological aspects, it is challenging to associate it with any known fossil group due to the overlapping geological processes occurring in a transitional deposit of Rio do Sul Formation (Itararé Group of the Paraná Basin), particularly in close proximity to a sill from the Serra Geral Group (Lower Cretaceous), which has undergone thermal effects. Given the absence of attributes essential for supporting the initial hypotheses proposing the material as a potential set of sponge spicules or a result of contact metamorphism in Pennsylvanian turbidites, the objects are now investigated as mineral dubiofossils. To address this challenge, we have developed a descriptive protocol for dubiofossils, building upon prior research in the field. This protocol evaluates the following aspects: (1) morphology, texture, and structure; (2) relationship with the matrix; (3) composition; and (4) context. This is done by assessing indigeneity and syngenicity and comparing the specimens with abiotic and biotic products. Applying this protocol to our samples revealed a wide range of morphologies with internal organization, predominantly composed of calcite with impurities such as iron, magnesium, aluminum, and oxygen. The inferred indigeneity suggests the presence of these minerals concurrently with or prior to the intrusion of the sill. Extensive comparisons were made between the studied samples and a broad spectrum of abiotic minerals, as well as controlled, induced, and influenced biominerals from similar contexts. These comparative analyses encompassed sponge spicules; sea urchin and algae skeletons; minerals induced or influenced by fungi, bacteria, and microbial mats; and inorganic pre- and synsedimentary–eodiagenetic minerals like evaporites, springs, and other precipitates, and mesodiagenetic–metamorphic crystals. Despite this comprehensive analysis, no hypothesis emerged as significantly more likely than others. The comparative analysis did allow us to exclude the possibility of the samples being controlled biominerals due to their patternless diversity of morphologies, as well as purely thermometamorphic in origin due to their branched elongated forms. The occurrence of these structures suggests a complex history: a syndepositional or eodiagenetic origin of some carbonate or sulfate (gypsum, ikaite, dolomite, calcite, aragonite, siderite), potentially associated with the presence of microbial mats, which may have served as templates for mineralization and mediated mineral growth. Mesodiagenesis could have further modified the occurrence through processes such as mineral stabilization, agglutination, aging, and growth. However, the

primary agent responsible for the formation of the dubiofossil was the Cretaceous intrusion, which dissolved and replaced the initial minerals, resulting in the precipitation of calcite. Throughout these steps, a combination of physical–chemical and biological reactions, influenced by intrinsic matrix characteristics, organic matter content, and distance from the intrusive body, may have contributed to the heightened morphological complexity observed, thus corroborating the origin of the material becomes even more challenging. Consequently, both the hypotheses pertaining to the formation of biotic and abiotic sulfates and carbonates remain plausible explanations, hence sustaining the classification of the material as a dubiofossil. This material illustrates how dubiofossils can be a result of a complex history and overlapping geological processes. It also highlights the difficulty in differentiating biominerals from abiotic minerals due to the scarcity of biogenicity arguments.

1 Introduction

Biogenicity refers to the signatures exclusively generated and/or transformed by past or present organisms. Comprising signs of morphology (structure, distribution, texture) and/or chemistry (composition and trace indicator) that diagnose life, these signatures can be created from the growth or decay of (once) living organisms and cannot be produced by purely abiotic processes (Slater, 2009; McLoughlin, 2011). The issue lies in the ability to discriminate the origins of different components within complex mixtures given the range of spatial scales, diversity of life forms, and succession of geologic processes (Schiffbauer et al., 2007; Botta et al., 2008; Neveu et al., 2018; Rouillard et al., 2021).

Acquiring substantial evidence to establish biogenicity is crucial not only for determining the biological origin (Neveu et al., 2018; Callefo et al., 2019a; Rouillard et al., 2021) specially to understand the intricate biosphere–lithosphere interface (McMahon and Ivarsson, 2019). Life forms inhabit all environments on the planet's surface, including extreme environmental conditions (Fig. 1; Merino et al., 2019; McMahon and Ivarsson, 2019, and references therein). Thus, in addition to the conventional perspective that organisms are delimited and conditioned to the environment, there is growing evidence of the significant influence of life on natural processes and events (Knoll, 2013; Davies et al., 2020). As a result, it has become increasingly challenging to recognize large-scale physical and chemical cycles on Earth that are unaffected by biosphere activity (Gargaud et al., 2015). Furthermore, accurately measuring the impact of organisms, which are ubiquitous, on erosion, sedimentation, diagenesis, and mineralization has also become a complex task (Fig. 1; Briggs, 2003; Dupraz et al., 2004; Gargaud et al., 2015; Knoll, 2013; Bower et al., 2015; Briggs and McMahon, 2016; McMahon and Ivarsson, 2019; Davies et al., 2020).

These biological and geological processes are part of the natural cycles of the Earth system and therefore tend to repeat and overlap on multiple scales (Zhang et al., 2017). A dynamic scenario of physical, chemical, and biological reactions occurs throughout the Earth's crust and surface, defining the geological record (Milliken, 1978; Worden and Burley, 2009; Zhang et al., 2017). Consequently, any geological object, whether abiotic or biotic, must be understood in terms of its formation and original conditions, as well as the subsequent processes that contribute to its maintenance, modification, or destruction. Due to the complex interplay of these processes and the ongoing changes throughout geological history, it becomes essential to discern specific life signatures (Schiffbauer et al., 2007; Knoll, 2013; McLoughlin and Grosch, 2015; Neveu et al., 2018; McMahon et al., 2021; Rouillard et al., 2021).

Dubiofossils, fossil-like structures formerly related to life with an ambiguous origin (Hofmanm, 1972), play a crucial role in enhancing biosignatures. Through testing and refinement, the biological nature of a dubiofossil can be established, leading to its classification as a genuine fossil; alternatively, if its origin is determined to be the result of abiotic processes, it is categorized as a pseudofossil (Hofmann, 1972; Monroe and Dietrich, 1990; McMahon et al., 2021). Once the biological origin is confirmed, these dubiofossils can be regarded as potential biosignatures or contain distinctive characteristics indicative of past life (McMahon et al., 2021). To verify the origin of dubiofossils, it is necessary to apply biogenicity criteria (Buick, 1990; McLoughlin and Grosch, 2015; Davies et al., 2016; Neveu et al., 2018; McMahon et al., 2021; Rouillard et al., 2021).

As an area of science that has received significant attention and prominence in recent years (see Rouillard et al., 2021), biogenicity criteria are arguments proposed to defend or refute the biotic origin of a given object. As they depend on the type of material studied, generally they can be grouped into four classes: (1) morphology, structure, and texture; (2) relationship with the matrix or inserted medium; (3) composition (including bioindicators); and (4) context (environment and age) and comparison with other similar biotic and/or abiotic objects (Buick, 1990; García Ruiz et al., 2002; Brasier et al., 2002, 2004; Schopf et al., 2002; Westall, 2008; Noffke, 2009, 2021; Slater, 2009; Wacey, 2009, 2010; Brasier and Wacey, 2012; Schopf and Kudryavtsev, 2012; McLoughlin and Grosch, 2015; Callefo et al., 2019a; Gomes et al., 2019; Neveu et al., 2018; Maldanis et al., 2020; McMahon et al., 2021; Rouillard et al., 2021). To refute the contamination hypothesis, it is important to verify the indigeneity and syngenicity of a proposed fossil (Rouillard et al., 2021). Additionally, comparing these materials with abiotic and biotic objects is essential for refining and defining their origins (Rouillard et al., 2021).

Minerals can be either biotic or abiotic, and they constitute the fundamental record of abiotic processes and one of the main records of life activity over time. Due to the ubiquity

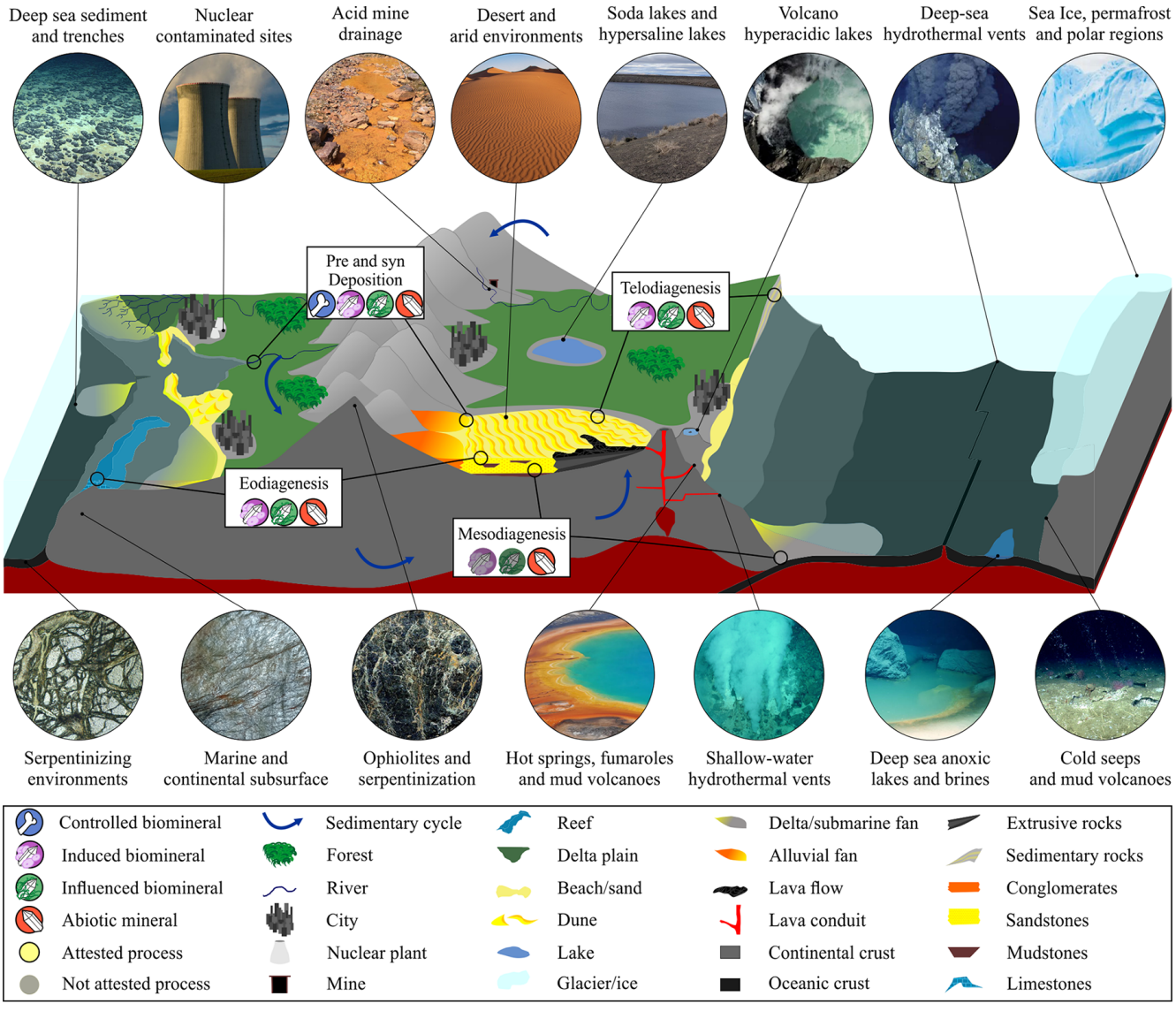

Figure 1. Representative cross-section of Earth's crust showing the diversity of inhabited extreme environments, besides the common biosphere, and the contribution of abiotic and biotic minerals in the sedimentary cycle from pre- and syn-deposition, eodiagenesis, mesodiagenesis, and telodiagenesis. Induced and/or influenced biominerals may be present in the diagenesis cycle, including mesodiagenesis (not attested). 3D geological model adapted from Dupraz et al. (2009), McMahon and Ivarsson (2019), and Merino et al. (2019); all the environment images (circles) were created using the AI Bing Image Creator.

of life forms in geological processes (from superficial processes to meso- and telodiagenesis; Fig. 1) and the existence of biomimetic inorganic minerals (Weiner and Dove, 2003; Weiner, 2008; Dupraz et al., 2009; Bindeschedler et al., 2014; Bower et al., 2015; Tisato et al., 2015; Muscente et al., 2017; McMahon and Ivarsson, 2019; Merino et al., 2019; Davies et al., 2020; Eymard et al., 2020; Suchý et al., 2021) arguments are lacking to differentiate purely abiotic minerals from controlled, induced, and influenced biominerals (Dupraz et al., 2009). Essentially, controlled biominerals are minerals that are directly produced and regulated by living organisms that exercise a high level of control over their formation and composition. Induced biominerals are indirectly formed by living organisms; these play an active role in triggering or influencing their formation, producing certain organic compounds or creating specific environmental conditions, often as an indirect result of the metabolic action. In influenced biominerals, there is a passive role in mineral formation or modification caused by the presence of living or dead organisms (see Dupraz et al., 2009, for a broader review); by exclusion abiotic minerals are the result of physical–chemical reactions without any biological interference. In practice, it is challenging to differentiate each of these products in the geological record due to the lack of diagnostic characteristics, such

as specific shapes or crystallographic properties and compositional signatures that resist modifications over time (see Weiner and Dove, 2003; Dupraz et al., 2009). To improve the biogenicity evidence for crystals it is essential to investigate mineral dubiofossils.

Recent investigations have focused on stick-shaped dubiofossils and alleged biominerals, leading to the development of some biogenicity criteria (Cailleau et al., 2009; Bindschedler et al., 2014; Tisato et al., 2015; Baucon et al., 2020; Green, 2022). However, due to the wide range of biominerals and biomimetic minerals (Dupraz et al., 2009), it is essential to examine more mineral dubiofossils and propose both biotic and abiotic evidence to strengthen these criteria. In this context, we present an example of a mineral dubiofossil from the Pennsylvanian age in Brazil. This material was previously proposed to be sponge spicules from the Paraná Basin (Mouro and Saldanha, 2021). Since some formats resemble spicules, the distribution of structures could delimit circular and ellipsoidal features such as flattened bodies; moreover, close to the outcrop, an earlier stratigraphic unit of similar context contains well-preserved fossil sponges in abundance (see Mouro and Saldanha, 2021). However, the diversity of formats and the absence of spicular nets prevented the classification of this material as Porifera. On the other hand, the diversity of formats demonstrates dissimilarities with diagenetic–metamorphic products in a preliminary comparison, so it remains a mineral dubiofossil.

The purpose of this study is to explore the origins of the multiple mineralized, elongated, and ramified dubiofossils in question. These elongated tubes will be examined across the four classes of biogenicity criteria, (1 to 4) explained above. Through additional analysis, we will diagnose the indigeneity and syngenicity of the material and compare it to both abiotic and biotic minerals in order to better understand its origins. We endeavor to unravel the intricate history of unique mineral occurrence, which has been shaped by the overlapping effects of abiotic and biotic geologic processes. Through our efforts, we aim to shed some light on the interplay between biotic and abiotic minerals. Ultimately, we propose this descriptive protocol that can facilitate investigations into dubiofossils.

Geological settings

Paraná Basin is an intracratonic Paleozoic–Mesozoic basin covering an area of about 1.5 million km^2, extending across southern Brazil, Paraguay, Argentina, and Uruguay (Fig. 2; Milani et al., 2007). The Rio Ivaí, Paraná, and Gondwana I Supersequences (Milani et al., 2007) register the Paleozoic transgressive–regressive cycles with evolution linked to the stabilization of West Gondwana, the active Andean margin, and the activity of the paleo-ocean Panthalassa, as well as the Supersequences Gondwana II and III deposited during the Mesozoic, whose continental sediments are associated with extensional events and volcanic rocks linked to the fragmentation of the supercontinent Gondwana (Milani et al., 2007). Most of the basin's units belong to the Gondwana I Supersequence, a record of the transgressive–regressive cycle at the end of the Paleozoic–Triassic caused by the establishment of the greatest Phanerozoic ice age and its transgressive and climatic response (Milani et al., 2007). The Itararé Group records the effects of this glaciation (Valdez Buso et al., 2019).

The Itararé Group records the glaciogenic deposits of the Late Paleozoic Ice Age (LPIA – Isbell et al., 2003) as glacioterrestrial, glaciomarine, and deglaciation successions of tillites, diamictites, sandstones, ritmites, and shales that lasted about 16 Myr from the Bashkirian to the Gzhelian (Daemon and Quadros, 1970; Schneider et al., 1974; Franca and Potter, 1988; Souza, 2006; Cagliari et al., 2016, Valdez Buso et al., 2019, 2020). The Itararé Group (Fig. 2c) is classified using field data by Schneider et al. (1974) in the Campo do Tenente, Mafra, and Rio do Sul formations and by Franca and Potter (1988), with subsurface data, in the Lagoa Azul, Campo Mourão, and Taciba formations. These units are similar in lithology and time, except for the Lontras member, which is the base of the Rio do Sul Formation and the top of the Campo Mourão Formation, respectively. As the material was collected in the outcrop, we prefer to use the first classification by Schneider et al. (1974).

In the study region (Fig. 2b), the Rio do Sul Formation crops out as sparse sandstones and a great abundance of diamictites and rhythmites, interpreted by Vesely and Assine (2006) as a distinct pattern of deglaciation, in which the turbidity currents of melting had a less important role than rain and resedimentation. The detailed outcrop description with sedimentary structures and biotic elements is presented in Sect. 3.1.4. Therefore, the regional interpretation corresponds to distal marine turbidites associated with delta systems caused by the deglaciation final phase, corresponding to the upper part of the Itararé Group (Salamuni et al., 1966; Schneider et al., 1974; Canuto et al., 2001; Weinschütz and Castro, 2006; Puigdomenech et al., 2014; Aquino et al., 2016; Schemiko et al., 2019; Vesely et al., 2021). The Paraná Basin Paleozoic section is cut by sills and dikes of the Serra Geral Group that fed the Large Igneous Province Paraná–Entendeka flows around 130 Ma (Zalán et al., 1985; de Almeida, 1987; Nardy et al., 2002; Frank et al., 2009).

2 Material and methods

Samples were collected at the Bemara quarry in the city of Itaiópolis (Santa Catarina, southern Brazil), approximately 12 km from the BR-116 Highway (km 29) at geographical coordinates 26°17′44.5″ S, 49°51′49.9″ W (Fig. 2a and b). The Rio do Sul Formation, the topmost unit of the Itararé Group in the Paraná Basin, crops out at this quarry. Approximately 250 siltstone and claystone slabs of different sizes with the structures have been described and are kept in the

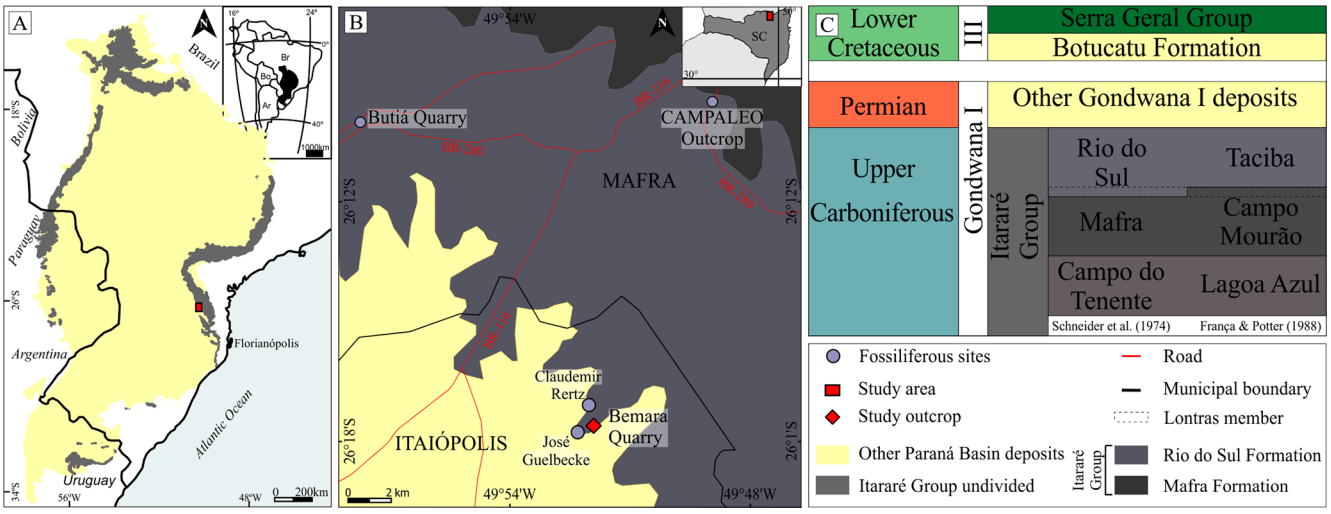

Figure 2. Location and geologic context of the collection area. **(a)** Coverage area of the Itararé Group in the Paraná Basin in south-central Brazil and neighboring countries (study area); modified from Vesely and Assine (2006). **(b)** Location of the collection area: Bemara quarry, municipality of Itaiópolis, and other paleontological sites in the region, including those similar to the Bemara Claudemir Retz and José Guelbecke locations, the geological units of study, Mafra Fm., Rio do Sul Fm. (Itararé Group), and other sequences of the Paraná Basin; the Campaleo outcrop is the fossil site with multiple sponge bodies – see Mouro and Saldanha (2021), modified from Silva (2020). **(c)** Temporal distribution of the studied units; Itararé divisions based on Schneider et al. (1974) and Franca and Potter (1988). Based on Weinschütz and de Castro (2006) and Valdez Buso et al. (2019).

fossil collection of the Laboratório de Paleontologia of the Universidade Federal de Santa Catarina (LABPaleo–UFSC) under the numbers UFSCLP 395–418, 877–971, and 993–1029, totaling 153 samples; the other 100 samples are not included in the collection to avoid redundancy. UFSCLP numbers 1023a–b and 1024–1029 have petrographic slides stored in the same collection under the number of the respective hand sample.

To guarantee a complete survey of the biotic and abiotic characteristics of the material in question, fulfilling the four attribute classes, the 250 hand samples were described and selected for more specific analyses as described below. To approach the (1) morphology, structure, and texture as well as the (2) relationship with the matrix, we used macroscopic description, petrographic microscopy, and X-ray computed microtomography. To describe (3) composition, in addition to the aforementioned techniques, we applied scanning electron microscopy, with energy-dispersive spectrometry, X-ray diffraction, and Raman spectroscopy. To discuss the (4) context (paleoenvironment and biotic elements) as well as (5) indigeneity and syngenicity, we used field-collected data, including some ichnofossils, which were also collected and observed under a stereomicroscope in the laboratory.

2.1 Macroscopic description and petrographic microscopy

The specimens were characterized in an Olympus SZ51 stereomicroscope and measured by an analogical caliper and through photos using Corel Draw software. The morphologies were described, and length, width, and relative angles of the branches were measured. Additional statistical analyses, such as the mean, median, and histograms, were performed using Excel tools. Eight thin sections, one perpendicular (sample UFSCLP 1023a) and seven others concordant to the bedding plane (samples UFSC LP 1023b, 1024–1029), were characterized in a Zeiss petrographic microscope at the Laboratório de Geoquímica of the Universidade Federal de Santa Catarina (LABGeoq–UFSC) and a Zeiss Stemi 305 at Universidade do Vale do Rio dos Sinos (UNISINOS) using 2.5, 10, and 25 × objective lenses.

2.2 X-ray computed microtomography (micro-CT)

One sample (not storage in the collection) was analyzed for three-dimensional structure and architecture using a Zeiss/XRadia Versa-500 microtomograph at the Laboratório de Meios Porosos e Propriedades Termofísicas of the Universidade Federal de Santa Catarina (LMPT–UFSC). This equipment operates with a 30 to 160 kV energy range, with power up to 10 W and 0.7 µm maximum spatial resolution, resulting in optical magnification of 3.982500 and pixel size 4.519758. Analysis was treated in FIJI open software (https://imagej.net/software/fiji/, last access: 17 August 2022) using simple processing, including adjusting brightness, contrast, and intensity, as well as stacking 2D slices and the volume viewer tool.

2.3 Scanning electron microscopy (SEM) and energy-dispersive spectrometry (EDS)

Three hand samples (UFSCLP 1024, 1026, 1029) and one thin section (UFSCLP 1026) were selected for SEM-EDS analysis at the Instituto Tecnológico de Paleoceanografia e Mudanças Climáticas (ITT OCEANEON–UNISINOS) using an EVO/MA15 Zeiss scanning electron microscope. They were metalized with 46 nm of gold. Tension ranged between 15 and 20 kV with five interactions.

2.4 X-ray diffraction (XRD)

For the mineralogical XRD analysis, one siltstone slab (not stored in the collection), containing at the same level a portion with distributed elongated material and the other only with matrix, was prepared through mechanical scraping of surfaces containing matrix and needles as well as only matrix. Two rock powder samples (one with the dubiofossil under study) were dried in an oven at 40 °C for 2 h, recovered, mounted in sample holders by the back-loading method, and taken to the diffractometer. XRD was performed at ITT OCEANEON–UNISINOS using an Empyrea PANanalytical, with reflection–transmission and a spinner set at two revolutions per second; this included a goniometric range from 2 to 75° (2θ), with a step of 0.01 for 330 s, a Cu tube (CuKα), and 40 kV and 40 mA.

2.5 Raman spectroscopy (RS)

One thin section (UFSCLP 1023b) was analyzed for mineralogical characterization using a micro-Raman Renishaw at the Laboratório de Astrobiologia of the Universidade de São Paulo (AstroLab–USP) using 5 × and 50 × lenses, a laser at 785 nm, and potency between 5 % and 10 %, with at least 30 acquisitions, capturing spectra of the first-order (150 to 1350 cm^{-1}) and second-order (1250 to 2250 cm^{-1}) ranges. The obtained 16 first-order and 11 second-order point signs (stacked spectra), as well as two compositional mappings, were treated on WiRE 4.4 and OrigingPro8.

3 Results and discussion

3.1 Description

3.1.1 Morphology, structure, and texture

The structures vary in size, shape, and packing, although there is a general needle-like shape of whitish material (Fig. 3). Size varies strongly between 0.04 and 16 mm in length and between 0.01 and 1.5 mm in thickness, with constant thickness within each needle. The packing can be loose or dispersed (Fig. 3), distributed freely concordantly in the matrix layer as a random texture, continuously covering the sample as a 2D pavement (Fig. 3a and b), or ending with increased packing in straight or curved contours (Fig. 3c and d). The needles appear as 3D tubules, flattened tubules, molds, and impressions, mainly straight, but some are curved and sinuous (Fig. 3e–i). Some 3D forms have a dark tubule inside the white layer (Fig. 3f), while others have a fainter white outer layer (Fig. 3g). In micro-CT, the needle is distinct from the matrix as a denser tube with a less dense central tube (Fig. 6), with true ramification and circular cross-section (Fig. 6f and g). The most common structures are small unbranched needles (Fig. 3d) and the second are elongated rods with multiple random short branches (Fig. 3f); there are also radial forms and little dots (Fig. 3e). Usually, one morphotype dominates each fine-grained slab, related to the matrix composition. Due to the range of shapes, we propose four informal classes (Fig. 4 and Table 1): (a) unramified rods in light gray siltstone, (b) ramified elongated forms in black to dark gray siltstone, (c) large radial forms in black mudstone, and (d) unramified needles with some ramified tubules and dots in dark to light gray siltstone. Of the nearly 250 samples, by visual estimation, approximately 40 % belong to class A, 35 % to class B, 15 % to class C, and 10 % to class D.

Class A (Fig. 4a and b) presents a random texture of straight small rods, with a length of 0.04 to 10 mm (mean 2.5 mm, standard deviation 1.9, Table 1), most of them with a 3D shape with well-defined limits in yellowish white material that can have a secondary pale white cover (Fig. 4b). Both ends are better preserved and gradually taper to the tip (some can have a spindle shape); the central area can have a dark axis or be completely faded. The black interior tubule is also recognized when the needles are broken longitudinally, presenting a circular transversal section. Longer than class A, the class B ramified elongate structures (Fig. 4c and d) can be straight or sinuous. In class B, length varies from 0.05 to 14 mm (mean 3 mm, SD 2.1; Table 1) and is variable between the main axis and the branches. The 3D structures are dark gray (Fig. 4c), occasionally showing a faded white margin, while the 2D structures are white well-defined impressions (Fig. 3h). Most structures have many primary short ramifications that do not show a periodicity of spacing, a trend of direction, or a regular angle with the main axis (ranging from 25 to 90° concerning the axis). Most of the branches depart from the main axis, but there are often branches emerging to both sides, crossing the feature (Fig. 4d). Secondarily, there are needles that ramify at only one end, separating into three or four points, and others with four tips forming irregular crosses. Rarely, there are sinuous structures with long primary branches and short secondary branches, also in aleatory directions.

Classes C and D are rarer. Class C seems linked to the darker matrix, presenting dispersed radial structures as impressions or flattened rods (Fig. 4e and f). The well-defined branches are of white material with straight walls (length 3 to 16 mm, mean 4.1, SD 3; Table 1), and the angles with the apparent central line have no pattern or periodicity (varying from 11 to 86°). The thickness and length of the branches

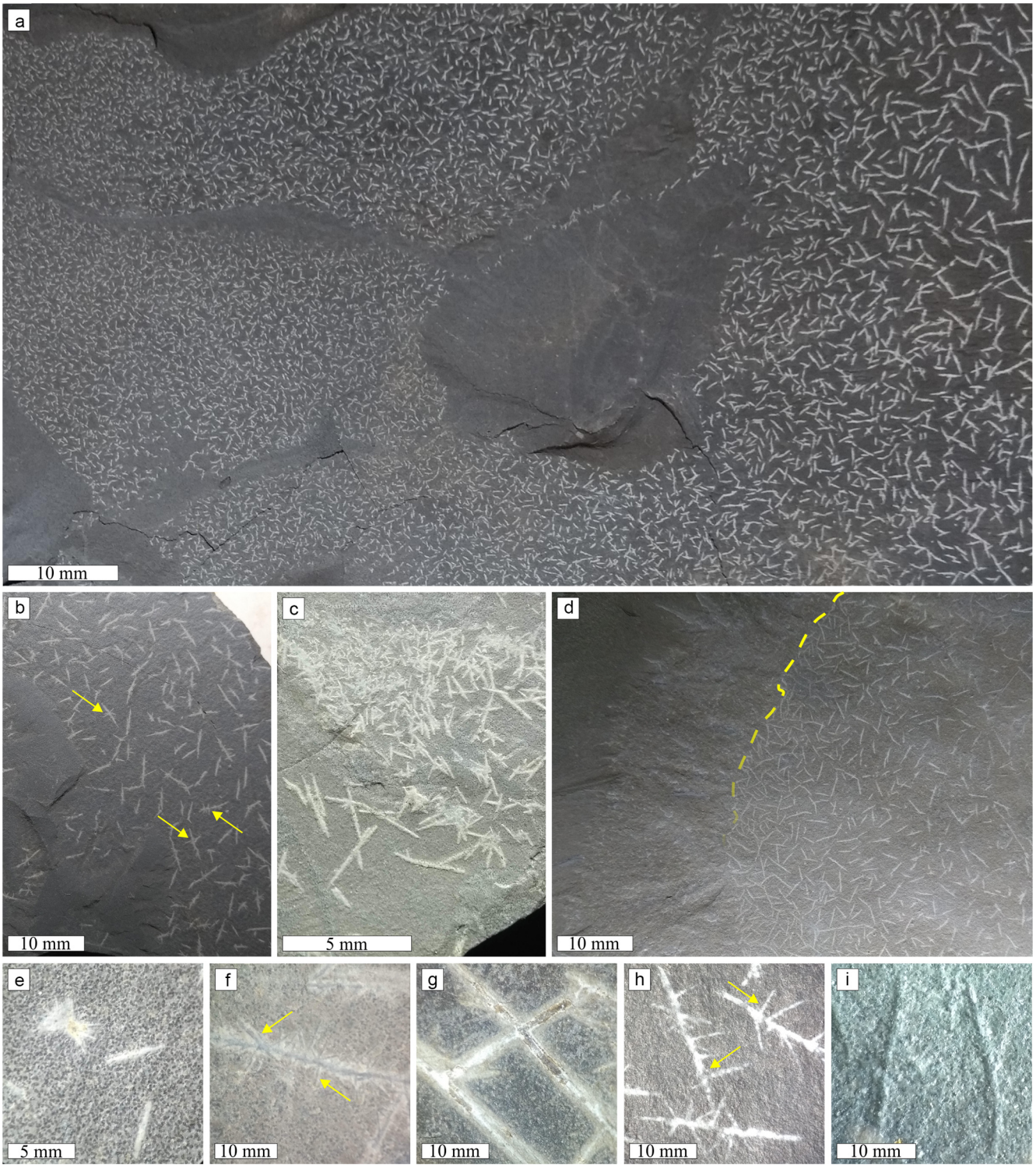

Figure 3. General distribution and morphology of dubiofossils: **(a)** 2D pavement of concordantly loose acicula; **(b)** dispersed ramified needles; **(c)** increased packing of needles in straight contours; **(d)** increased packing of needles in yellow curved contours; **(e)** non-ramified acicula and radial forms; **(f)** elongated ramified 3D needles, with a dark central axis; **(g)** flattened needles, with a dark central axis and fainter external layers; **(h)** 2D white lateral ramified needles; **(i)** mold of the slightly curved needles. Examples of branches are indicated by yellow arrows.

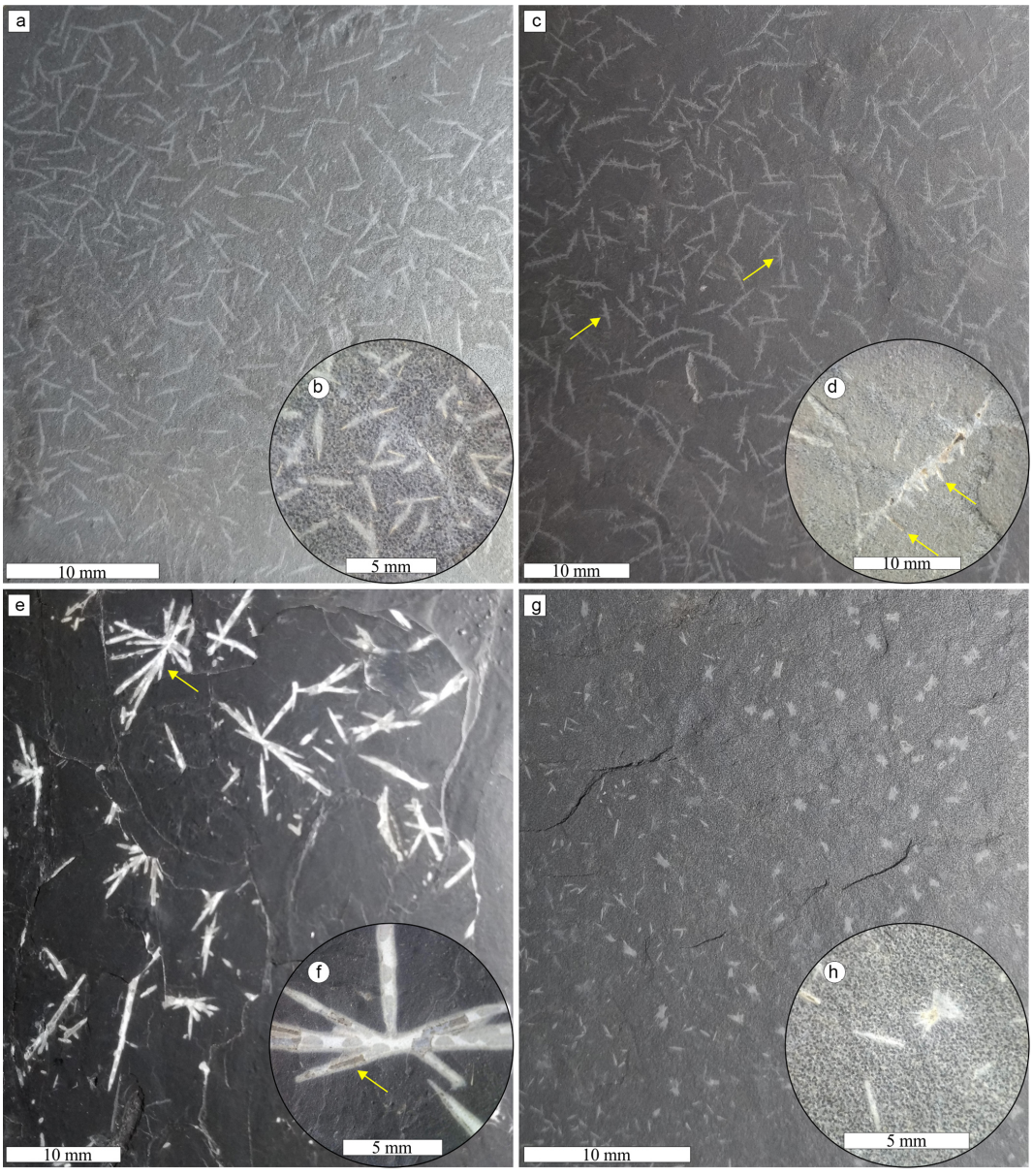

Figure 4. Informal classes of dubiofossil forms related to the matrix: **(a)** general view of class A, with loosely packed unramified acicula; **(b)** close-up view of class A showing yellowish–white needles with tapered tips and fainter regions; **(c)** general view of class B with laterally ramified needles; **(d)** example of class B ramified acicula – branches depart from and cross the main axis; **(e)** general view of class C – radially ramified dubiofossil; **(f)** detail of class C radially ramified structures, with tapered tips, external fainter layer, and internal dark layer; **(g)** general view of class D, with small needles and dots, each dominating one side of the slab; **(h)** close-up view of class D non-ramified needles and "dots", with small radially ramified forms. Examples of branches are indicated by yellow arrows.

are variable, and the tips, when present, gradually taper towards the end. Moreover, in the direction of the center, they also seem to taper (Fig. 4f). Class D (Fig. 4g and h) is composed of unbranched or less branched rods associated with dot structures that appear to be small radial features (0.013 to 1 mm); ramification angles vary from 9 to 86° (Table 1). Typically, one of these structures dominates one side of the plate, showing a transition of shape dominance (Fig. 4g). The needles are in 3D and 2D white material with different degrees of alteration, similar to class A, with lengths of 1 to 10 mm. In general, classes B, C, and D present greater variation in size, as well as greater diversity in format than class A.

Despite the limited stratigraphic control of the collections, the grouping of classes based on different colors and matrix compositions suggests that the morphologies are not consistently present at the same stratigraphic level. It is possible that these forms may occur at various levels with similar compositions. For instance, class A may or may not be found

Table 1. Informal classes of dubiofossil morphology related to the associated matrix, mode of occurrence, length, and branching angles.

Class	Morphology	Associated matrix	Mode of preservation	Length (mm)	Main axis angles
A	Non-ramified straight	Light gray siltstone	3D white tubes with dark core faded border present or not, molds, and 2D impressions	0.04 to 10 (mean 2.5, SD 1.9)	–
B	Laterally ramified	Black to dark gray siltstone	3D black tubes and white tubes, faded border present or not, 2D white impressions	0.05 to 14 (mean 3, SD 2.1)	25 to 90°
C	Radially ramified	Black mudstone	White 2D impressions or 3D flattened tubules	3 to 16 (mean 4.1, SD 3)	11 to 86°
D	Less branched needles associated with dots	Dark to light gray siltstone	2D impressions, molds, and 3D white tubes with dark core faded border present or not	Acicula: 1 to 10 Dots: 0.013 to 1	9 to 86°

in the lighter siltstone layers, while class C may or may not be present in the darker claystone layers. Additionally, it is important to note that there is a possibility of variation within classes occurring at the same stratigraphic level, particularly in the case of class D. This class exhibits a transition from small needles, similar to the morphotypes of class A, to dots.

Despite the different external shapes found in a hand sample, common elements were described in a petrographic thin section that allow inferring that they are the same product (Fig. 5). The needles have a distinct crystallinity from the matrix, generally with well-defined edges, euhedral to subhedral shape, low relief, and nanocrystalline texture. The needles do not show color, twinning, or cleavage (Fig. 5a–c). It may have a black opaque central axis in the elongation direction and, less commonly, an opaque brownish outer edge (Fig. 5a–c). Incomplete extinction is oblique with a mottled, undulating appearance in larger needles. Birefringence is variable depending on needle size, usually low first order, but second order is present in larger features (Fig. 5c, d, g, and h). In general, the needles are organized in layers and may have a central axis that is always opaque, a surrounding layer of greater crystallinity (up to microcrystalline) and high birefringence, and a second layer of first-order birefringence; other layers may also occur externally as brown linings or a faded edge that appears as an irregular gray texture (never extinct).

The order and number of these layers are different between classes. Class A has only the opaque interior and the first-order layer (Fig. 5a and c). Class B has a more extinct interior, with two layers of distinct birefringence (second order and first order; Fig. 5b), sometimes delimited by the opaque lining; lateral branches present a generally extinct central region or the opaque axis (Fig. 5d). Class C presents two opaque axes (different from the others) delimiting an internal portion of second order (Fig. 5e and f), and class D presents, in radial forms, a less centralized axis and a predominance of second-order nanocrystalline material (Fig. 5g and h).

In general, the needles show irregular layers in the direction of the central axis of microporous texture intercalated with smooth or microgranular texture (Fig. 5c), sometimes aligned subspherical blocks (Fig. 5f). The texture and the crystallographic and birefringence variations between the needles make mineral inference difficult. Certainly, the lining is an iron oxide–hydroxide film present in the matrix and that surrounds the needles. The interior, with the most extinguished region or the entirely opaque axis, seems to be linked to impurities inside the needle. Mottled extinction refers to a possible clay or phyllosilicate (white mica?); however, birefringence resembles a possible carbonate (calcite?) – see the composition discussion in Sect 3.1.3.

3.1.2 Relationship with the matrix

The needles are embedded in the matrix composed of an agglomerate of circular–subcircular transparent forms and brown opaque cement, in petrography. The subspherical shape is demonstrated in the vertical thin section and micro-CT (Figs. 5i–l and 6f–i). Some look to be joined and aligned in groups of two to six spheres, forming ellipses and straight to sinuous lines with a globose limit (length up to 0.5 mm). Each circle has a low birefringence and is never extinct (Fig. 5c and d), with the diameter ranging from 0.04 to 0.1 mm. Some show a central black point or are polyhedric with subhedral faces delimited by brown lines. The needles are inserted in the lamina, are always horizontal, as demonstrated by micro-CT (Fig. 6g–i), and never cross or disarray the matrix spheres; both are covered by cement (darker, amorphous gray tone in micro-CT; Fig. 6a–e). Despite similar microstructures (central or wall), dubiofossils are distinguished from matrix spheres by size, degree of crystallinity, density differences, and higher birefringence;

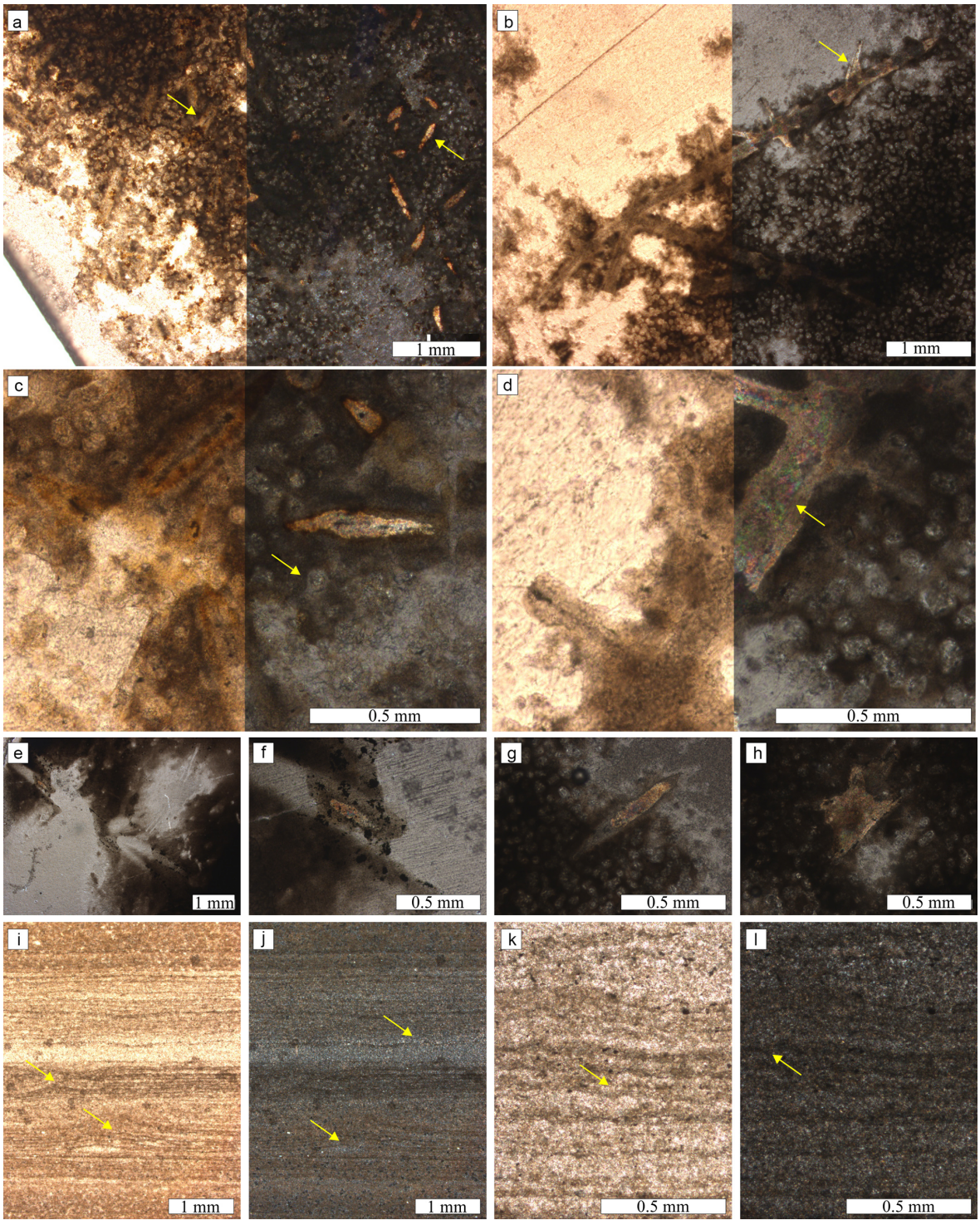

Figure 5. Petrographic thin sections: **(a)** class A needles (arrow) distributed with the spheres inside the matrix – left: natural light, right: polarized light, acicula in higher birefringence. **(b)** Class B ramified needle with the spheres inside the matrix – left: natural light, right: polarized light, dubiofossil in higher birefringence, arrow pointed to a dark main axis in a branch. **(c)** Close view of class A needles with a main dark axis, white layer, brown layer, and a second white layer – left: natural light, right: polarized light, dubiofossil in higher birefringence, arrow pointed to a matrix sphere. **(d)** Close view of a class B needle – left: natural light, right: polarized light, arrow pointed to the microcrystalline texture with higher birefringence (corresponding to the white layer), with nanocrystalline externally. **(e)** Close view of class C radially ramified mold – polarized light. **(e)** Close view of class C – internal composition partially preserved with second-order birefringence, polarized light. **(g, g)** Close view of a needle and radially ramified structures of class D – polarized light. **(i–l)** Microfabric of the matrix in vertical thin section – well-laminated, undulated, and disrupted lamina (arrows) related to sinusoidal and laminated leveling microstructures. **(i–k)** Natural light. **(j–l)** Polarized light.

there is greater morphological complexity, more layers, and branching (Figs. 5 and 6d).

3.1.3 Composition

The composition corroborates the difference between the elongated structures and the matrix. The matrix EDS shows an expected composition for siliciclastic muds and silts of O, Mg, Al, Si, K, and Fe (Fig. 7e), while the needles exhibit a complex element distribution following the pattern of texture described above (Fig. 7d and e). The main dark axis has O, Mg, Al, and Fe composition. The first layer (crystalline white–yellowish white) is dominated only by calcium and depleted in other elements. The second layer seems similar to the main axis, presenting a brown or dark appearance in which O, Mg, Al, and Fe occur. Another external layer of irregular gray texture, not always present, has O, Na, Al, Si, and K composition. C, Mn, and S appear weakly dispersed throughout the material, while Ti and sometimes S are concentrated in spots in the matrix and needles (Fig. 7f). Although Mg, Al, Si, K, and Fe cover the whole matrix, sometimes Mg and Fe appear concentrated in the matrix spheres, and Al and Si seem less concentrated in the same areas (Fig. 7e).

Between classes (A, B, and C), there was no difference in elemental composition, which varies, in addition to the external shape and crystallinity described above, in coverage and the compositional sequence. As class A is composed of smaller needles, it had a smaller coverage of Ca and Fe layers, with central axes (Mg, Al, K, and Fe) better defined. Class B is organized similarly with relatively greater coverage of Ca. Class C appears a little more distinct with less calcium coverage, as well as a wider central axis of O, Mg, Al, and Fe with a higher iron concentration towards the edges before the calcium wall.

The mineralogical composition agrees with the EDS elemental data. The brown amorphous material in the matrix can be assigned to hematite (as measured by Raman spectroscopy, peaks 400, 510, and 640 cm^{-1}, and XRD; Fig. 7a and g) and possibly magnetite (captured by XRD; Table 2), and organic matter is not encountered in RS or XRD. The spheres are probably clay minerals and micas, as measured by RS (Fig. 7a, peaks of 200, 260, 470, and 700 cm^{-1}) and corroborated by XRD (undefined clay minerals 14 and 7 Å). The XRD also indicated the presence of quartz, biotite, and albite. As in the EDS, the needles have a different composition, and the RS peaks at 1060 and 1420 cm^{-1} were interpreted as possible disordered carbonate minerals due to deviation and formation of additional peaks, which makes it hard to characterize the material (Fig. 7a). Calcite inferred by XRD is present only in the powder sample that contained the needles (Fig. 7g and Table 2).

Therefore, by the distribution of the elements in the needles, as corroborated by RS and EDS, it is possible to infer a calcite composition with impurities in the central area and a purer calcitic to the surrounding layer, whose main dark axis concentrates O, Al, Mg, and Fe with the whiter layers concentrating calcium. The external brown layers of O, Al, Mg, and Fe are considered clayey cement in the matrix, and the outermost layers are interpreted as a posterior alteration of the material from clays rich in Na and K.

Table 2. XRD powder results with and without needles.

Matrix with needles	Only matrix
Quartz	Quartz
Calcite	
Muscovite	Muscovite
Albite	Albite
Magnetite	Magnetite
Clay mineral 14 Å	Clay mineral 14 Å
Clay mineral 7 Å	Clay mineral 7 Å

3.1.4 Context, paleoenvironment, and associated biotic elements

The outcrop exhibits 14 m of centimetric heterolithic layers, measuring 0.2 to 4 cm (Fig. 8a), defined by tabular normally graded siltstones, rhythmically alternated with black mudstones, which are usually massive or present sub-millimetric lamination. There is a thinning-upward tendency with the predominance of sand layers at the base and mud layers at the top (Fig. 8a). Very fine to fine-grained sandstone layers with ripples are rare. Erosive structures such as sole marks, tool marks, flute casts, bounce, grooves, flames, and pseudonodules are frequent (Fig. 8c–f). Few dispersed granule clasts disturb the mudstone laminations, while erosive bases occur in sandstones.

Horizontal trace fossils and microbially induced sedimentary structures (MISSs) are distributed throughout the section, present in different silty and muddy layers, and became rare towards the top (Fig. 8a). Both fossil elements are widely investigated in other outcrops of the Itararé Group (Balistieri et al., 2002, 2003, 2021; Buatois et al., 2006; Gandini et al., 2007; Netto et al., 2009, 2021; Lima et al., 2015, 2017; Noll and Netto, 2018; Callefo et al., 2019b; De Barros et al., 2021) and help to understand the depositional environment.

As systematic ichnology is not one of our aims, here we present a brief description and identification of ichnotaxons. Simple shallow burrows of *Helminthoidichnites tenuis* and *Treptichnus pollardi* are very common in the Bemara outcrop, as well as others in the Itararé Group (see Balistieri et al., 2021). The first, *H. tenuis*, appears in concave hyporelief on muddy and silty facies (some associated with the rods, Fig. 9e), with a curved to meandering shape and many crosses between specimens, identified as non-specialized grazing traces, produced by arthropod larvae or a worm-like animal in non-marine settings. The former, *T. pollardi*, appears as concave or convex epirelief of

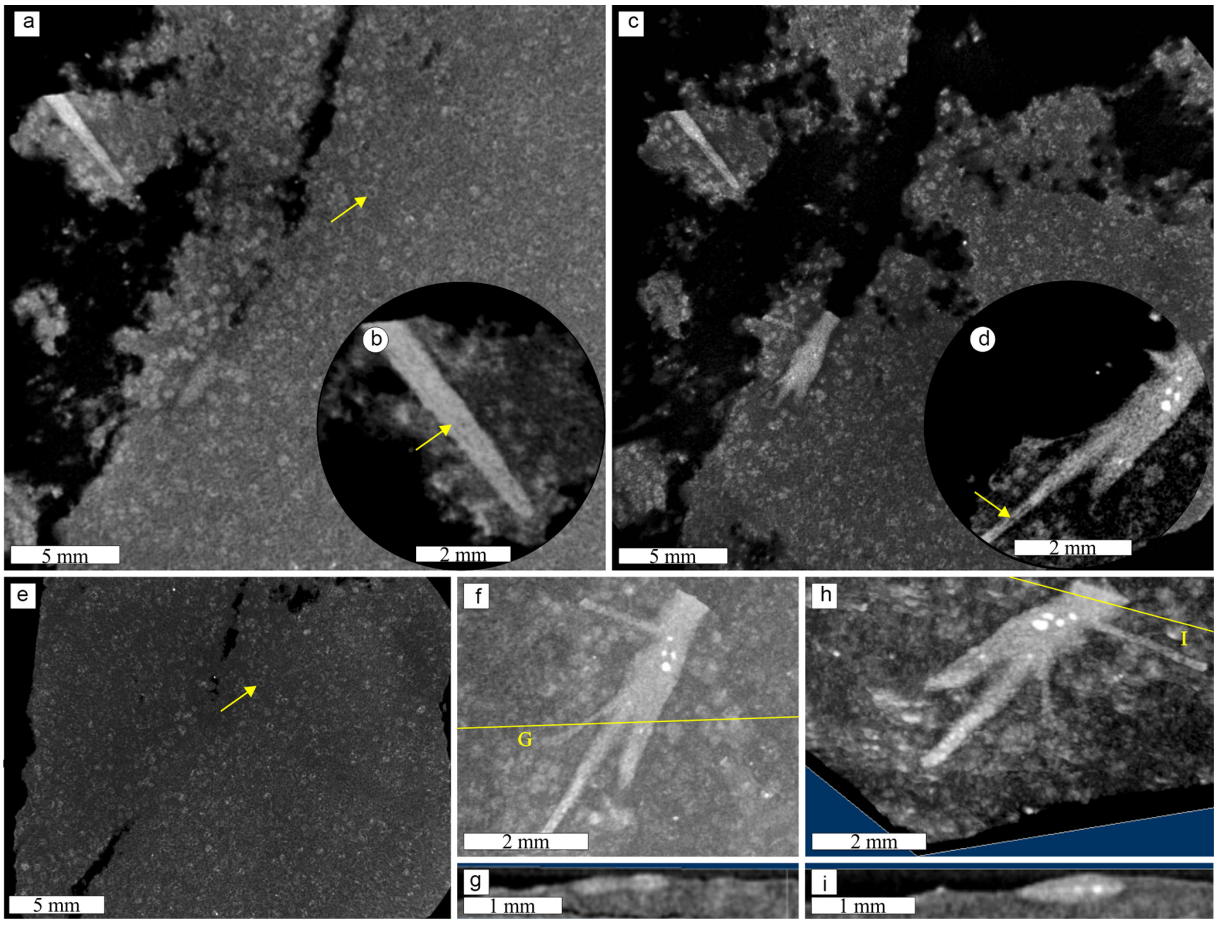

Figure 6. Micro-CT results for a needle (lighter gray structure), matrix (darker gray), and matrix spheres (gray circles): **(a)** general view of a non-ramified needle – yellow arrow points to matrix sphere; **(b)** close view showing the internal structure (slight density differences inside the tube, yellow arrow); **(c)** view of ramified structure; **(d)** close view of the ramified tubule – middle tubule less dense (yellow arrow). **(e)** Matrix view with multiple matrix spheres (one indicated by the yellow arrow). **(f–h)** Cross-section demonstrating the true ramification and insertion in the matrix. **(a–e)** 2D micro-CT slices. **(f–i)** 3D volume viewer composition showing **(f, g)** horizontal and **(g, i)** vertical.

straight to curvilinear segments joined by small round pits, interpreted as a feeding trace probably produced by worm-like animals also in subaqueous non-marine conditions. In addition, there are slightly curved to straight shallow bilobed intrastratal structures, ornamented by fine striations arranged obliquely to the median groove, preserved by convex hyporelief, diagnosed as *Cruziana problematica* and *Cruziana* isp., interpreted as a product of arthropod locomotion into the substrate (Fig. 9b and f). Epistratal structures were recognized: there are sinuous and straight trails of *Diplopodichnus biformis*, composed of two parallel grooves separated by a median ridge, which may or may not be ornamented with podial imprints, preserved as concave epirelief, possibly produced by millipedes on a soft-ground substrate (Fig. 9a); straight to strongly curved trackways consist of two parallel rows of podal impressions, without series, preserved as convex epirelief, recognized as *Diplichnites gouldi* also produced by millipedes on a stiff-ground substrate (Fig. 9a), as well as arthropod resting impressions like *Gluckstadella* isp. This suite can be interpreted as Mermia–Scoyenia ichnofacies, with the palimpsest already diagnosed in other Itararé localities (Netto et al., 2009; Balistieri et al., 2021).

MISSs are widely distributed in the Bemara quarry (Fig. 8a). Principally flattened unidirectional ripples with slightly sinuous parallel ridges (wavelength: 5 to 30 mm) occur in several muddy and silty layers throughout the outcrop, including those associated with the needles (Figs. 8i and 9d and h), presenting laminated leveling structures, the most common feature related to the microbial mat at the study area. The dubiofossils are distributed following the morphology of the ripples or are concentrated in the trough forming parallel clusters (Fig. 9h). Wrinkle structures are irregular parallel to subparallel crests or very sinuous ridges (Fig. 9c) that form a wrinkled pavement of claystone layers, typically non-transparent wrinkles. In addition, there are clusters of wrinkle types *Arumberia* (delicate subparallel lines) and

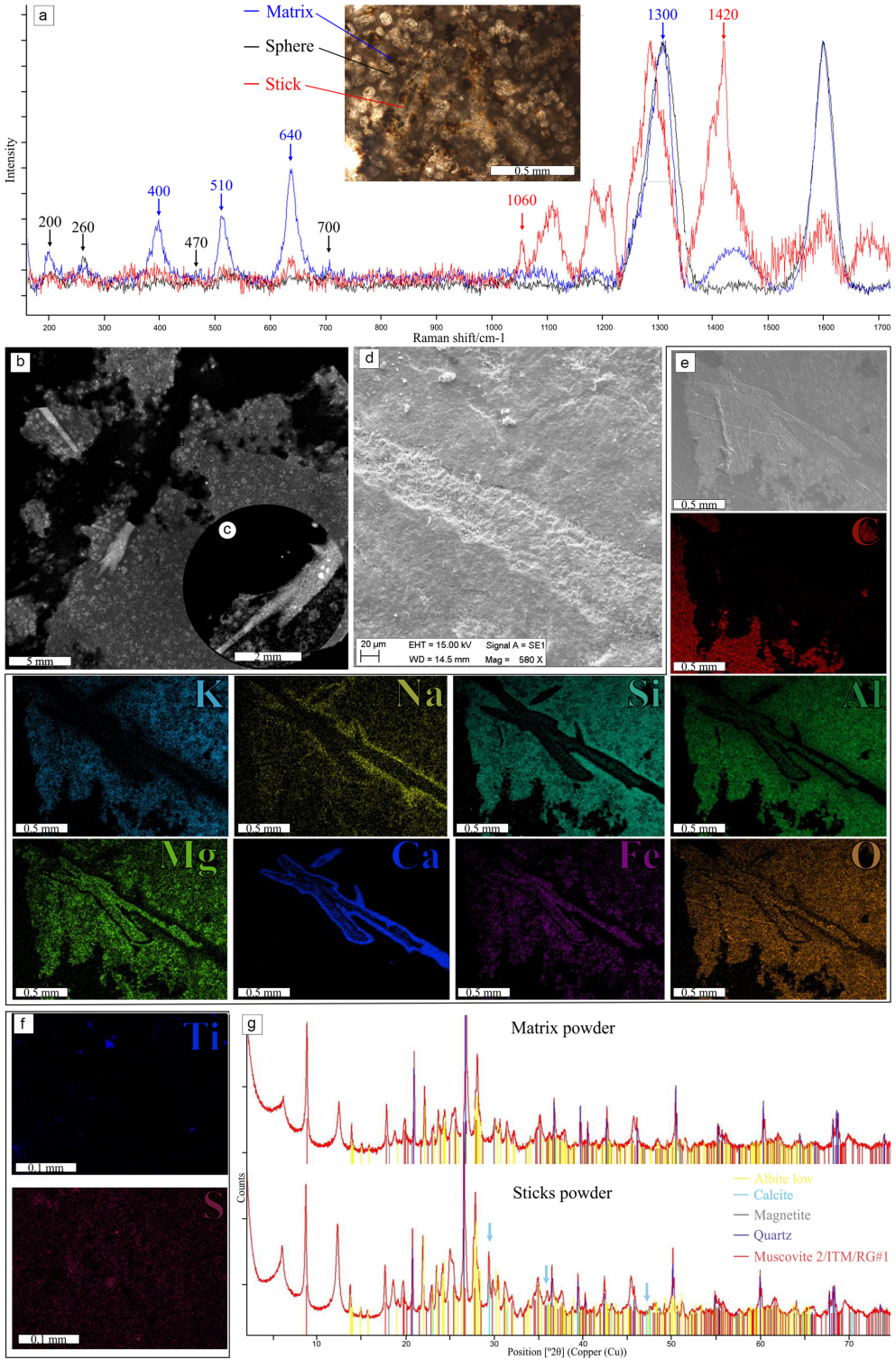

Figure 7. Paleometric results: **(a)** Raman spectra of the thin section – matrix show by blue, consistent with hematite peaks (~ 400, 510, 640, and 1300 cm^{-1}); spheres shown by black, with possible clay mineral composition (~ 200, 260, 470, and 700 cm^{-1}); needle shown by red, related to carbonate peaks (~ 1060 and 1420 cm^{-1}). **(b, c)** Density differences between the matrix (dark gray), spheres (gray), and needles (light gray). **(d–f)** SEM-EDS results: **(d0** secondary electron image of part of the needle in a hand sample, with different textures of the matrix, margin, and center of the needle. **(e)** Backscatter electron image and EDS composition of a ramified needle in thin section; C, K, Na, Si, Al, Mg, Ca, Fe, and O detected in different distributions. **(f)** EDS results of dispersed S and points of Ti in the matrix (other sample measured). **(g)** Graphical signs of XRD powder analysis, showing a matrix without (upper) and with (lower) acicula; the difference in the peaks of calcite present in the needles (blue arrows) is shown.

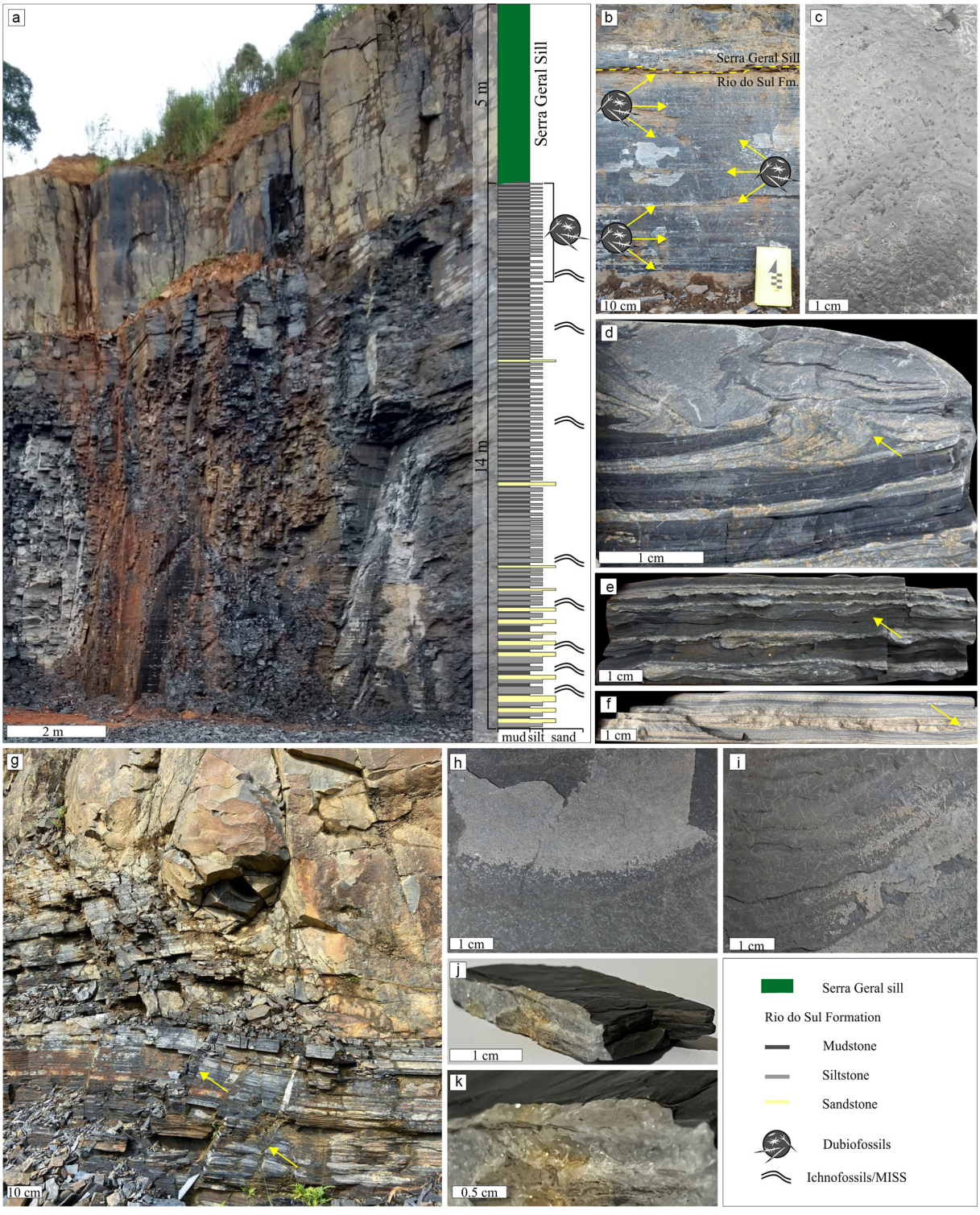

Figure 8. Geological setting and sample features of the Bemara quarry. **(a)** Bemara quarry – a section of 14 m of heteroliths enclosed by the sill of the Serra Geral Group, followed by a schematic section of the lithological distribution and presence of ichnofossils, microbially induced sedimentary structures (MISSs), and the dubiofossil under study;. **(b)** Occurrence section of the dubiofossils in the Rio do Sul Formation, close to the contact with the sill (dashed line); they are present in some layers but not all strata. **(c)** Pseudo-nodules on the mudstone slab, seen in plain view. **(d)** Flames and syn-depositional folds (arrow). **(e)** Flute cast and syn-depositional charge structures (arrow), cross-sectional view. **(f)** Sand layer with silt–clay load structures (arrow), cross-sectional view. **(g)** Irregular contact between the Paleozoic section and Cretaceous sill, fractured zone (arrows). **(h)** Horizontal quartz vein covering the silt layer with the needles. **(i)** Horizontal quartz vein partially covering flattened ripples with acicula. **(j)** Vertical quartz vein cutting the siltstone and mudstone layers. **(k)** Detail of the vertical quartz vein presenting the euhedral quartz crystals and brown cement.

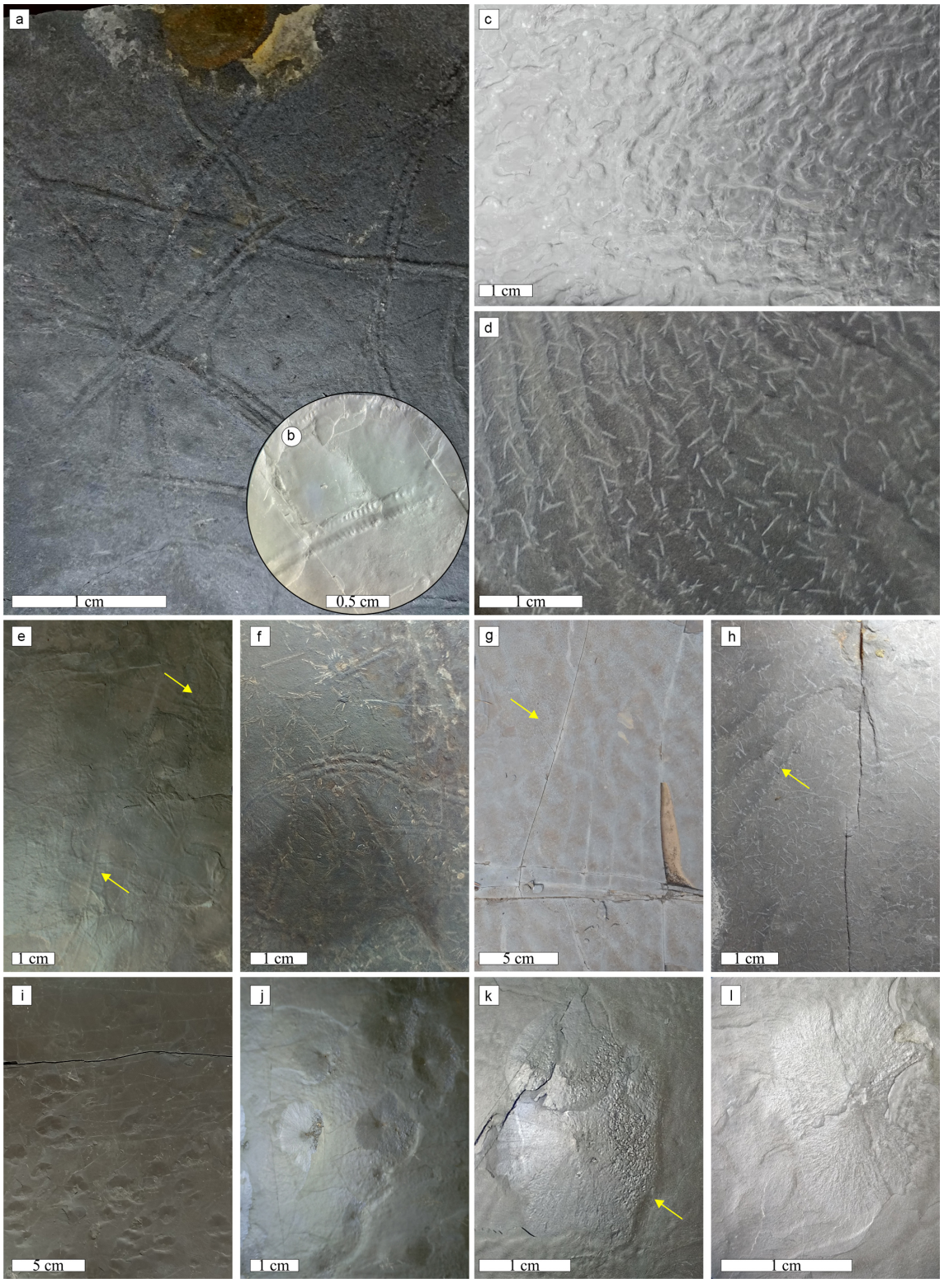

Figure 9. Associated biotic elements: **(a, b, e, f)** ichnofossils, **(c, d, g, h)** wrinkle structures, and microbial mat elements. **(i–l)** Small disks in the mudstones: **(a)** *Diplichnites gouldi* and *Diplopodichnus biformis*; **(b)** *Cruziana problematica*. **(c)** Wrinkle structures and **(d)** flattened unidirectional ripples with needles. **(e)** Helminthoidichnites *tenuis* (arrows). **(f)** *Cruziana* isp. at the center and *Cruziana problematica* at the top with the needles. **(g)** multi-directed ripple marks with needles (arrow). **(h)** Flattened ripples with needles aligned in parallel clusters. **(i)** Counted slab with many cones. **(j)** Aligned disks. **(k)** Cone with a flower form, vitreous luster, and a micro-wrinkle (arrow) on one side. **(l)** Detail of the disk with a flat top.

elephant skin (fine corrugations). Some levels also present multi-directed ripple marks (Fig. 9g).

The microfabric seen in the vertical thin section corroborates the macroscopic structures related to microbial mats (Fig. 5i–l). Despite not having layers composed of sand, hampering the visualization of oriented grains, the alternating laminar layers of silt and clay present a characteristic microfabric, undulated and disruptive features related to sinoidal and laminated leveling microstructures (Fig. 5i–l). In addition, the microfabric contains mat-layer-bound small grains (spheres, clays detected in XRD and RS) and possibly heavy minerals (opaque minerals and hematite detected in RS; Fig. 7a). The gradual alternation of dark and light layers may be related to micro-sequences, defined by Noffke et al. (1997) and Noffke (2010) and presented for other Itararé locality by Noll and Netto (2018) and Callefo et al. (2019b).

Some black argillaceous levels have clusters of small radial cones (1–4 mm in height and diameter ranging from 2 to 23 mm, with the mean of the largest and smallest diameter at 15.1 and 8.3 mm, respectively) with a straight top of circular to subangular shape (maximum of 3 mm), whose sides are formed by radial lines or elevations (Fig. 9i–l). A vitreous luster distinguishes them from the matrix with lobed edges that resemble a flower. In a slab measuring 1200 cm^2, 157 objects were counted; most are aligned and elongated in one direction, sometimes with two or three disks joined (Fig. 9j), and normally one of the faces orthogonal to this alignment presents a micro-wrinkle (Fig. 9k). In the vertical section, a central tube is not observable, and the same massive texture occurs inside and outside the disks, likely related to gas dome products of microbial metabolism (see Noffke, 2010, and Inglez et al., 2021).

All the features described favor the interpretation of extensive microbial mats throughout the Bemara outcrop, suggesting the presence of epibenthic communities, and possibly endobenthic, in a transitional lower supratidal to upper intertidal environment (see Noffke, 2010, 2018, and references therein). The association between microbial mats and trace fossils is common in the rhythmic deposits of the Itararé Group (see Lima et al., 2015, 2017; Noll and Netto, 2018, and Callefo et al., 2019b) and reveals the colonization of the bottom of shallow water bodies by microbial mats and animals. The mats favored preservation and served as a food substrate for undermat miners (*H. tenuis* and *T. pollardi*) and overmat grazers (myriapods traces of *D. biformis* and *Gluckstadella* isp.) (see Lima et al., 2015).

The stratigraphic data corroborate the regional interpretation of large turbiditic systems related to melt discharge. The dominance of clayey and silty layers and deformations favors the interpretation of distal turbidites (regional interpretation by Weinschütz and Castro, 2006; Aquino et al., 2016; Schemiko et al., 2019; Vesely et al., 2021). On the other hand, the extensive MISS and Mermia–Scoyenia ichnofacies are interpreted as shallow freshwater lakes in near-marginal marine settings that are tidally influenced (lower supratidal) and intensively colonized by microbial mats and trace fossil producers. These environments quickly dried up or reduced the water column, evidenced by the dominance of myriapods (other locations interpreted by Balistieri et al., 2002, 2003, 2021; Netto et al., 2009; Lima et al., 2015; Noll and Netto, 2018, and Callefo et al., 2019b). Both interpretations are postulated for other outcrops of the Itararé Group, and further work must be carried out to resolve the issue. As a more detailed description of the outcrop was not carried out and the paleoenvironmental interpretation is not the main objective of this work, both interpretations were considered in the discussion. Even so, the distribution of sand layers and the number of ichnofossils decreasing towards the top may signify a shallowing pattern in any of the interpretations.

The outcrop is closed at the top by a diabase sill with irregular contact (approximately 5 m; Fig. 8a, b and g), related to the Lower Cretaceous intrusions of Serra Geral Group (Silva, 2020), in which the last 3 cm of the sedimentary package close to the contact has a much higher hardness than the rest of the unit. The dubiofossils were collected in the last $\sim$ 2 m of the top of the outcrop, close to this diabase sill (Fig. 8). These problematic structures found in some, but not all, silt–mud layers, dispersed as abundant concordant macrotextures and clusters, are sometimes associated with trace fossils and MISS as described above. The systematic collection showed an increase in dubiofossil layers towards the top, with the highest abundance between 50 and 20 cm below the sill contact.

The sill facilitates the correlation of the Bemara outcrop with two other very close ones, Claudemir Rertz and José Guelbecke (Fig. 2b), which have the same Paleozoic succession (sedimentary structures and biotic elements) and the same occurrence of dubiofossils close to contact. In the José Guelbecke outcrop, approximately 600 m from the study point, Silva (2020) identified a halo of thermal effect, measured in palynomorphs from the sill contact up to 2.5 m below, and a zone of intense thermal influence $>$ 50 cm (gray phytoclasts). In the Bemara outcrop, a similar thermal effect can be interpreted by an increase in the hardness of the Rio do Sul Formation laminae as it approaches contact.

Furthermore, the study area is cut by several vertical and subvertical fractures, some of them filled with whitish crystals that are linked to the placement of the Cretaceous intrusive rock (Fig. 8g–k). This filling is different from dubiofossils because, in addition to cutting the sedimentary layers, it has a prismatic euhedral habit of regular size, transparent vitreous luster, and high crystallinity (Fig. 8j and k); quartz crystals possibly filled in the fractures (see Hartmann et al., 2012; Teixeira et al., 2018; De Vargas et al., 2022). The same crystallization rarely occurs in slides following the layering plane and covering the sedimentary structures and the dubiofossils (Fig. 8h and i), which makes it easier to distinguish the needles from this filling.

The geological history of this outcrop is complex, resulting from a range of processes including synsedimentary–

eodiagenetic processes, mesodiagenetic lithification, and thermal alteration during and after the intrusion of the sill. As a result, the origin of the dubiofossil may be linked to one or more of these processes or their superimposition. Further investigation of similar products is therefore necessary to shed light on the potential origins of this dubiofossil.

3.2 Indigeneity and syngenicity

Indigeneity and syngenicity are two concepts used to establish the origin and temporal history of materials. Indigeneity refers to the origin of the material and aims to eliminate the possibility of recent or procedural contamination. Syngenicity, on the other hand, seeks to establish synchronism between the material and its matrix or inserted medium, providing evidence of its temporal history (Buick, 1990; Wacey, 2009; McLoughlin and Grosch, 2015; Rouillard et al., 2021). In the case of the material under study, the brown cement coating over the dubiofossils and on the matrix suggests indigeneity, ruling out procedural contamination (Fig. 5). Additionally, the presence of needles predating the alteration and hematitic coat, which may have resulted from posterior cementation (Al-Agha et al., 1995), supports this hypothesis. The cement is also found in parts of the filled fractures, and the crystallized layer covering the dubiofossils strongly suggests that the needles are older than the fill and the intrusive rock (Fig. 8h–k). Therefore, the needles likely predate or are synchronous with the placement of the intrusive rock.

The dubiofossils always inserted in the clay or silt sheets indicate indigeneity, not growing later over the layers (Figs. 5 and 6). The fact that the elongated minerals do not cut the laminations and cross or disarrange the spheres may be an argument for a previous origin or during deposition–diagenesis (syngenicity). However, it does not rule out the possibility of later growth taking advantage of the horizontal weakness of the sediment laminations and regions without spheres (e.g., Makovicky et al., 2006). Or it may indicate the concomitant metamorphic growth of spheres and needles (Fig. 5). Therefore, the dubiofossil can be considered indigenous, but its syngenicity remains open.

3.3 Comparison with similar objects

The origin of the dubiofossils is suggested by the observed distribution of the needles only close to the contact and prior to the filled veins linked to the intrusion. Formation through the thermal effect is chemically plausible since ions and acids are produced by thermal degradation of organic matter (microbial C found in the matrix) and by magma degassing capable of crystallizing these carbonates (Saxby and Stephenson, 1987; Aarnes et al., 2010; Agirrezabala et al., 2014; Liu et al., 2016). Nevertheless, the morphology of the needles is different from products of contact metamorphism in mudstones: (1) usually these carbonates are cements or pore fillers, occupying the available space and generally amorphous–subhedral and unbranched (e.g., Finkelman et al., 1998; Huntington et al., 2011; Fig. 10c and s); (2) they occur as fractures breaking the sedimentary layers, forming irregular, sharp to serrated branches, which are features missing from needles (e.g., Golab et al., 2007; Huntington et al., 2011); (3) dendrites, as a branched radial growth structure from a point, usually have more than one order of branches (see Jones, 2017). As the origin by contact metamorphism seems implausible, the dubiofossils may be earlier and have been modified by the thermal effect, resulting in the calcitic composition found. In this way, the needles were compared with several abiotic and biotic objects from similar contexts, regardless of composition, to assess the most likely origin. Controlled minerals from sponge spicules, skeletons of sea urchins and algae, minerals induced and/or influenced by fungi and bacteria, inorganic pre- and synsedimentary–eodiagenetic minerals such as evaporites, springs, and other precipitation and mesodiagenetic crystals were surveyed, looking for resemblances to the needles (Fig. 10).

Most objects observed had similarities to the elements of dubiofossils described in Sect. 3.1, including their external form, internal structures, texture, and composition. The random distribution, packing, and branching seen in the objects are similar to algae and fungi, as well as evaporitic, tufaceous, and diagenetic minerals. The internal features, such as variations in crystallinity and a dark central axis, may resemble internal structures of algal skeletons and sponge spicules or features of induction and/or influence of algae, bacteria, or fungi; nevertheless, they may also be diagnostic textures produced by diagenetic processes.

The wide range of morphologies observed among the needles made it difficult to immediately associate them with any of the compared products. Each morphotype or shape class could be associated with a specific object, but when compared to another class, the association appeared less likely. For example, radial forms of class C with tapered ends (Fig. 4e and f) strongly resemble "chrysanthemum stones" (eodiagenetic mineralization of celestine or calcite; see Makovicky et al., 2006; Fig. 10d), while when compared with the other classes they are very distinct. However, the morphological complexity does not necessarily indicate a higher probability of biogenic origins (McLoughlin and Grosch, 2015), since complex and diverse forms are common in depositional minerals such as calcite and gypsum (see Maiklem et al., 1969; Garber et al., 1987; Aleali et al., 2013; Schultz et al., 2022; Fig. 10h), as well as diagenetic minerals (e.g., diagenetic calcites; Maliva, 1989; Ren and Jones, 2021; Fig. 10p and t).

The internal organization in layers as well as the textural and compositional variations found in the needles do not refer to specific mineral products. However, the features described here resemble layered structures, central features, and other textures produced by bacteria and fungi, which during their formation and growth generate zoned minerals and cell, hyphae, or EPS allocation sites within the biomin-

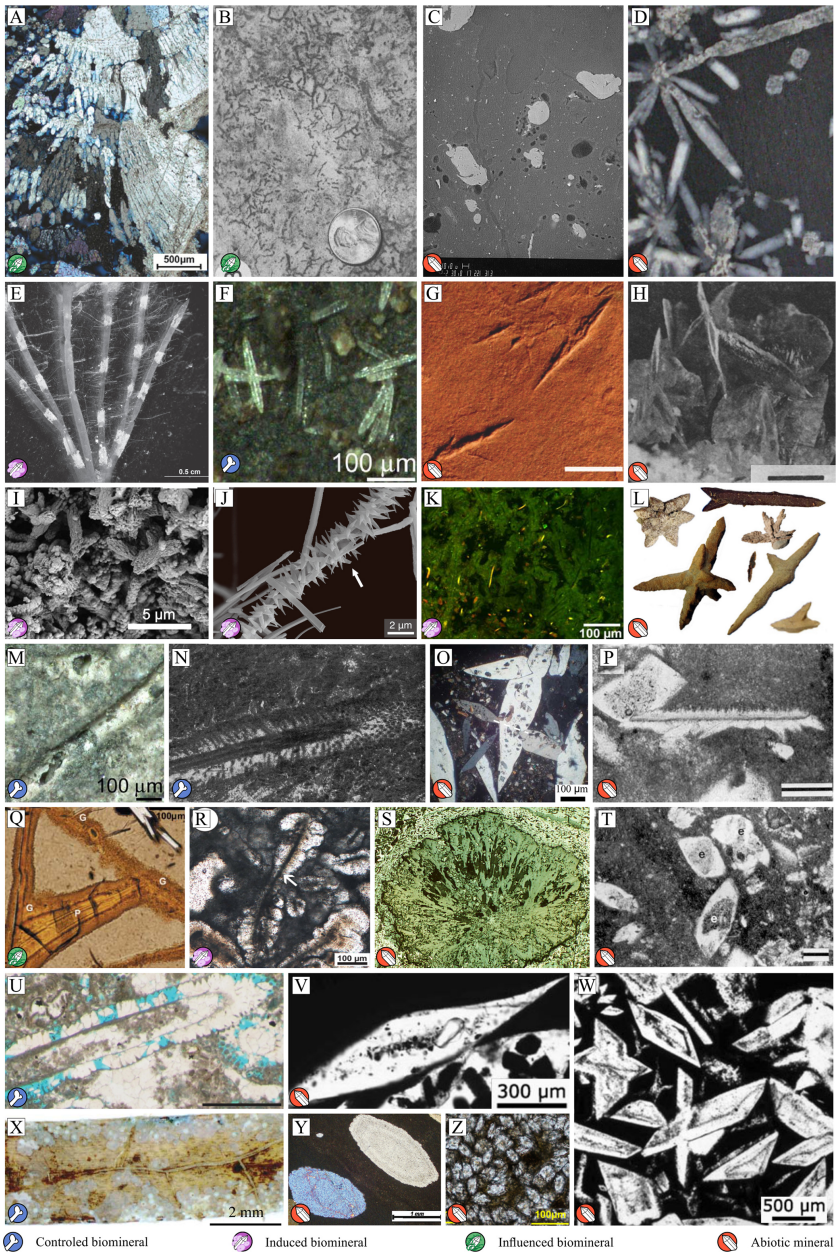

Figure 10. Comparison examples: **(a)** carbonate ($CaCO_3$) influenced by bacteria (Kraus et al., 2018); **(b)** carbonatic rizolith (influenced substitution) (Loope, 1988); **(c)** calcite (light gray spheres) produced by thermometamorphism in mudstone (dark gray) (Finkelman et al., 1998); **(d)** chrysanthemum stone (diagenetic radial celestine – $SrSO_4$); **(e)** carbonate precipitation over specific regions of the algae (induced crystallization) (Apolinarska et al., 2011); **(f)** silicious sponge spicules (skeleton) (Müller et al., 2006); **(g)** ice cast (Voigt et al., 2021); **(h)** evaporitic gypsum ($CaSO_4 \cdot 2H_2O$) (Garber et al., 1987); **(i)** tube-like forms of induced calcite in a microbial mat (Vasconcelos et al., 2006); **(j)** ramified and ornamented calcium oxalate produced by fungi (induced mineralization) (Bindschedler et al., 2016); **(k)** vertical section of a modern microbial mat with a filamentous network inducing calcite crystallization (Arp et al., 2010); **(l)** diverse habits of glendonite (ikaite pseudomorph $CaCO_3 \cdot 6H_2O$, cold-water precipitation) (Schultz et al., 2022); **(m)** close view of siliceous sponge spicule, internal detail (skeleton) (Müller et al., 2006); **(n)** carbonate algae (skeleton), internal detail (Wolf, 1965); **(o)** thin section of evaporitic elongated gypsum (Aref and Mannaa, 2021); **(p** diagenetic calcite ($CaCO_3$), internal structures (Maliva, 1989); **(q)** volcanic glass fracture containing banded palagonite (P), microbially deposited (influenced) (McLoughlin et al., 2009); **(r)** tufa crystal with micritic central filament, with supposed biotic origin (influenced) (Della Porta, 2015); **(s)** siderite ($FeCO_3$) nodule from a thermal-affected mudstone (Golab et al., 2007); **(t)** diagenetic calcite, internal details (Maliva, 1989); **(u)** Dasycladales (algae) in wackestone, original skeleton and mold (Granier, 2012); **(v)** glauberine ($CaNa_2(SO_4)_2$), evaporitic with inclusions of faecal pellets (influence not proved) (Salvany et al., 2007); **(w)** zoned glauberine, evaporitic precipitation in the substrate–water interface (Salvany et al., 2007); **(x)** coralline red algae growing on leaves of seagrass (skeleton) (Beavington-Penney et al., 2004); **(y)** evaporitic sparse anhydrite ($CaSO_4$) crystals in mudstones, concentrically zoned (Aleali et al., 2013); **(z)** diagenetic siderite presenting internal impurities (Wang et al., 2021).

eral (e.g., Golubic et al., 2000; Arp et al., 2010; Della Porta, 2015; Bindschedler et al., 2016). On the other hand, these features also resemble zonations, inclusions, and areas of impurities generated during diagenetic mineral growth (e.g., Maliva, 1989).

Comparing the matrix relationships of dubiofossils and other products can be problematic due to morphological variability. Flat, 2D topologies and impressions that accompany lamination may resemble diagenetic minerals (e.g., Maliva, 1989; Makovicky et al., 2006), while 3D features such as tubular or flattened shapes that do not cut through layers may resemble pre- and syn-depositional objects, such as evaporitic minerals, tufaceous minerals, and biominerals (e.g., Baąbel, 2004; Vasconcelos et al., 2006). Additionally, mineralized structures that do not cut through layers can also occur as a result of diagenetic growth (e.g., Makovicky et al., 2006).

The comparison revealed a low likelihood that the dubiofossil is a controlled biomineral. Skeletal biominerals typically exhibit greater regularity in size, shape, and branching due to their specific physiological origins (Dupraz et al., 2009). For instance, despite similarities to sponge diactinal spicules (such as tapered ends, outer layers, and a dark central feature thought to be axial filament, as seen in Uriz et al., 2003; Weaver and Morse, 2003; Müller et al., 2006; Fig. 10f and m), the dubiofossil's irregular branches in angle (ranging from 8 to 90° with the main axis) and length, as well as the morphological variations between classes, make this hypothesis less likely. Therefore, the absence of a controlled angular pattern or branching spacing and the wide variation in shapes preclude classification as a skeletal biomineral from sources such as sponge, sea urchin, coral, and coralline algae (Fig. 10a, n, u, and x; e.g., Wolf, 1965; Hooper and Van Soest, 2002; Beavington-Penney et al., 2004; Sethmann and Whörheide, 2008; Leonov and Fedonkin, 2009; Granier, 2012; Grgasović, 2022).

Regarding the composition, minerals (abiotic and biotic) with similar composition capable of posterior calcitic replacement were surveyed: carbonates and sulfates. Some of these minerals were excluded from the comparison because they did not have an origin compatible with the context observed for the acicula, such as aragonite, magnesite, gaylussite, ankerite, and kutnohorite (Lippmann, 1973; Alhaddad and Ahmed, 2022; Xu et al., 2019; Reijmer, 2021). The rest can be deposited abiotically as evaporites, biotically by bacteria, or by diagenetic crystallization. Most may have elongated habits like needles, but only calcite, dolomite, ikaite, gaylussite, and gypsum commonly have the diversity of habits of a dubiofossil: radial, laterally branched, and elongated. The specific patterns of size, shape, and distribution of these needles have not been found in the literature for these minerals (e.g., Warren, 2000, 2010; Baąbel, 2004; Schultz et al., 2022). Therefore, the shape may be the result of further thermal modification of the material, and therefore vaterite, aragonite, siderite, dawsonite, and gypsum–anhydrite also remain as putative original materials. As the comparison did not result in a more likely hypothesis, the proposals will be further evaluated in the next section.

3.4 Evaluating proposals

How should we proceed when comparison with objects from the literature does not significantly reduce the number of possibilities for the dubiofossil? Although controlled biomineral hypotheses have been eliminated, the descriptive and visual comparison of the dubiofossil did not yield a conclusive result. Therefore, a detailed discussion is necessary to determine its proposed origin. The lack of comparative parallels suggests that the complex environmental conditions in which it was formed – a transitional environment with strong climatic influences, such as variations in temperature, water volume, salinity, and mixing of saline and continental waters, in addition to a significant interface with extensive microbial mats – played a crucial role in shaping the final composition and morphology of the material. The dubiofossil underwent common diagenesis during the Itararé strata formation and subsequently experienced thermal effects resulting from the Cretaceous intrusion. Accordingly, dubiofossils seem to be the result of this complex history due to the following. (1) The large population morphology range prevents the identification of the material as a product that is only depositional or diagenetic or only metamorphic or biotic, mediated by microbial mats. (2) A distribution restricted to this contact does not occur far from it in the previous layers of the Rio do Sul Formation, which disfavors the explanation of a purely depositional product, whether abiotic or biotic. (3) A relatively wide geographic distribution occurs in the three outcrops, always closer to the sill contact, but is not found in other Cretaceous thermal aureoles within the Paraná Basin (see Santos et al., 2009; Hartmann et al., 2012; Teixeira et al., 2018; De Vargas et al., 2022), which precludes characterization as an artifact of purely contact metamorphism. Thus, the dubiofossil may have been formed through the combination of a syn-depositional or diagenetic process with a thermal effect.

3.4.1 Syn-depositional or diagenetic product

Based on the hypothesis of a subsequent thermal alteration that modified and replaced the needles, the original conditions of the material are evaluated, whether syn-depositional or diagenetic, induced and/or influenced biominerals, or abiotic minerals. To test the needles as a pre-thermal mineral, the minerals selected in Sect. 3.3 are evaluated.

Ice casts – freezing minerals. Certain characteristics of dubiofossils suggest that they could be interpreted as ice molds or ice casts. These elongated features are formed when water freezes within silt-dominated mudstones and fine-grained sandstones in fluvio-lacustrine, marginal marine, or aeolian environments (Dionne, 1985; Pfeifer et al., 2021; Voigt et al.,

2021), making their occurrence plausible in a periglacial setting. Moreover, these features are often randomly distributed within the bedding plane without disrupting the layers, as epistratal ice typically grows horizontally (Voigt et al., 2021). The various shapes observed in these elongated features resemble the different ways in which ice forms under varying temperature conditions, including needle-shaped, branched forms, stubby rods, fanned needles, rosette, and stellate structures (Mason et al., 1963; Pfeifer et al., 2021; Voigt et al., 2021). Additionally, the predominance of a specific morphotype within each slab corresponds to the monotypic pattern observed in ice molds (Voigt et al., 2021). The branching features are explained by cycles of freezing and thawing of water-saturated mud events, possibly occurring on a daily basis, which result in branches forming at acute angles without crossing the principal elongation (Voigt et al., 2021). Particular aspects of dubiofossils, such as crossing branches, distinct from ice casts, can be attributed to diagenetic or thermal modifications. Although similar features have been found in the fossil record, such as those reported by Bandel and Shinaq (2003) and Retallack (2021) in the Precambrian as well as Pfeifer et al. (2021) and Voigt et al. (2021) in the Permian, linked to the LPIA, the corroboration of this hypothesis is hindered by the fact that these structures are typically preserved as epirelief or hyporelief molds formed through the melting of ice crystals and subsequent sedimentary deposition within the resulting cavities (Fig. 10g; Voigt et al., 2021). It is challenging to explain the syn- or post-depositional preservation of other materials, such as calcite, within these spaces.

Gypsum – evaporitic mineral. The interpretation of needles as evaporitic gypsum (and anhydrite as gypsum that lost water) is supported by shape and context. Elongated and radiated morphologies are common for non-agglomerated crystals, as are tapered points (Baąbel 2004; Warren, 2016). Furthermore, the size fits the definition of selenite (gypsum > 2 mm in length), which evidences subaqueous evaporitic deposition (Baąbel, 2004). In this way, the proximity to the sea could contribute the necessary salinity, the semiarid to arid conditions would favor evaporation, and climate control such as cycles of melting and freshwater input would generate temperature changes, brine mixing, or brine freezing and freeze-drying that together would culminate in the crystallization of the needles (Baąbel, 2004; Warren, 2010). The low to no salinity inferred by the trace fossils (see Netto et al., 2009) does not interfere with the presence of these evaporites, as only saturation in calcium sulfate is required; in addition, more saline moments and intense stratification could be seasonally or daily controlled in a monomictic to polymictic lake (see Baąbel, 2004; Ayllón-Quevedo et al., 2007). The presence of needles in the top section of the quarry is indicative of these specific conditions of higher salinity inferred by the reduction of trace fossils, contrary to the base of the quarry with more trace fossils and shallower conditions, more conducive to dissolution by the input and interference of fresh water (Baąbel, 2004). Microbial mats, common in evaporitic systems (Trichet et al., 2001; Bontognali et al., 2010; Warren, 2010, 2016; Perillo et al., 2019), would favor the preservation of the needles on and within mats, as the gas domes indicate low substrate permeability, allowing the concentration of ions for precipitation (e.g., Paso Seco, in Argentina, Perillo et al., 2019). Thus, evaporitic gypsum precipitation is plausible in this context: as required by the Usiglio precipitation sequence, the deposition of carbonates comes before sulfates (see Baąbel, 2004; Warren, 2010). In addition, these earlier carbonates may have replaced the gypsum needles through the Cretaceous thermal effect.

Other evaporitic minerals. Other sulfates, such as thenardite, mirabilite, bloedite, loeweite, and glauberite, also exhibit a needle-like morphology in similar geological contexts (Warren, 1996, 2016; Hamdi-Aissa et al., 2004; Benison and Bowen, 2013). The Bemara environment, due to its local temperature conditions, may have provided favorable settings for the formation of these sulfate needles. Modern evaporites demonstrate that the nocturnal temperature reduction during winter, reaching close to 0 °C, creates the necessary thermodynamic equilibrium for the crystallization of mirabilite and other evaporitic minerals (Hamdi-Aissa et al., 2004; Espinosa-Marzal and Scherer, 2010; Jassim and Al-Badri, 2019). It is worth noting that glauberite has also been found in the Karoo basin, in a similar context of LPIA deglacial sequences, although it occurs in concretions (McLachlan and Anderson, 1973). These less common sulfates require a high concentration of specific cations for deposition (Hamdi-Aissa et al., 2004; Warren, 2016) and follow the Usiglio precipitation sequence, necessitating prior carbonate precipitation before their crystallization (see Baąbel, 2004; Warren, 2010). Consequently, the hypothesis of dubiofossils as evaporitic products becomes less plausible.

Ikaite – depositional–eodiagenetic mineral. Composition, multiple external branching forms, and internal features may denote origin as ikaite. Although the specific conditions for the formation of this mineral are still little known, they occur as surface precipitated minerals (e.g., Oehlerich et al., 2013) or eodiagenetic minerals (Lu et al., 2012; Zhou et al., 2015) in multiple cold-water environments (continental to abyssal; see Rogov et al., 2021, and Schultz et al., 2022, for a review). These crystals are extremely unstable, quickly dissolving or changing to glendonite (a variety of calcite that replaces ikaite; Huggett et al., 2005; Schultz et al., 2022). The multiple shapes of the needles match the morphologies of this unstable mineral (Schultz et al., 2022). The central internal features rich in iron and magnesium (e.g., Schubert et al., 1997) may be nuclei of magnesium ions that would guarantee mineral stability (Purgstaller et al., 2017; Stockmann et al., 2018), and the concentric layers may be marks of the transformation of ikaite into glendonite (proposed by Vickers et al., 2018). This mineralization can occur in the sulfate reduction zone or in the sulfate–methane transition, well

established by microbial mats, whose high pH and organic content also favor the maintenance of ikaite, promote glendonite replacement, and prevent dissolution (see Lu et al., 2012; Zhou et al., 2015; Trampe et al., 2016). The mat can also contribute to a rise in the phosphorous content related to the ikaite stability, like hyper-eutrophy in Manito Lake, Canada (Last et al., 2013); calcium phosphate was reported by Callefo et al. (2019b) in a similar Itararé outcrop linked to MISS. Furthermore, the occurrence of needles on some of the top laminae of the outcrop section could be caused by climate or environmental control, such as colder seasonal moments of the lake or specific depth conditions (see Oehlerich et al., 2013, and Schultz et al., 2022).

Dolomite – syn-depositional or eodiagenetic precipitation. The context interpreted for the needles fits into some of the various subenvironments and conditions in which dolomite can form and, together with the texture of the dubiofossils, makes this interpretation plausible. Cloudy-centered and clear-rimmed crystals are common textures in dolomites, denoting the replacement of high Mg-calcite by dolomite and the increase in order and size during diagenesis, since these minerals tend to age and/or evolve throughout burial history (Sibley et al., 1994; Warren, 2000; Ayllón-Quevedo et al., 2007). As syn-depositional dolomites in evaporitic environments (similar to gypsum discussed above), marine and lacustrine types tend to form laminae or surface strata (Warren, 2000; Trichet et al., 2001; Baąbel 2004), with the pattern of distribution and packing of needles having greater resemblance to eodiagenetic products such as interstitial, intrapore, or intramat mineralization (Warren, 2000). The eodiagenetic needles can be mixing zone dolomite or hemipelagic organogenic products (see Warren, 2000). The transitional conditions interpreted for the outcrop allow the mixing of phreatic pore water close to saturation in calcite with fresh water that leads to a state of undersaturation (Warren, 2000), with the mineral growing as void fillings in the mixing zone (Ward and Halley, 1985). The other plausible explanation is the origin of the needles related to the subsurface degradation of layers rich in organic matter and the increase in alkalinity in the zones of sulfate reduction or methanogenesis, well developed at the outcrop and diagnosed by the gas domes of the mats, which would favor mineralization (Roberts et al., 2004; Wright and Wacey, 2004, 2005). Several authors point to the reduction of sulfate by bacteria as essential and link most occurrences of eodiagenetic dolomite to the presence and mediation of microbial mats (Roberts et al., 2004; Wright and Wacey, 2004; Vasconcelos et al., 2006; Bontognali et al., 2010). Thus, the interaction of the MISS with the needles reinforces this hypothesis, since the mats are preponderant for crystallization, acting as nucleation centers (Vasconcelos et al., 1995).

Calcite – abiotic mineral. The needles can be made of calcite, as it fits into the various subenvironments as well as depositional and diagenetic contexts presented in the previous hypotheses as marginal evaporites, diagenetic products, or the result of biotic interaction with the environment and can generate unconventional and/or multiple forms of calcites (e.g., Wright and Barnett, 2015; Payandi-Rolland et al., 2019). In chemical and evaporitic deposits, shrub-like, dendritic, stellate, and spheroidal forms are abiotically precipitated (Wright and Barnett, 2015; Kraus et al., 2018; Farias et al., 2019), controlled, or modified by the presence of Mg^{2+}, which can, for example, promote growth parallel to the crystalline *c* axis (Zhu et al., 2006). Thus, the presence of this element in the water, in the conditions of a restricted or saline lake, can be the justification for the unusual precipitation of the needles, maintaining the centers rich in magnesium. Most diagenetic calcites are amorphous and fill the pores of the sediment like cement, originating from the concentration of Ca^{2+} in the interstitial space. However, there are occurrences of euhedral and distinct forms, with the presence of relicts and growth in layers (Cardoso et al., 2022; Sommer et al., 2022); thus, the needles may have formed during diagenesis, with the dark center as a relict, impurities that favored its growth, and the final shape modified by metamorphism.

Calcite – biomineral. Many authors emphasize the importance of sulfate bacteria, cyanobacteria, microbial mats, and EPS in syn-depositional and eodiagenetic calcite crystallization (Kropp et al., 1996, 1997; Bosak and Newman, 2005; Baumgartner et al., 2006; Vasconcelos et al., 2006; Dupraz et al., 2009; Arp et al., 2010, among others). In this sense, the formation of needles may be related to the organic content of the mats in three degrees of relevance. The first results from the presence of the mat with EPS only as a nucleation center, providing carboxyl groups for the initial binding of Ca^{2+} ions from water and subsequent abiotic growth of calcite (Turner and Jones, 2005; Baumgartner et al., 2006). In the second degree, in addition to serving as a nucleus, the degradation of bacteria and EPS (CO^{2-} degassing) may have influenced mineral growth by establishing a favorable microenvironment (pH, [Ca^{2+}], alkalinity, temperature). Moreover, the distribution of EPS on the mat can serve as a crystallization template, which partially explains the arrangement of needles in the matrix (Kropp et al., 1996, 1997; Turner and Jones, 2005; Spadaforda et al., 2010; Arp et al., 2010; Payandi-Rolland et al., 2019). In the third degree, in addition to serving as a nucleation center, the metabolism of bacteria, whether sulfate reducers or cyanobacteria, may have induced the crystallization of the needles (Kropp et al., 1997; Bosak and Newman, 2005; Baumgartner et al., 2006; Vasconcelos et al., 2006; Spadaforda et al., 2010). Kropp et al. (1997) exemplified this EPS control on carbonates in temperate-water intertidal siliciclastic sediments. Microorganisms can control calcification by secreting inhibitors and influencing binding of Ca^{2+} and Mg^{2+} ions (Braissant et al., 2003; Bosak and Newman, 2005; Arp et al., 2010). The bacterial metabolism and EPS degradation promote the precipitation of ovoid carbonates, and the continued degradation favors the aggregation and formation of larger ovoid crystals (e.g., Spadaforda et al., 2010; Payandi-Rolland et al., 2019). The variety of

stick morphologies, also recognized in induced and/or influenced biominerals of current biofilms, can be explained by the transformation from one form to another over time, changes in EPS chemistry during crystallization, or modifications in the degree of supersaturation of carbonates (Turner and Jones, 2005; Spadaforda et al., 2010; Arp et al., 2010; Liang et al., 2013; Payandi-Rolland et al., 2019). In addition, the shape may be an exotic deviation produced by unique physicochemical conditions such as the calcite dendrites reported by Turner and Jones (2005), which would have undergone further thermal modification.

Aragonite – biotic and abiotic mineral. Aragonite is commonly found in mollusk shells and nacre and as a high-pressure metamorphic mineral (Lippmann, 1973; Ramakrishna et al., 2017; Toffolo, 2021). While it is typically metastable compared to calcite, there are other occurrences where it is found. Needle-shaped aragonite, normally ranging from 5 to 100 µm, can be secreted by algae or deposited in various environments such as caves, hot springs, shallow seas, and lakes (Lowenstam and Epstein, 1957; Lippmann, 1973; Frisia et al., 2002; Jones, 2017; Ramakrishna et al., 2017). The factors contributing to the precipitation of aragonite needles instead of calcite are the influence of temperature, usually above 25 °C (Lipmann, 1973; Jones, 2017; Ramakrishna et al., 2017), a high concentration of Mg^{+} or a high Mg/Ca ratio (Kitano and Hood, 1962; Hu et al., 2009; Jones, 2017; Ramakrishna et al., 2017), and environments with high CO_2 degassing rates (Frisia et al., 2002; Sanchez-Moral et al., 2003; Jones, 2017). In the case of dubiofossils at Bemara, the larger needle size cannot be attributed to higher temperatures, as the paleoenvironmental conditions do not support this explanation. However, the presence of a central axis rich in Mg in the needles may indicate remnants of the high concentration necessary for aragonite deposition, in addition to the possible high rate of degassing due to the mediation and/or degradation of the mats (see Sanchez-Moral et al., 2003). Despite the fact that aragonite can easily be replaced by calcite, the large needle size, exceeding what is commonly reported in the literature, poses challenges in classifying the material as acicular aragonite.

Other carbonate minerals. The needles can be other carbonate minerals, which have less diversity of habits and morphologies and are generally presented in relatively smaller spheres than the needles. Despite that, the final form of the needles can be caused by metamorphism. Although vaterite is a very rare mineral, found mainly as a controlled biomineral of mollusk shells, the needles can be a rare depositional occurrence associated with bacteria usually forming microspheres (high NH_3 and high pH are required to promote the carbonate supersaturation, easily achieved in the mat). Once naturally precipitated, it has low stability and a tendency toward recrystallization; the morphology is easily modified (Lippmann, 1973; Rodriguez-Navarro et al., 2007). Dawsonite is a common authigenic mineral that can have an acicular shape, more elongated than classes A and B; usually it forms in the eodiagenesis of continental alkaline saline environments, when pore water is concentrated in Al, or in mesodiagenetic CO_2 storage environments (Eugster, 1980; Hellevang et al., 2013; Xia et al., 2022). However, Al was detected inside and outside the dubiofossils. The needles can be siderite growing during eodiagenesis as cement in pore water by the decomposition of organic matter, with methanogenesis produced in highly reducing anoxic non-sulfidic environments, whether lake, lagoon, or marine (Mücke, 2006; Vuillemin et al., 2019; Lin et al., 2020); that fits the Bemara interpretation. Several authors emphasize the mediation of sulfate-reducing bacteria in the process, and others point to the presence of Mg that helps in the reaction (Sapota et al., 2006; Lin et al., 2020).

Oxalate minerals. Oxalates such as whewellite, weddellite, and glushinskite, known as organic minerals, occur mainly as biominerals in plants, fungi, and algae as well as in diagenetic and hydrothermal occurrences (Baran, 2014; Hofmann and Bernasconi, 1998). The hydrothermal origin of the needles is completely discarded, as they do not present features that cut the layers like veins and that should be found as late-stage hydrothermal products in the form of whewellite (Baran, 2014; Hofmann and Bernasconi, 1998) after crystallization of calcite, inversely to what is found in the Bemara outcrop. The shapes and crystallinity also argue against the diagenetic origin of the needles; although the occurrence of diagenetic whewellite is generally a result of low migration in rocks rich in organic matter, the products are druses, vugs, and fissures within septarian concretions, normally larger than 1 cm (see Hofmann and Bernasconi, 1998, for a review). The needles cannot be skeletal parts of the plants and algae due to their generally elongated format, regular or in small globules (Franceschi and Horner, 1980; Hofmann and Bernasconi, 1998; Francheschi and Nakata, 2005; Baran, 2014), or in the rare occurrences of oxalate crosses included in algae (Pueschel, 2001), which are much smaller than Bemara needles. However, the origin of dubiofossils as products of mineralization induced and/or influenced by fungi or lichens is still plausible, mainly the result of the microenvironmental modification of the substrate by the action of hyphae, which leads to the mineralization of whewellite, weddellite (Gadd, 2007; Gadd et al., 2012, 2014; Baran, 2014), or glushinskite for some lichens (Wilson et al., 1980; Baran, 2014). These minerals have varied forms: some branched or ornamented with lateral spines (Whitney, 1989; Dutton and Evans, 1996), similar to dubiofossils. Fungi have a fossil record since the Proterozoic (e.g., Retallack, 2022) and are important degraders of rock and sediments on the surface (Chen et al., 2000; Gadd, 2007; Gadd et al., 2012, 2014). In addition, oxalates are easily modified to calcite under increasing temperature (Baran, 2014). One of the points that argues against this origin is that the needle features are not penetrative in the subsurface (generally subvertical to vertical, Friedmann et al., 1987; Chen et al., 2000; Gadd et al., 2014; Retallack, 2022) and do not present an expansive dis-

tribution from one or more centers, which would be the starting point of mycorrhizae, hyphae, or lichens (see Gadd et al., 2014).

Evaluating the proposals within the complex context of the needles and considering the analyzed composition as a probable thermal modification, it is possible, based on the descriptive criteria (Sect. 3.1), to determine the needles' chances of being each of these proposed minerals. Although plausible, sulfates need prior precipitation of carbonates (Baąbel, 2004), which leads to the following question: how did the carbonate precipitate to favor the growth of these needles? For dawsonite, alkalinity conditions are not proven. For vaterite specific conditions of high pH, NH_3, and supersaturation (see Rodriguez-Navarro et al., 2007) are required, which are also not proven but more possible because of the presence of bacteria. For ice casts, the features should be molds without containing any mineral fillers other than the matrix. For fungi or lichen oxalates, it is challenging to explain the purely horizontal forms. The other proposals remain with equal weight, as all of them show multiple forms, with similar textures and internal features. The compositional details and the distribution of elements contribute to keeping the proposals valid. The presence of Mg and Fe mainly inside the structures can be the centers of nucleation of the material. For ikaite and siderite, magnesium may have favored its stability (Purgstaller et al., 2017; Lin et al., 2020), and for calcite it could contribute to the generation of unusual external forms (see Zhu et al., 2006). For dolomite, it may be the trace of the original ions that, when replaced by Ca in metamorphism, were separated into the inside. Fe can still be a strong indication of the existence of organic matter, as a filamentous structure or EPS, which, due to the following mesodiagenetic, metamorphic, and epigenetic reactions, was replaced and/or complexed by this element (see Roden et al., 2010; Kunoh et al., 2016; Lepot et al., 2017), favoring the hypotheses linked to microbial mats.

3.4.2 Thermal effect

The effect of the intrusion on the sedimentary package is evidenced by the greater hardness in contact and the presence of multiple fractures and veins, in addition to the thermal effect indirectly diagnosed by altered palymorphs (Silva, 2020) in an aureole with gradual reduction of thermo-alteration up to 2.5 m below the contact, which agrees with the model proposed by Aarnes et al. (2010) of aureole thickness of up to 200 % of the thickness of their respective sills, in this case ~ 50 % (see Silva, 2020). Two more features may be evidence of this metamorphism: (1) the matrix spheres described as clays may be metamorphic mineral such as chlorite, which explains the interior impurity features and rounded to straight outer walls as a result of thermal growth (see Brammall, 1915; Weaver, 1984; Pitra and De Waal, 2001). As the spheres are never cut by the needles, it is possible that there was a later or concomitant development; (2) the needles themselves with impurity and zoning features as well as final calcite composition may be due to metamorphism.

Several authors highlight the presence of carbonates in shales and coals only close to the contact of sills and dikes, generated by the thermal alteration of organic matter (Saxby and Stephenson, 1987; Meyers and Simoneit, 1999; Santos et al., 2009; Agirrezabala et al., 2014; Liu et al., 2016, and references therein). This reaction, by mineral dehydration as well as organic matter decarbonization and decomposition, produces inorganic and organic acids such as CO, CO_2, CH_4, HCO^{3-}, and water, and the intrusion adds alkali cations (Fe^{2+}, Mg^{2+}, and Ca^{2+}), which together can circulate the sedimentary package by hydrothermal convection (Finkelman et al., 1998; Agirrezabala et al., 2014; Liu et al., 2016). This highly acidic environment can cause the dissolution of pre-existing carbonates and the precipitation of new ones (generally cementing the pores) by decreasing hydrothermal flow, overpressure buildup, and ion concentration (Zekri et al., 2009; Liu et al., 2016). The conditions presented above support the presence of needles only in this thermal aureole but do not justify their morphological diversity, pattern of distribution between layers, and packing.

Compositional differences in carbonates have been found to be linked to their proximity to intrusive bodies, with varying percentages of calcite, ankerite, dolomite, and siderite observed along the aureole, resulting from differences in Fe and Mg contents (Kisch and Taylor, 1966). These variations are influenced by the chemistry of the intrusive body, its distance from the dike or sill, and diagenesis specific to each thermal event (Finkelman et al., 1998). Furthermore, the petrophysical and chemical properties of the sedimentary package can also affect the circulation of fluids and the precipitation of carbonates, with mudstones contributing to overpressure buildup due to their very low permeability (Brace, 1980; Gerdes et al., 1998; Aarnes et al., 2012; Agirrezabala et al., 2014). As a result, the variation in the needles can be partially explained by the heterogeneity and differences in saturation, diffusion, and viscosity between mudstones and siltstones, as well as their distance from the contact (see Brace, 1980; Douglas and Beveridge, 1998; Mason et al., 2010; Sánchez-Navas et al., 2012).

3.5 Deciphering the complex history

Based on the proposed physicochemical conditions, it is possible to partially reconstruct the complex history of the needles. This history resulted from overlapping processes and the evolution of depositional, eodiagenetic, mesodiagenetic, and metamorphic environments. The following discussion aims to link the various features of the needles to these stages of the geological cycle (Fig. 11).

The carbonates discussed above, including ikaite, dolomite, calcite, and siderite, are more likely associated with microbial mats, whether syn-depositional or diagenetic (Fig. 11a). The occurrence of needles with mats suggests

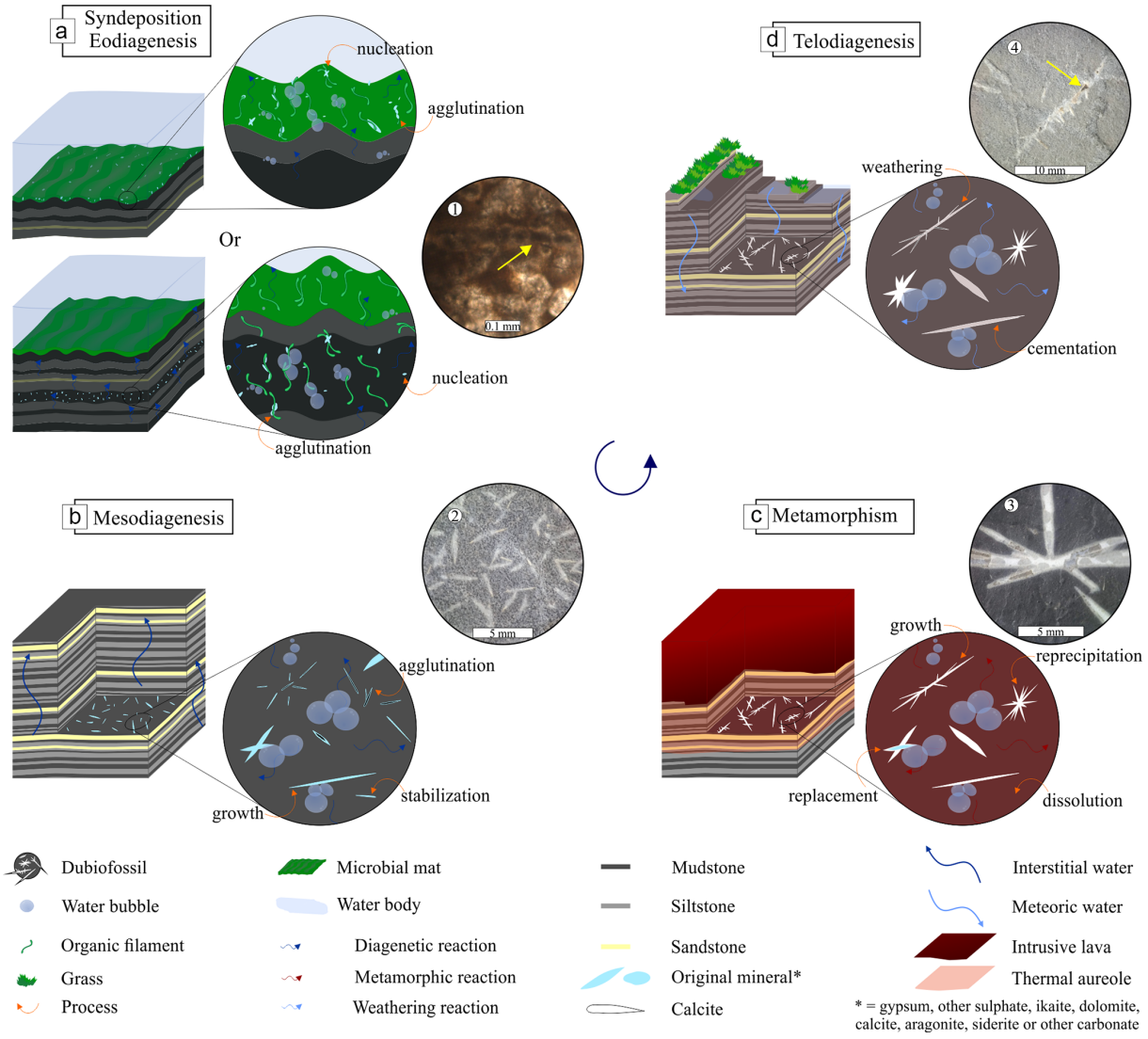

Figure 11. History of the formation of dubiofossils. **(a)** Syn-depositional or eodiagenesis associated with microbial mats; upper part – model deposition on the mat in life, lower part – authigenesis in eodiagenesis by mat degradation. **(b)** Mesodiagenesis and mineralization modifications. **(c)** Thermal effect, dissolution, modification, and replacement of the initial minerals by calcite and precipitation. **(d)** Telodiagenesis process of oxidation and cementation by hematite in recent exposure. (1–4) Examples of the result of interpreted processes; yellow arrows point to crystal alignment on the "filament" in 1 and cemented interior in 4. In each phase processes like nucleation, agglutination, stabilization, growth, dissolution, reprecipitation, replacement, cementation, and weathering have acted to produce and modify the dubiofossils.

an unlikely abiotic origin. The distribution of crystals may have been morphologically controlled by the EPS or the bacteria, serving as nucleation centers (Arp et al., 2010; Payandi-Rolland et al., 2019). However, it is unlikely that the EPS withstood later diagenetic and thermal modifications (see Turner and Jones, 2005), resulting in the transformation of the dark central axes into iron and magnesium. The rare occurrence of a dark central axis lining mineralized circles may indicate the original mineralization (see no. 1 in Fig. 11).

The form of needles may be linked to branched mineral habits, which are common in ikaite and less frequent in dolomite and calcite, as well as to the mineral evolution over time due to deposition and diagenesis processes that tend to modify or age them (see Warren, 2000; Payandi-Rolland et al., 2019; Schultz et al., 2022). Growth may have occurred abiotically after nucleation, driven by the physicochemical conditions of the microenvironment (see Turner and Jones, 2005), which are specific to each mineral, as discussed in Sect. 3.4. Alternatively, the metabolism or degradation of the microbial mat may have induced or influenced the transformation of these crystals, causing the ovoids to unite into elongated structures and resulting in elongated or branched crystals with central axes (see Spadaforda et al., 2010).

The evolution of these minerals may have been mediated by the eodiagenetic alteration of the mat, as evidenced by the gas domes, and the degradation of the organic content, which established methanogenetic or sulfate-reducing conditions and contributed to morphological transformations. Changes in the chemistry of EPS or modifications in the degree of carbonate supersaturation may have also played a role (Fig. 11a; Warren, 2000; Wright and Wacey, 2004; Turner and Jones, 2005; Zhou et al., 2015; Payandi-Rolland et al., 2019).

Crystallization commonly occurs around filaments or EPS in laboratory and modern environments, where it tends to grow vertically alongside biofilms (Pratt, 2001; Vasconcelos et al., 2006; Arp et al., 2010). However, in some cases, purely horizontal occurrences may be the result of water loss from clays and subsequent diagenetic flattening. Other modifications may have taken place during diagenesis, such as the complete replacement of ikaite by glendonite or crystallographic changes in dolomite and calcite (Fig. 11b).

Contact metamorphism is believed to be the primary modifying agent responsible for the observed phenomena (Fig. 11c). The thermal effect of the intrusion likely contributed to the simultaneous growth of matrix spheres and needles. This thermal alteration may have also caused the acidification and significant degradation of organic matter, which could have dissolved previous carbonate minerals and recrystallized and precipitated calcite (as described by Liu et al., 2016), replacing the original calcite, dolomite, siderite, or ikaite–glendonite. As a result of this process, impurity separation features may have formed, creating a dark center and Ca-rich external layers, which may or may not retain the central axis structure. Additionally, recrystallization and precipitation may have facilitated the union of aligned smaller needles to form larger needles, with branches composed of other mineralized tubes that were fused to the axis, resulting in the morphologies of class B (see no. 4 in Fig. 11). The irregularity in branching angles can be attributed to the random distribution of EPS or filaments that served as nuclei within the matrix. Thermal-alteration-induced precipitation may have generated radial morphologies of classes C and D (see no. 3 in Fig. 11), starting from a core, such as an old EPS and/or cell or a pre-existing mineralized structure.

The observed variations in morphologies between classes A, B, C, and D linked to the color of the matrix appear to be related to initial sedimentological differences (variations in the amounts of mud and silt between layers), the amount of organic matter and original crystals, and specific physicochemical conditions during thermometamorphism and contact distance (Brace, 1980; Finkelman et al., 1998). For example, class C, occurring in darker mud layers, seems to have lower permeability, resulting in larger radial shapes (see no. 3 in Figs. 11 and 12). Conversely, the smaller needles of class A (Fig. 12), linked to the light gray matrix, appear to be less influenced by reprecipitation and possibly retain an appearance closer to the original with a central "filament" and without the growth of long needles, possibly due to greater relative permeability or smaller amounts of organic matter to be degraded at that level (see no. 2 in Fig. 11). Class B may have sufficient organic matter and permeability to reprecipitate, grow, and unify the crystals into elongated branched forms (Fig. 12). Class D appears to have higher permeability, keeping the crystals as separate rods, with less permeable regions or organic cores allowing for the growth of radial dots (Fig. 12).

During the final intrusion process, both vertical and horizontal fractures were filled with quartz, likely as a result of hydrothermalism, as observed in other sedimentary sections of the Paraná Basin with the intrusive suite of the Paraná–Entendeka LIP (e.g., Hartmann et al., 2012; Teixeira et al., 2018). Finally, the posterior exposure of the outcrop resulted in hematite oxidation and cementation in the matrix spaces, covering the spheres and needles and replacing the organic filaments inside the needles (Fig. 11d).

Therefore, the diversity of morphologies and internal structures seems to be a result of the complex history and inherent properties of the matrix (Fig. 12). In the syndepositional–eodiagenetic stage, initial mineral nucleation and agglutination may have occurred abiotically. However, due to the association with MISS, biologically mediated processes seem more likely, and permeability and sediment composition may have determined differences in ion distribution, microenvironment formation, and the distribution of filamentous structures (Fig. 12). In the next phase, mesodiagenesis, stabilization, mineral growth, and rock compression may have occurred. There is a lack of evidence of biotic activity, but the different petrophysical properties between siltstones and mudstones may have favored greater or lesser grouping of minerals between layers. During metamorphism, several processes occurred such as growth, dissolution, replacement by calcite, and reprecipitation (Fig. 12), whose intensities may have been determined by the characteristics of the matrix. Other later modifications in telodiagenesis may have occurred, such as cementation and weathering. In all stages, biotic or abiotic processes may have occurred due to the ubiquity of life on Earth; this is a likely hypothesis, but there are no sufficient arguments to rule out others (Fig. 12).

Remaining questions

Does the composition found indicate that the original composition was not calcite? Despite the fact that, according to the data, calcite is the main material present, the distribution of elements found by EDS suggests that regions of high calcium concentration are mainly found around the needles, with iron and magnesium located in the center and the matrix. This raises questions about whether Fe and Mg should have covered a smaller area if they were only impurities in the original calcite. One possibility is that the concentration of these elements indicates the presence of another mineral,

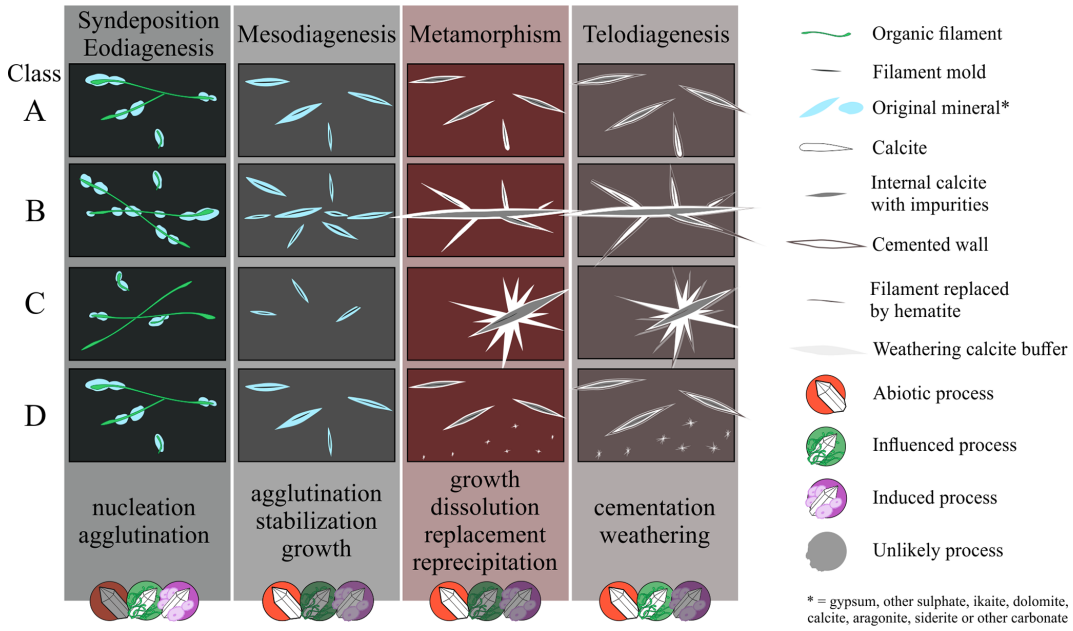

Figure 12. Model of differences between morphological classes (A–D) generated by variations in matrix properties in each of the stages of the complex history of mineralization. Associated matrix: class A – light gray siltstone; class B – black to dark gray siltstone; class C – black mudstone; class D – dark to light gray siltstone. Different intensities of the processes occurred, determining the morphologies and increasing the final morphological complexity. At each stage, the most likely process is indicated: biotic or abiotic, without being able to rule out the other hypotheses.

either original or substituted during metamorphism, such as ankerite, siderite, dolomite, or high Mg-calcite.

If these morphologies are mineralized by microbial mats, why are features with a certain similarity not found at the base of the outcrop? For this, three possible explanations are suggested. One is that environmental factors, such as depth or circulation, may have restricted deposition to only the top of the Bemara section. Another possibility is that some diagenetic or posterior process consumed the mineral from the needles far from the thermal aureole, as metamorphism may have conditioned greater resistance to weathering. The third option is that mineralization was entirely promoted by the thermal effect, with the intrusion contributing ions and degrading the organic matter necessary for calcite crystallization. The needles may have used the filamentous structure of fossilized EPS as a template for growth in different forms, which would justify their absence away from contact.

Although the hypothesis discussed above considers the possibility of biofilms and the needles being involved in the mineralization process, it is still unclear whether the abiotic hypothesis is completely refuted. Two hypotheses can be tested: one is that the needles are depositional–diagenetic abiotic calcite, which, due to specific geochemical conditions (such as the influence of Mg^{2+} ions on growth; see Zhu et al., 2006), could result in the exotic forms found. The second is that the rods are purely metamorphic abiotic calcite, since internal features of opaque axis in the center, compositional changes, crystallinity, and zonation can also be produced by metamorphism (Pitra and De Waal, 2001; Mason and Liu, 2018). The varied shapes and distribution are explained by physicochemical conditions of the substrate and intrusion (Brace, 1980; Finkelman et al., 1998; Agirrezabala et al., 2014).

Considering the current proposal of the ubiquity of life across the Earth's crust (see Merino et al., 2019; MacMahon and Ivarsson, 2019), is it possible that both early mineralization (syn-depositional or diagenetic) and thermal modification are mediated by bacteria? Although few studies have been conducted on this topic (Bengtson et al., 2017; Ivarsson et al., 2020, 2021), the heat of the intrusion, the presence of organic material, and the chemical reactions involved could create favorable conditions for the establishment of a deep biosphere that would help increase the diversity and complexity of needle morphologies. However, the lack of information prevents testing this hypothesis, so it is unclear whether the occurrence is mostly biotic.

3.6 Biogenity criteria for biominerals and biomimetic minerals

The needles described in this study demonstrate the lack of conclusive evidence for the biogenicity of biominerals and inorganic minerals. Despite a thorough description and comparison, there were not enough convincing arguments to discard any hypothesis, although an origin as a controlled biomineral seems less likely. The size, shape, structure, tex-

ture, and arrangement with the matrix observed in the needles are not necessarily diagnostic of abiotic or biotic products. These characteristics can be present in natural materials regardless of their origin, which is consistent with the views of several authors who have emphasized the challenges of using these features as biogenicity criteria (García Ruiz et al., 2002; Weiner and Dove, 2003; McLoughlin and Grosch, 2015; McMahon et al., 2021; Rouillard et al., 2021; McMahon and Cosmidis, 2022). This highlights the importance of further investigation of both biominerals and biomimetic inorganic minerals (Dupraz et al., 2009).

The irregular spacing and periodicity of branches observed in the needles are not typical of controlled biominerals but are rather common in induced, influenced, and abiotic biominerals (e.g., Shearman et al., 1989; Bindschedler et al., 2014). The composition of calcite, a mineral produced by various abiotic and biotic processes (Maliva, 1989; Weiner and Dove, 2003; Davies and Smith, 2006; Baąbel, 2007; Salvany et al., 2007; Benzerara and Menguy, 2009; Warren, 2016; Benzerara et al., 2019), is a result of complex histories and thermal transformations, making it challenging to eliminate any hypothesis. Furthermore, the biotic origin of the needles is supported by their co-occurrence with microbial mats, a feature that is associated in the literature with the crystallization of several minerals, whether induced or influenced. However, in transitional environments, abiotic crystallizations are also common (see Warren, 2000; Baąbel, 2004; Noffke, 2010).

The high variability in morphology and taphonomic characteristics has often been used as evidence of biogenicity for microfossil-like and biomineral-like objects (Whitney, 1989; Buick, 1990; Verrecchia and Verrecchia, 1994; Douglas and Beveridge, 1998; Weiner and Dove, 2003; Dodd et al., 2017). However, as demonstrated by the needles, this variability can also be the result of a complex history involving overlapping processes, physicochemical and microenvironmental variations, and other factors, making it a less conclusive criterion for mineral biogenicity.

Although the descriptive survey and comparison provide strong evidence for a biogenic origin of the needles, it is still not possible to completely rule out an abiotic hypothesis. Therefore, the needles exemplify the challenges of investigating biominerals and highlight the need to consider the complex history, superimposed processes, and ubiquity of life in the investigation of biomineral-like objects.

4 Conclusion

We have proposed a descriptive protocol for dubiofossils, building upon previous research in the field. Our protocol comprises four classes of attributes: morphology, structure, and texture; relationship with the matrix; composition; and context. By thoroughly examining these attributes, we can gather valuable insights that aid in determining the indigenous and syngenetic nature of dubiofossils, as well as comparing them to similar biotic and abiotic objects. Itararé's dubiofossils are products of nature, exhibiting a wide range of morphologies that distinguish them from any known minerals. The absence of a consistent pattern in their diverse forms helps dismiss hypotheses suggesting controlled biomineralization. However, it remains uncertain whether the material could have originated as an abiotic mineral or as an induced or influenced biomineral. The complexity of their geological history and the multitude of contributing factors have resulted in this distinctiveness. Consequently, we propose that dubiofossils are likely the outcome of a combination of processes and a complex geological history.

1. *Environment*. A Pennsylvanian transitional setting was established, characterized by a shallow lake close to the sea and the reception of continental deglaciation fluxes, in conjunction with semi-arid conditions that can reduce the water column and extensive microbial mats at the bottom. This environment provides many possibilities for the presence of original minerals, such as evaporitic sulfate, depositional–eodiagenetic ikaite and dolomite, abiotic calcite, biofilm-mediated calcite, and eodiagenetic aragonite, vaterite, dawsonite, or siderite. Although the co-occurrence with MISS reinforces the likelihood of biotic origin, the possibility of an abiotic origin cannot be completely ruled out.

2. *First precipitation*. Regardless of the type of mineral, the deposition occurred on or within the mats (underwater or eodiagenetic conditions) in which the EPS and bacterial filamentous structures would serve as nucleation centers and in which initial spheres would be deposited by influence or induction of bacteria.

3. *Diagenesis*. The various eodiagenetic and mesodiagenetic chemical reactions, including mat degradation, would serve to modify and age the crystals, aggregating spheres in rods or growing ramifications.

4. *Intrusion and thermal alteration*. The intrusion of a Cretaceous sill from the Serra Geral Group has caused significant changes in the sedimentary package in contact. The heat generated by the intrusion led to the occurrence of new reactions, high degradation of organic matter, dissolution, reprecipitation, and replacement of original minerals by calcite. These thermometamorphic processes have resulted in considerable variability in forms, primarily due to physicochemical differences in the matrix.

5. *Posterior processes*. Quartz filling of fractures and veins at the end of intrusion (Cretaceous) and cementation–hematite replacement in the matrix occurred through telodiagenetic exposure.

At each stage, variations in the environmental and physical–chemical characteristics of the substrate play a significant

role in shaping the resulting products. Factors such as water content, organic matter, mineral composition, and specific properties of silt and clay layers contribute to the unique conditions for reactions that form and modify the needle-like structures. As a result, distinct processes occur with varying intensities in each silty and muddy layer within this contact section of the turbidites and the sill. These processes include nucleation and agglutination reactions during syndeposition–eodiagenesis, agglutination, aging, stabilization, and mineral growth in mesodiagenesis, dissolution, reprecipitation, replacement, and growth during contact metamorphism, as well as cementation, weathering, and subsequent processes. It is through the interplay of these processes that the diverse forms of dubiofossils emerge.

The precise definition of the original material remains a subject of debate for two primary reasons. Firstly, the morphological diversity observed can be attributed to a succession of processes that have occurred throughout the complex history of the specimen. This has resulted in the presence of diagnostic forms that support a particular hypothesis, as well as other forms that do not refute it. Secondly, the final composition has been influenced by thermometamorphic alteration, which has led to the replacement and modification of the original composition of the recovered calcite needles. This alteration has obscured the initial mineralogy, making it challenging to determine conclusively. As a result, the hypotheses of both biotic and abiotic sulfates and carbonates remain plausible explanations, and the material remains as a dubiofossil.

The needles described in this study serve as an example of how complex forms, wide-ranging morphology, organized textures, and composition can be the result of a complex history for dubiofossils. Therefore, these attributes should be carefully investigated and used with caution as evidence of biogenicity for biomineral-like objects. It is important to note that exotic forms can be present in both abiotic and biotic products of nature, emphasizing the need for thorough analysis and evaluation.

Data availability. Data presented in this work can be shared upon request.

Author contributions. JPS designed the study with help from JC and RSH. JPS conducted the study with technical assistance from MLAFP and LDM. All co-authors analyzed the results. JPS prepared the paper with contributions from all co-authors.

Competing interests. The contact author has declared that none of the authors has any competing interests.

Disclaimer. Publisher's note: Copernicus Publications remains neutral with regard to jurisdictional claims in published maps and institutional affiliations.

Acknowledgements. We appreciate and are thankful for the support of the Universidade do Vale do Rio do Sinos, Universidade Federal de Santa Catarina, and ITT OCEANEON. We are grateful for advice from and discussions with Joseph Botting, Francisco Manoel Wohnrath Tognoli, Cristina Silveira Vega, Heinrich Frank, and Andrea Sander, as well as Renata Guimarães Netto for help and guidance.

Financial support. This research has been supported by the Coordenação de Aperfeiçoamento de Nível Superior (CAPES) for funding the scholarship and by Conselho Nacional de Desenvolvimento Científico e Tecnológico (CNPq) (grant nos. CNPq PQ 310970/2022-9 and CNPq 420748/2018-0).

Review statement. This paper was edited by Helge Niemann and reviewed by Flavia Callefo, Luana Morais, and Gregory Retallack.

References

Aarnes, I., Svensen, H., Connolly, J. A. D., and Podladchikov, Y. Y.: How contact metamorphism can trigger global climate changes: Modeling gas generation around igneous sills in sedimentary basins, Geochim. Cosmochim. Ac., 74, 7179–7195, https://doi.org/10.1016/j.gca.2010.09.011, 2010.

Aarnes, I., Podladchikov, Y., and Svensen, H.: Devolatilization-induced pressure build-up: Implications for reaction front movement and breccia pipe formation, Geofluids, 12, 265–279, https://doi.org/10.1111/j.1468-8123.2012.00368.x, 2012.

Agirrezabala, L. M., Permanyer, A., Suárez-Ruiz, I., and Dorronsoro, C.: Contact metamorphism of organic-rich mudstones and carbon release around a magmatic sill in the Basque-Cantabrian Basin, western Pyrenees, Org. Geochem., 69, 26–35, https://doi.org/10.1016/j.orggeochem.2014.01.014, 2014.

Al-Agha, M. R., Burley, S. D., Curtis, C. D., and Esson, J.: Complex cementation textures and authigenic mineral assemblages in Recent concretions from the Lincolnshire Wash (east coast, UK) driven by Fe(0) to Fe(II) oxidation, J. Geol. Soc. Lond., 152, 157–171, https://doi.org/10.1144/gsjgs.152.1.0157, 1995.

Aleali, M., Rahimpour-Bonab, H., Moussavi-Harami, R., and Jahani, D.: Environmental and sequence stratigraphic implications of anhydrite textures: A case from the Lower Triassic of the Central Persian Gulf, J. Asian Earth Sci., 75, 110–125, https://doi.org/10.1016/j.jseaes.2013.07.017, 2013.

Alhaddad, M. S. and Ahmed, H. A. M.: A Review of Magnesite Mineral and its Industrial Application, Arab. J. Sci. Publ., 2663, 1–13, 2022.

Apolinarska, K., Pełechaty, M., and Pukacz, A.: $CaCO_3$ sedimentation by modern charophytes (Characeae): can calcified remains and carbonate $\delta^{13}C$ and $\delta^{18}O$ record the ecological state of lakes? – a review, Stud. Limnol. Telmatolog., 5, 55–66, 2011.

Aquino, C. D., Buso, V. V., Faccini, U. F., Milana, J. P., and Paim, P. S. G.: Facies and depositional architecture according to a jet efflux model of a late Paleozoic tidewater grounding-line system from the Itararé Group (Paraná Basin), southern Brazil, J. S. Am. Earth Sci., 67, 180–200, https://doi.org/10.1016/j.jsames.2016.02.008, 2016.

Aref, M. A. and Mannaa, A. A.: The significance of gypsum morphology in interpreting environmental changes caused by human construction, Red Sea coastal evaporation environment, Saudi Arabia, Environ. Earth Sci., 80, 1–21, 2021.

Arp, G., Bissett, A., Brinkmann, N., Cousin, S., Beer, D. D. E., Friedl, T., Mohr, K. I., Neu, T. R., Reimer, A., Shiraishi, F., Stackebrandt, E., and Zippel, B.: Tufa-forming biofilms of German karstwater streams: microorganisms, exopolymers, hydrochemistry and calcification, Microb. Phys. Control., 336, 83–118, 2010.

Ayllón-Quevedo, F., Souza-Egipsy, V., Sanz-Montero, M. E., and Rodríguez-Aranda, J .P.: Fluid inclusion analysis of twinned selenite gypsum beds from the Miocene of the Madrid basin (Spain). Implication on dolomite bioformation, Sediment. Geol., 201, 212–230, https://doi.org/10.1016/j.sedgeo.2007.06.001, 2007.

Bąbel, M.: Models for evaporite, selenite and gypsum microbialite deposition in ancient saline basins, Acta Geol. Pol., 54, 219–249, 2004.

Bąbel, M.: Depositional environments of a salina-type evaporite basin recorded in the Badenian gypsum facies in the northern Carpathian Foredeep, Geol. Soc. London, Spec. Publ., 285, 107–142, https://doi.org/10.1144/SP285.7, 2007.

Balistieri, P., Netto, R. G., and Lavina, E. L. C.: Icnofauna de ritmitos do topo da Formação Mafra (Permo-Carbonífero da Bacia do Paraná) em Rio Negro, Estado do Paraná (PR), Brasil. Asoc. Paleontológica Argentina. IV Reun. Argentina Icnología y II Reun. Icnología del Mercosur, 9, 131–139, 2003.

Balistieri, P., Netto, R. G., and Sedorko, D.: Paleoichnology of the Itararé Group in the State of Santa Catarina and Rio Negro City (PR), Brazil: a revision, Terr. Plur., 15, e2118322, https://doi.org/10.5212/TerraPlural.v.15.2118322.039, 2021.

Balistieri, P. R. M. N., Netto, R. G., andLavina, E. L. C.: Ichnofauna from the Upper Carboniferous-Lower Permian rhythmites from Mafra, Santa Catarina State, Brazil: ichnotaxonomy, Revista Brasileira de Paleontologia, 4, 13–26, 2002.

Bandel, K. and Shinaq, R.: Sediments of the Precambrian Wadi Abu Barqa Formation influenced by life and their relation to the Cambrian sandstones in southern Jordan, Freib. Forschungshefte C, 499, 78–91, 2003.

Baran, E. J.: Review: Natural oxalates and their analogous synthetic complexes, J. Coord. Chem. 67, 3734–3768, https://doi.org/10.1080/00958972.2014.937340, 2014.

Baucon, A., De Carvalho, C. N., Felletti, F., and Cabella, R.: Ichnofossils, cracks or crystals? A test for biogenicity of stick-like structures from vera rubin ridge, mars, Geosciences, 10, 39, https://doi.org/10.3390/geosciences10020039, 2020.

Baumgartner, L. K., Reid, R. P., Dupraz, C., Decho, A. W., Buckley, D. H., Spear, J. R., Przekop, K. M., and Visscher, P. T.: Sulfate reducing bacteria in microbial mats: Changing paradigms, new discoveries, Sediment. Geol., 185, 131–145, https://doi.org/10.1016/j.sedgeo.2005.12.008, 2006.

Beavington-Penney, S. J., Paul Wright, V., and Woelkerling, W. J.: Recognising macrophyte-vegetated environments in the rock record: a new criterion using 'hooked' forms of crustose coralline red algae, Sediment. Geol., 166, 1–9, https://doi.org/10.1016/j.sedgeo.2003.11.022, 2004.

Bengtson, S., Rasmussen, B., Ivarsson, M., Muhling, J., Broman, C., Marone, F., Stampanoni, M., and Bekker, A.: Fungus-like mycelial fossils in 2.4-billion-year-old vesicular basalt, Nat. Ecol. Evol., 1, 1–6, https://doi.org/10.1038/s41559-017-0141, 2017.

Benison, K. C. and Bowen, B. B.: Extreme sulfur-cycling in acid brine lake environments of Western Australia, Chem. Geol., 351, 154–167, https://doi.org/10.1016/j.chemgeo.2013.05.018, 2013.

Benzerara, K. and Menguy, N.: Looking for traces of life in minerals, Comptes Rendus Palevol., 8, 617–628, https://doi.org/10.1016/j.crpv.2009.03.006, 2009.

Benzerara, K., Bernard, S., and Miot, J.: Mineralogical Identification of Traces of Life, Springer, 123–144, https://doi.org/10.1007/978-3-319-96175-0_6, 2019.

Bindschedler, S., Cailleau, G., Braissant, O., Millière, L., Job, D., and Verrecchia, E. P.: Unravelling the enigmatic origin of calcitic nanofibres in soils and caves: Purely physicochemical or biogenic processes?, Biogeosciences, 11, 2809–2825., https://doi.org/10.5194/bg-11-2809-2014, 2014.

Bindschedler, S., Cailleau, G., and Verrecchia, E.: Role of Fungi in the Biomineralization of Calcite, Minerals, 6, 41, https://doi.org/10.3390/min6020041, 2016.

Bontognali, T. R. R., Vasconcelos, C., Warthmann, R. J., Bernasconi, S. M., Dupraz, C., StrohmengeR, C. J., and McKenzie, J. A.: Dolomite formation within microbial mats in the coastal sabkha of Abu Dhabi (United Arab Emirates), Sedimentology, 57, 824–844, https://doi.org/10.1111/j.1365-3091.2009.01121.x, 2010.

Bosak, T. and Newman, D. K.: Microbial Kinetic Controls on Calcite Morphology in Supersaturated Solutions, J. Sediment. Res., 75, 190–199, https://doi.org/10.2110/jsr.2005.015, 2005.

Botta, O., Bada, J. L., Gomez-Elvira, J., Javaux, E., Selsis, F., and Summons, R.: Strategies of Life Detection, in: Space Sciences Series of ISSI, Springer Science & Business Media, Springer US, Boston, MA, https://doi.org/10.1007/978-0-387-77516-6, 2008.

Bower, D. M., Hummer, D. R., Steele, A., and Kyono, A.: The Co-Evolution of Fe-Oxides, Ti-Oxides, and Other Microbially Induced Mineral Precipitates. In: Sandy Sediments: Understanding the Role of Cyanobacteria In Weathering and Early Diagenesis., J. Sediment. Res., 85, 1213–1227, https://doi.org/10.2110/jsr.2015.76, 2015.

Brace, W. F.: Permeability of crystalline and argillaceous rocks, Int. J. Rock Mech. Min. Sci. Geomech., 17, 241–251, https://doi.org/10.1016/0148-9062(80)90807-4, 1980.

Braissant, O., Cailleau, G., Dupraz, C., and Verrecchia, E. P.: Bacterially induced mineralization of calcium carbonate in terrestrial environments: the role of exopolysaccharides and amino acids., J. Sediment. Res., 73, 485–490, https://doi.org/10.1306/111302730485, 2003.

Brammall, A.: VI – The Genesis of Chiastolite; and its suspected Occurrence in Association with a Basic Intrusive, Geolog. Mag., 2, 224–228, 1915.

Brasier, M., Green, O., Lindsay, J., and Steele, A.: Earth's Oldest (∼ 3.5 Ga) Fossils and the 'Early Eden Hypothesis': Ques-

tioning the Evidence, Orig. Life Evol. Biosph. 34, 257–269, https://doi.org/10.1023/B:ORIG.0000009845.62244.d3, 2004.

Brasier, M. D. and Wacey, D.: Fossils and astrobiology: new protocols for cell evolution in deep time, Int. J. Astrobiol., 11, 217–228, https://doi.org/10.1017/S1473550412000298, 2012.

Brasier, M. D., Green, O. R., Jephcoat, A. P., Kleppe, A. K., Van Kranendonk, M. J., Lindsay, J. F., Steele, A., and Grassineau, N. V.: Questioning the evidence for Earth's oldest fossils, Nature, 416, 76–81, https://doi.org/10.1038/416076a, 2002.

Briggs, D. E. G.: The Role of Decay and Mineralization in the Preservation of Soft-Bodied Fossils, Annu. Rev. Earth Planet. Sci., 31, 275–301, https://doi.org/10.1146/annurev.earth.31.100901.144746, 2003.

Briggs, D. E. G. and McMahon, S.: The role of experiments in investigating the taphonomy of exceptional preservation, Palaeontology, 59, 1–11, https://doi.org/10.1111/pala.12219, 2016.

Buatois, L. A., Netto, R. G., Mángano, M. G., and Balistieri, P. R. M. N.: Extreme freshwater release during the late Paleozoic Gondwana deglaciation and its impact on coastal ecosystems, Geology, 34, 1021, https://doi.org/10.1130/G22994A.1, 2006.

Buick, R.: Microfossil Recognition in Archean Rocks: An Appraisal of Spheroids and Filaments from a 3500 M.Y. Old Chert-Barite Unit at North Pole, Western Australia, Palaios, 5, 441, https://doi.org/10.2307/3514837, 1990.

Cagliari, J., Philipp, R. P., Buso, V. V., Netto, R. G., Klaus Hillebrand, P., da Cunha Lopes, R., Stipp Basei, M. A., and Faccini, U. F.: Age constraints of the glaciation in the Paraná Basin: evidence from new U–Pb dates, J. Geol. Soc. Lond., 173, 871–874, https://doi.org/10.1144/jgs2015-161, 2016.

Cailleau, G., Verrecchia, E. P., Braissant, O., and Emmanuel, L.: The biogenic origin of needle fibre calcite, Sedimentology, 56, 1858–1875, https://doi.org/10.1111/j.1365-3091.2009.01060.x, 2009.

Callefo, F., Maldanis, L., Teixeira, V. C., de Abans, R. A. O., Monfredini, T., Rodrigues, F., and Galante, D.: Evaluating Biogenicity on the Geological Record with Synchrotron-Based Techniques, Front. Microbiol., 10, 1–12, https://doi.org/10.3389/fmicb.2019.02358, 2019a.

Callefo, F., Ricardi-Branco, F., Hartmann, G. A., Galante, D., Rodrigues, F., Maldanis, L., Yokoyama, E., Teixeira, V. C., Noffke, N., Bower, D. M., Bullock, E. S., Braga, A. H., Coaquira, J. A. H., and Fernandes, M. A.: Evaluating iron as a biomarker of rhythmites – An example from the last Paleozoic ice age of Gondwana, Sediment. Geol., 383, 1–15, https://doi.org/10.1016/j.sedgeo.2019.02.002, 2019b.

Canuto, J. R., dos Santos, P. R., and Rocha-Campos, A. C.: Estratigrafia de sequênicas do grupo Itararé (Neopaleozoico), Revista Brasileira de Geociências, 31, 107–116, 2001.

Cardoso, A. R., Basilici, G., and da Silva, P. A. S.: Early diagenetic calcite replacement of evaporites in playa lakes of the Quiricó Formation (Lower Cretaceous, SE Brazil), Sediment. Geol., 438, 106212, https://doi.org/10.1016/j.sedgeo.2022.106212, 2022.

Chen, J., Blume, H.-P., and Beyer, L.: Weathering of rocks induced by lichen colonization – a review, Catena, 39, 121–146, https://doi.org/10.1016/S0341-8162(99)00085-5, 2000.

Daemon, R. F. and Quadros, L. D.: Bioestratigrafia do Neopaleozóico da bacia do Paraná, Congresso Brasileiro de Geologia, 24, 359–412, 1970.

Davies, G. R. and Smith, L. B.: Structurally controlled hydrothermal dolomite reservoir facies: An overview, Am. Assoc. Pet. Geol. Bull. 90, 1641–1690, https://doi.org/10.1306/05220605164, 2006.

Davies, N. S., Liu, A. G., Gibling, M. R., and Miller, R. F.: Resolving MISS conceptions and misconceptions: A geological approach to sedimentary surface textures generated by microbial and abiotic processes, Earth-Sci. Rev., 154, 210–246, https://doi.org/10.1016/j.earscirev.2016.01.005, 2016.

Davies, N. S., Shillito, A. P., Slater, B. J., Liu, A. G., and McMahon, W. J.: Evolutionary synchrony of Earth's biosphere and sedimentary-stratigraphic record, Earth-Sci. Rev., 201, 102979, https://doi.org/10.1016/j.earscirev.2019.102979, 2020.

de Almeida, F. F. M.: Distribuição regional e relações tectônicas do magmatismo pós-paleozoico no brasil, Rev. Bras. Geociências, 17, 325–349, https://doi.org/10.25249/0375-7536.1986325349, 1987.

De Barros, G. E. B., Becker-Kerber, B., Sedorko, D., Lima, J. H. D., and Pacheco, M. L. A. F.: Ichnological aspects of the Aquidauana Formation (Upper Carboniferous, Itararé Group, Brazil): An arthropod-colonized glacial setting, Palaeogeogr. Palaeoclim. Palaeoecol., 578, 110575, https://doi.org/10.1016/j.palaeo.2021.110575, 2021.

Della Porta, G.: Carbonate build-ups in lacustrine, hydrothermal and fluvial settings: comparing depositional geometry, fabric types and geochemical signature, Geol. Soc. Lond. Spec. Publ., 418, 17–68, https://doi.org/10.1144/SP418.4, 2015.

De Vargas, T., Boff, F. E., Belladona, R., Faccioni, L. F., Reginato, P. A. R., and Carlos, F. S.: Influence of geological discontinuities on the groundwater flow of the Serra Geral Fractured Aquifer System, Groundw. Sustain. Dev., 18, 100780, https://doi.org/10.1016/j.gsd.2022.100780, 2022.

Dionne, J. C.: Formes, figures et faciès sédimentaires glaciels des estrans vaseux des régions froides, Palaeogeogr. Palaeoclim. Palaeoecol., 51, 415–451, https://doi.org/10.1016/0031-0182(85)90097-5, 1985.

Dodd, M. S., Papineau, D., Grenne, T., Slack, J. F., Rittner, M., Pirajno, F., O'Neil, J., and Little, C. T. S.: Evidence for early life in Earth's oldest hydrothermal vent precipitates, Nature, 543, 60–64, https://doi.org/10.1038/nature21377, 2017.

Douglas, S. and Beveridge, T.: Mineral formation by bacteria in natural microbial communities, FEMS Microbiol. Ecol., 26, 79–88, https://doi.org/10.1016/S0168-6496(98)00027-0, 1998.

Dupraz, C., Visscher, P. T., Baumgartner, L. K., and Reid, R. P.: Microbe-mineral interactions: early carbonate precipitation in a hypersaline lake (Eleuthera Island, Bahamas), Sedimentology, 51, 745–765, https://doi.org/10.1111/j.1365-3091.2004.00649.x, 2004.

Dupraz, C., Reid, R. P., Braissant, O., Decho, A. W., Norman, R. S., and Visscher, P. T.: Processes of carbonate precipitation in modern microbial mats, Earth-Sci. Rev., 96, 141–162, https://doi.org/10.1016/j.earscirev.2008.10.005, 2009.

Dutton, M. V. and Evans, C. S.: Oxalate production by fungi: its role in pathogenicity and ecology in the soil environment, Can. J. Microbiol., 42, 881–895, https://doi.org/10.1139/m96-114, 1996.

Espinosa-Marzal, R. M. and Scherer, G. W.: Advances in understanding damage by salt crystallization, Acc. Chem. Res., 43, 897–905, https://doi.org/10.1021/ar9002224, 2010.

Eugster, H. P.: Geochemistry of Evaporitic Lacustrine Deposits, Annu. Rev. Earth Planet. Sci., 8, 35–63, https://doi.org/10.1146/annurev.ea.08.050180.000343, 1980.

Eymard, I., Alvarez, M., Bilmes, A., Vasconcelos, C., and Ariztegui, D.: Tracking Organomineralization Processes from Living Microbial Mats to Fossil Microbialites, Minerals, 10, 605, https://doi.org/10.3390/min10070605, 2020.

Farias, F., Szatmari, P., Bahniuk, A., and França, A. B.: Evaporitic carbonates in the pre-salt of Santos Basin – Genesis and tectonic implications, Mar. Pet. Geol., 105, 251–272, https://doi.org/10.1016/j.marpetgeo.2019.04.020, 2019.

Finkelman, R. B., Bostick, N. H., Dulong, F. T., Senftle, F. E., and Thorpe, A. N.: Influence of an igneous intrusion on the inorganic geochemistry of a bituminous coal from Pitkin County, Colorado, Int. J. Coal Geol., 36, 223–241, https://doi.org/10.1016/S0166-5162(98)00005-6, 1998.

Franca, A. B. and Potter, P. E.: Estratigrafia, ambiente deposicional e análise de reservatório do Grupo Itararé (Permocarbonifero), Bacia do Parana (Parte 1), Bol. Geociencias – Petrobras, 2, 147–191, 1988.

Franceschi, V. R. and Horner, H. T.: Calcium oxalate crystals in plants, Bot. Rev., 46, 361–427, https://doi.org/10.1007/BF02860532, 1980.

Franceschi, V. R. and Nakata, P. A.: Calcium oxalate in plants: Formation and function, Annu. Rev. Plant Biol., 56, 41–71, https://doi.org/10.1146/annurev.arplant.56.032604.144106, 2005.

Frank, H. T., Gomes, M. E. B., and Formoso, M. L. L.: Revisão da extensão areal e do volume da Formação Serra Geral, Bacia do Paraná, América do Sul, Pesqui. em Geociências, 36, 49–57, https://doi.org/10.22456/1807-9806.17874, 2009.

Friedmann, E. J., Weed, R., and Land, V.: Abiotic Weathering in the Antarctic Cold Desert, Science, 236, 703–705, 1987.

Frisia, S., Borsato, A., Fairchild, I. J., McDermott, F., and Selmo, E. M.: Aragonite-Calcite Relationships in Speleothems (Grotte De Clamouse, France): Environment, Fabrics, and Carbonate Geochemistry, J. Sediment. Res., 72, 687–699, https://doi.org/10.1306/020702720687, 2002.

Gadd, G. M.: Geomycology: biogeochemical transformations of rocks, minerals, metals and radionuclides by fungi, bioweathering and bioremediation, Mycol. Res., 111, 3–49, https://doi.org/10.1016/j.mycres.2006.12.001, 2007.

Gadd, G. M., Rhee, Y. J., Stephenson, K., and Wei, Z.: Geomycology: Metals, actinides and biominerals, Environ. Microbiol. Rep., 4, 270–296, https://doi.org/10.1111/j.1758-2229.2011.00283.x, 2012.

Gadd, G. M., Bahri-Esfahani, J., Li, Q., Rhee, Y. J., Wei, Z., Fomina, M., and Liang, X.: Oxalate production by fungi: significance in geomycology, biodeterioration and bioremediation, Fungal Biol. Rev., 28, 36–55, https://doi.org/10.1016/j.fbr.2014.05.001, 2014.

Gandini, R., Netto, R. G., and Souza, P. A.: Paleoicnologia e a palinologia dos ritmitos do Grupo Itararé na pedreira de Águas Claras (Santa Catarina, Brasil), Gaea, 3, 47–59, 2007.

Garber, R. A., Levy, Y., and Friedman, G. M.: The sedimentology of the Dead Sea, Carbon. Evapor., 2, 43–57, https://doi.org/10.1007/BF03174303, 1987.

García Ruiz, J. M., Carnerup, A., Christy, A. G., Welham, N. J., and Hyde, S. T.: Morphology: An Ambiguous Indicator of Biogenicity, Astrobiology, 2, 353–369, https://doi.org/10.1089/153110702762027925, 2002.

Gargaud, M., Irvine, W. M., Amils, R., Cleaves, H. J., Pinti, D. L., Quintanilla, J. C., Rouan, D., Spohn, T., Tirard, S., and Viso, M. (Eds.): Encyclopedia of Astrobiology, Springer, Berlin, Heidelberg, https://doi.org/10.1007/978-3-662-44185-5, 2015.

Gerdes, M. L., Baumgartner, L. P., and Person, M.: Convective fluid flow through heterogeneous country rocks during contact metamorphism, J. Geophys. Res.-Solid, 103, 23983–24003, https://doi.org/10.1029/98jb02049, 1998.

Golab, A. N., Hutton, A. C., and French, D.: Petrography, carbonate mineralogy and geochemistry of thermally altered coal in Permian coal measures, Hunter Valley, Australia, Int. J. Coal Geol., 70, 150–165, https://doi.org/10.1016/j.coal.2006.01.010, 2007.

Golubic, S., Seong-Joo, L., and Browne, K. M.: Cyanobacteria: Architects of Sedimentary Structures, in: Microbial Sediments, Springer, Berlin, Heidelberg, 57–67, https://doi.org/10.1007/978-3-662-04036-2_8, 2000.

Gomes, A. L. S., Becker-Kerber, B., Osés, G. L., Prado, G., Becker Kerber, P., de Barros, G. E. B., Galante, D., Rangel, E., Bidola, P., Herzen, J., Pfeiffer, F., Rizzutto, M. A., and Pacheco, M. L. A. F.: Paleometry as a key tool to deal with paleobiological and astrobiological issues: some contributions and reflections on the Brazilian fossil record, Int. J. Astrobiol., 18, 575–589, https://doi.org/10.1017/S1473550418000538, 2019.

Granier, B.: The contribution of calcareous green algae to the production of limestones: a review, Geodiversitas, 34, 35–60, https://doi.org/10.5252/g2012n1a3, 2012.

Green, S.: Polymerized Tubular Silicates in Lower Cambrian Carbonates – Biology or Chemistry?. Independent Project in Earth Science, Department of Earth Sciences, Uppsala University, Uppsala, https://urn.kb.se/resolve?urn=urn:nbn:se:uu:diva-476830 (last access: 30 March 2023), 2022.

Grgasović, T.: Taxonomy of the fossil calcareous algae: Revision of genera Physoporella Steinmann and Oligoporella Pia (Dasycladales), Carnets géologie, Notebooks Geol., 22, 171–310, https://doi.org/10.2110/carnets.2022.2207, 2022.

Hamdi-Aissa, B., Valles, V., Aventurier, A., and Ribolzi, O.: Soils and Brine Geochemistry and Mineralogy of Hyperarid Desert Playa, Ouargla Basin, Algerian Sahara, Arid L. Res. Manage., 18, 103–126, https://doi.org/10.1080/1532480490279656, 2004.

Hartmann, L. A., da Cunha Duarte, L., Massonne, H.-J., Michelin, C., Rosenstengel, L. M., Bergmann, M., Theye, T., Pertille, J., Arena, K. R., Duarte, S. K., Pinto, V. M., Barboza, E. G., Rosa, M. L. C. C., and Wildner, W.: Sequential opening and filling of cavities forming vesicles, amygdales and giant amethyst geodes in lavas from the southern Paraná volcanic province, Brazil and Uruguay, Int. Geol. Rev., 54, 1–14, https://doi.org/10.1080/00206814.2010.496253, 2012.

Hellevang, H., Aagaard, P., and Jahren, J.: Will dawsonite form during CO_2 storage?, Greenh. Gases Sci. Technol., 4, 191–199, https://doi.org/10.1002/ghg.1378, 2014.

Hofmann, B. A. and Bernasconi, S. M.: Review of occurrences and carbon isotope geochemistry of oxalate minerals: implications for the origin and fate of oxalate in diagenetic and hydrothermal fluids, Chem. Geol., 149, 127–146, https://doi.org/10.1016/S0009-2541(98)00043-6, 1998.

Hofmann, H. J.: Precambrian remains in Canada: fossils, dubiofossils, and pseudofossils, in: International Geological Congress, 24th Session, Proceedings, Montreal, 20–30, 1972.

Hooper, J. N. A. and Van Soest, R. W. M.: Systema Porifera. A Guide to the Classification of Sponges, in: Systema Porifera, Springer US, 1–7, https://doi.org/10.1007/978-1-4615-0747-5_1, 2002.

Hu, Z., Shao, M., Li, H., Cai, Q., Zhong, C., Xianming, Z., and Deng, Y.: Synthesis of needle-like aragonite crystals in the presence of magnesium chloride and their application in papermaking, Adv. Compos. Mater., 18, 315–326, https://doi.org/10.1163/156855109X434720, 2009.

Huggett, J. M., Schultz, B. P., Shearman, D. J., and Smith, A. J.: The petrology of ikaite pseudomorphs and their diagenesis, Proc. Geol. Assoc., 116, 207–220, https://doi.org/10.1016/S0016-7878(05)80042-2, 2005.

Huntington, K. W., Budd, D. A., Wernicke, B. P., and Eiler, J. M.: Use of Clumped-Isotope Thermometry To Constrain the Crystallization Temperature of Diagenetic Calcite, J. Sediment. Res., 81, 656–669, https://doi.org/10.2110/jsr.2011.51, 2011.

Inglez, L., Warren, L. V., Quaglio, F., Netto, R. G., Okubo, J., Arrouy, M. J., Simões, M. G., and Poiré, D. G.: Scratching the discs: evaluating alternative hypotheses for the origin of the Ediacaran discoidal structures from the Cerro Negro Formation, La Providencia Group, Argentina, Geolog. Mag., 159, 1192–1209, https://doi.org/10.1017/S0016756821000327, 2021.

Isbell, J. L., Miller, M. F., Wolfe, K. L., and Lenaker, P. A.: Timing of late Paleozoic glaciation in Gondwana: Was glaciation responsible for the development of Northern Hemisphere cyclothems?, in: Extreme Depositional Environments: Mega End Members in Geologic Time, Geological Society of America, 5–24, https://doi.org/10.1130/0-8137-2370-1.5, 2003.

Ivarsson, M., Drake, H., Neubeck, A., Sallstedt, T., Bengtson, S., Roberts, N. M. W., and Rasmussen, B.: The fossil record of igneous rock, Earth-Sci. Rev., 210, 103342, https://doi.org/10.1016/j.earscirev.2020.103342, 2020.

Ivarsson, M., Drake, H., Neubeck, A., Snoeyenbos-West, O., Belivanova, V., and Bengtson, S.: Introducing palaeolithobiology, Geologiska Föreningen i Stockholm Förhandlingar, 143, 305–319, https://doi.org/10.1080/11035897.2021.1895302, 2021.

Jassim, R. Z. and Al-Badri, A. S.: Mineral resources and occurrences of sodium chloride in Iraq: an overview, Iraqi Bulletin of Geology and Mining, 8, 263–287, 2019.

Jones, B.: Review of aragonite and calcite crystal morphogenesis in thermal spring systems, Sediment. Geol., 354, 9–23, 2017.

Kisch, H. J. and Taylor, G. H.: Metamorphism and alteration near an intrusive-coal contact, Econ. Geol., 61, 343–361, https://doi.org/10.2113/gsecongeo.61.2.343, 1966.

Kitano, Y. and Hood, D. W.: Calcium Carbonate Crystal Forms Formed from Sea Water by Inorganic Processes, J. Oceanogr. Soc. Jpn., 18, 141–145, https://doi.org/10.5928/kaiyou1942.18.141, 1962.

Knoll, A. H.: Systems paleobiology, Geol. Soc. Am. Bull., 125, 3–13, https://doi.org/10.1130/B30685.1, 2013.

Kraus, E. A., Beeler, S. R., Mors, R. A., Floyd, J. G., Stamps, B. W., Nunn, H. S., Stevenson, B. S., Johnson, H. A., Shapiro, R. S., Loyd, S. J., Spear, J. R., and Corsetti, F. A.: Microscale biosignatures and abiotic mineral authigenesis in Little Hot Creek, California, Front. Microbiol., 9, 1–13, https://doi.org/10.3389/fmicb.2018.00997, 2018.

Kropp, J., Von Bloh, W., and Klenke, T.: Calcite formation in microbial mats: Modeling and quantification of inhomogeneous distribution patterns by a cellular automaton model and multifractal measures, Int. J. Earth Sci., 85, 857–863, https://doi.org/10.1007/s005310050117, 1996.

Kropp, J., Block, A., Von Bloh, W., Klenke, T., and Schellnhuber, H. J.: Multifractal characterization of microbially induced magnesian calcite formation in recent tidal flat sediments, Sediment. Geol., 109, 37–51, https://doi.org/10.1016/S0037-0738(96)00059-0, 1997.

Kunoh, T., Hashimoto, H., McFarlane, I. R., Hayashi, N., Suzuki, T., Taketa, E., Tamura, K., Takano, M., El-Naggar, M. Y., Kunoh, H., and Takada, J.: Abiotic deposition of Fe complexes onto Leptothrix sheaths, Biology (Basel), 5, 26, https://doi.org/10.3390/biology5020026, 2016.

Last, F. M., Last, W. M., Fayek, M., and Halden, N. M.: Occurrence and significance of a cold-water carbonate pseudomorph in microbialites from a saline lake, J. Paleolimnol., 50, 505–517, https://doi.org/10.1007/s10933-013-9742-6, 2013.

Leonov, M. V. and Fedonkin, M. A.: Discovery of the first macroscopic algal assemblage in the Terminal Proterozoic of Namibia, southwest Africa, Commun. Geol. Surv. Namib., 14, 87–93, 2009.

Lepot, K., Addad, A., Knoll, A. H., Wang, J., Troadec, D., Béché, A., and Javaux, E. J.: Iron minerals within specific microfossil morphospecies of the 1.88 Ga Gunflint Formation, Nat. Commun., 8, 14890, https://doi.org/10.1038/ncomms14890, 2017.

Liang, A., Paulo, C., Zhu, Y., and Dittrich, M.: $CaCO_3$ biomineralization on cyanobacterial surfaces: Insights from experiments with three Synechococcus strains, Colloids Surf. B Biointerf., 111, 600–608, https://doi.org/10.1016/j.colsurfb.2013.07.012, 2013.

Lima, J. H. D., Netto, R. G., Corrêa, C. G., and Lavina, E. L. C.: Ichnology of deglaciation deposits from the Upper Carboniferous Rio do Sul Formation (Itararé Group, Paraná Basin) at central-east Santa Catarina State (southern Brazil), J. S. Am. Earth Sci., 63, 137–148, https://doi.org/10.1016/j.jsames.2015.07.008, 2015.

Lima, J. H. D., Minter, N. J., and Netto, R. G.: Insights from functional morphology and neoichnology for determining tracemakers: a case study of the reconstruction of an ancient glacial arthropod-dominated fauna, Lethaia, 50, 576–590, https://doi.org/10.1111/let.12214, 2017.

Lin, C. Y., Turchyn, A. V., Krylov, A., and Antler, G.: The microbially driven formation of siderite in salt marsh sediments, Geobiology, 18, 207–224, https://doi.org/10.1111/gbi.12371, 2020.

Lippmann, F.: Sedimentary Carbonate Minerals, Springer, Berlin, Heidelberg, https://doi.org/10.1007/978-3-642-65474-9, 1973.

Liu, C., Xie, Q., Wang, G., Zhang, C., Wang, L., and Qi, K.: Reservoir properties and controlling factors of contact metamorphic zones of the diabase in the northern slope of the Gaoyou Sag, Subei Basin, eastern China, J. Nat. Gas Sci. Eng., 35, 392–411, https://doi.org/10.1016/j.jngse.2016.08.070, 2016.

Loope, D. B.: Rhizoliths in ancient eolianites, Sediment. Geol., 56, 301–314, https://doi.org/10.1016/0037-0738(88)90058-9, 1988.

Lowenstam, H. A. and Epstein, S.: On the Origin of Sedimentary Aragonite Needles of the Great Bahama Bank, J. Geol., 65, 364–375, https://doi.org/10.1086/626439, 1957.

Lu, Z., Rickaby, R. E. M., Kennedy, H., Kennedy, P., Pancost, R. D., Shaw, S., Lennie, A., Wellner, J., and Anderson, J. B.: An ikaite record of late Holocene climate at the Antarctic Peninsula, Earth Planet. Sc. Lett., 325–326, 108–115, https://doi.org/10.1016/j.epsl.2012.01.036, 2012.

Maiklem, W. R., Bebout, D. G., and Glaister, R. P.: Classification of anhydrite – practical approach, Bull. Canad. Petrol. Geo., 17, 194–233, 1969.

Makovicky, E., Karup-Møller, S., and Li, J.: Mineralogy of the chrysanthemum stone, Neues Jahrb. für Mineral. – Abhandlungen, 182, 241–251, https://doi.org/10.1127/0077-7757/2006/0048, 2006.

Maldanis, L., Hickman-Lewis, K., Verezhak, M., Gueriau, P., Guizar-Sicairos, M., Jaqueto, P., Trindade, R. I. F., Rossi, A. L., Berenguer, F., Westall, F., Bertrand, L., and Galante, D.: Nanoscale 3D quantitative imaging of 1.88 Ga Gunflint microfossils reveals novel insights into taphonomic and biogenic characters, Sci. Rep., 10, 8163, https://doi.org/10.1038/s41598-020-65176-w, 2020.

Maliva, R. G.: Displacive Calcite Syntaxial Overgrowths in Open Marine Limestones, SEPM J. Sediment. Res., 59, 397–403, https://doi.org/10.1306/212F8FA3-2B24-11D7-8648000102C1865D, 1989.

Mason, B. J., Bryant, G. W., and Van den Heuvel, A. P.: The growth habits and surface structure of ice crystals, Philos. Mag., 8, 505–526, https://doi.org/10.1080/14786436308211150, 1963.

Mason, R. and Liu, R.: The Origin of Spots in Contact Aureoles and Over-Heating of Country Rock Next to a Dyke, J. Earth Sci., 29, 1005–1009, https://doi.org/10.1007/s12583-018-0882-5, 2018.

Mason, R., Burton, K. W., Yuan, Y., and She, Z.: Chiastolite, Gondwana Res., 18, 222–229, https://doi.org/10.1016/j.gr.2010.03.005, 2010.

McLachlan, I. R. and Anderson, A.: A review of the evidence for marine conditions in Southern Africa during Dwyka times, Palaeont. Afr., 15, 37–64, 1973.

McLoughlin, N.: Biogenicity, in: Encyclopedia of Astrobiology, edited by: Gargaud, M., Amils, R., and Cleaves, H. J., Springer, Berlin, Heidelberg, https://doi.org/10.1007/978-3-642-11274-4_17, 2011.

McLoughlin, N., Furnes, H., Banerjee, N. R., Muehlenbachs, K., and Staudigel, H.: Ichnotaxonomy of microbial trace fossils in volcanic glass, J. Geol. Soc. Lond., 166, 159–169, https://doi.org/10.1144/0016-76492008-049, 2009.

McLoughlin, N. and Grosch, E. G.: A Hierarchical System for Evaluating the Biogenicity of Metavolcanic- and Ultramafic-Hosted Microalteration Textures in the Search for Extraterrestrial Life, Astrobiology, 15, 901–921, https://doi.org/10.1089/ast.2014.1259, 2015.

McMahon, S. and Cosmidis, J.: False biosignatures on Mars: anticipating ambiguity, J. Geol. Soc. Lond., 179, jgs2021-050, https://doi.org/10.1144/jgs2021-050, 2022.

McMahon, S. and Ivarsson, M.: A New Frontier for Palaeobiology: Earth's Vast Deep Biosphere, BioEssays, 41, 1900052, https://doi.org/10.1002/bies.201900052, 2019.

McMahon, S., Ivarsson, M., Wacey, D., Saunders, M., Belivanova, V., Muirhead, D., Knoll, P., Steinbock, O., and Frost, D. A.: Dubiofossils from a Mars-analogue subsurface palaeoenvironment: The limits of biogenicity criteria, Geobiology, 19, 473–488, https://doi.org/10.1111/gbi.12445, 2021.

Merino, N., Aronson, H. S., Bojanova, D. P., Feyhl-Buska, J., Wong, M. L., Zhang, S., and Giovannelli, D.: Living at the Extremes: Extremophiles and the Limits of Life in a Planetary Context, Front. Microbiol., 10, 780, https://doi.org/10.3389/fmicb.2019.00780, 2019.

Meyers, P. A. and Simoneit, B. R. T.: Effects of extreme heating on the elemental and isotopic compositions of an Upper Cretaceous coal, Org. Geochem., 30, 299–305, https://doi.org/10.1016/S0146-6380(99)00015-7, 1999.

Milani, E. J., De Melo, J. H. G., De Souza, P. A., Fernandes, L. A., and França, A. B.: Bacia do Paraná, B. Geoci. Petrobras, Rio de Janeiro, Brazil, 15, 265–287, 2007.

Milliken, K. L.: Diagenesis, in: Encyclopedia of Sediments and Sedimentary Rocks. Encyclopedia of Earth Sciences Series, edited by: Middleton, G. V., Church, M. J., Coniglio, M., Hardie, L. A., and Longstaffe, F. J., Springer, Dordrecht, 339–349, https://doi.org/10.1007/978-1-4020-3609-5_66, 1978.

Monroe, J. S. and Dietrich, R. V.: Pseudofossils, Rocks Miner., 65, 150–158, https://doi.org/10.1080/00357529.1990.11761667, 1990.

Mouro, L. D. and Saldanha, J. P.: Sponge fossil of Brazil: review and perspectives. Paleontol. Em Destaque – Bol. Inf. da Soc. Bras. Paleontol., 36, 46–61, https://doi.org/10.4072/paleodest.2021.36.75.03, 2021.

Mücke, A.: Chamosite, siderite and the environmental conditions of their formation in chamosite-type Phanerozoic ooidal ironstones, Ore Geol. Rev., 28, 235–249, https://doi.org/10.1016/j.oregeorev.2005.03.004, 2006.

Müller, W. E. G., Belikov, S. I., Tremel, W., Perry, C. C., Gieskes, W. W. C., Boreiko, A., and Schröder, H. C.: Siliceous spicules in marine demosponges (example Suberites domuncula), Micron, 37, 107–120, https://doi.org/10.1016/j.micron.2005.09.003, 2006.

Muscente, A. D., Schiffbauer, J. D., Broce, J., Laflamme, M., O'Donnell, K., Boag, T. H., Meyer, M., Hawkins, A. D., Huntley, J. W., McNamara, M., MacKenzie, L. A., Stanley, G. D., Hinman, N. W., Hofmann, M. H., and Xiao, S.: Exceptionally preserved fossil assemblages through geologic time and space, Gondwana Res., 48, 164–188, https://doi.org/10.1016/j.gr.2017.04.020, 2017.

Nardy, A. J. R., Oliveira, M. D., Betancourt, R. H. S., Verdugo, D. R. H., and Machado, F. B.: Geologia e estratigrafia da Formação Serra geral, Geociências, 21, 15–32, 2002.

Netto, R. G., Balistieri, P. R. M. N., Lavina, E. L. C., and Silveira, D. M.: Ichnological signatures of shallow freshwater lakes in the glacial Itararé Group (Mafra Formation, Upper Carboniferous–Lower Permian of Paraná Basin, S Brazil), Palaeogeogr. Palaeoclim. Palaeoecol., 272, 240–255, https://doi.org/10.1016/j.palaeo.2008.10.028, 2009.

Netto, R. G., Corrêa, C. G., Lima, J. H. D., Sedorko, D., and Villegas-Martín, J.: Deciphering myriapoda population dynamics during Gondwana deglaciation cycles through neoichnology, J. S. Am. Earth Sci., 109, 103247, https://doi.org/10.1016/j.jsames.2021.103247, 2021.

Neveu, M., Hays, L. E., Voytek, M. A., New, M. H., and Schulte, M. D.: The Ladder of Life Detection, Astrobiology, 18, 1375–1402, https://doi.org/10.1089/ast.2017.1773, 2018.

Noffke, N.: The criteria for the biogeneicity of microbially induced sedimentary structures (MISS) in Archean and younger, sandy deposits, Earth-Sci. Rev. 96, 173–180, https://doi.org/10.1016/j.earscirev.2008.08.002, 2009.

Noffke, N.: Geobiology, Springer, Berlin, Heidelberg, https://doi.org/10.1007/978-3-642-12772-4, 2010.

Noffke, N.: Comment on the paper by Davies et al. "Resolving MISS conceptions and misconceptions: A geological approach to sedimentary surface textures generated by microbial and abiotic processes" (Earth Science Reviews, 154 (2016), 210–246), Earth-Sci. Rev., 176, 373–383, https://doi.org/10.1016/j.earscirev.2017.11.021, 2018.

Noffke, N.: Microbially Induced Sedimentary Structures in Clastic Deposits: Implication for the Prospection for Fossil Life on Mars, Astrobiology, 21, 866–892, https://doi.org/10.1089/ast.2021.0011, 2021.

Noffke, N., Gerdes, G., Klenke, T., and Krumbein, W. E.: A microscopic sedimentary succession of graded sand and microbial mats in modern siliciclastic tidal flats, Sediment. Geol., 110, 1–6, https://doi.org/10.1016/S0037-0738(97)00039-0, 1997.

Noll, S. H. and Netto, R. G.: Microbially induced sedimentary structures in late Pennsylvanian glacial settings: A case study from the Gondwanan Paraná Basin, J. S. Am. Earth Sci., 88, 385–398, https://doi.org/10.1016/j.jsames.2018.09.010, 2018.

Oehlerich, M., Mayr, C., Griesshaber, E., Lücke, A., Oeckler, O. M., Ohlendorf, C., Schmahl, W. W., and Zolitschka, B.: Ikaite precipitation in a lacustrine environment – implications for palaeoclimatic studies using carbonates from Laguna Potrok Aike (Patagonia, Argentina), Quaternary Sci. Rev., 71, 46–53, https://doi.org/10.1016/j.quascirev.2012.05.024, 2013.

Payandi-Rolland, D., Roche, A., Vennin, E., Visscher, P. T., Amiotte-Suchet, P., Thomas, C., and Bundeleva, I. A.: Carbonate Precipitation in Mixed Cyanobacterial Biofilms Forming Freshwater Microbial Tufa, Minerals, 9, 409, https://doi.org/10.3390/min9070409, 2019.

Perillo, V. L., Maisano, L., Martinez, A. M., Quijada, I. E., and Cuadrado, D. G.: Microbial mat contribution to the formation of an evaporitic environment in a temperate-latitude ecosystem, J. Hydrol., 575, 105–114, https://doi.org/10.1016/j.jhydrol.2019.05.027, 2019.

Pfeifer, L. S., Birkett, B. A., Van Den Driessche, J., Pochat, S., and Soreghan, G. S.: Ice-crystal traces imply ephemeral freezing in early Permian equatorial Pangea, Geology, 49, 1397–1401, https://doi.org/10.1130/G49011.1, 2021.

Pitra, P. and De Waal, S. A.: High-temperature, low-pressure metamorphism and development of prograde symplectites, Marble Hall Fragment, Bushveld Complex (South Africa), J. Metamorph. Geol., 19, 311–325. https://doi.org/10.1046/j.1525-1314.2001.00313.x, 2001.

Pratt, B. R.: Calcification of cyanobacterial filaments: Girvanella and the origin of lower Paleozoic lime mud, Geology, 29, 763, https://doi.org/10.1130/0091-7613(2001)029<0763:COCFGA>2.0.CO;2, 2001.

Pueschel, C. M.: Calcium oxalate crystals in the green alga Spirogyra hatillensis (Zygnematales, Chlorophyta), Int. J. Plant Sci., 162, 1337–1345, https://doi.org/10.1086/322943, 2001.

Puigdomenech, C. G., Carvalho, B., Paim, P. S. G., and Faccini, U. F.: Lowstand Turbidites and Delta Systems of the Itararé Group in the Vidal Ramos region (SC), southern Brazil, Brazil. J. Geol., 44, 529–544, https://doi.org/10.5327/Z2317488920140004000 2, 2014.

Purgstaller, B., Dietzel, M., Baldermann, A., and Mavromatis, V.: Control of temperature and aqueous Mg^{2+}/Ca^{2+} ratio on the (trans-)formation of ikaite, Geochim. Cosmochim. Ac., 217, 128–143, https://doi.org/10.1016/j.gca.2017.08.016, 2017.

Ramakrishna, C., Thenepalli, T., and Ahn, J. W.: A brief review of aragonite precipitated calcium carbonate (PCC) synthesis methods and its applications, Korean Chem. Eng. Res., 55, 443–455, https://doi.org/10.9713/kcer.2017.55.4.443, 2017.

Reijmer, J. J. G.: Marine carbonate factories: Review and update, Sedimentology, 68, 1729–1796, https://doi.org/10.1111/sed.12878, 2021.

Ren, M. and Jones, B.: Modern authigenic amorphous and crystalline iron oxyhydroxides in subsurface Ordovician dolostones (Jinan, North China Block): Biomineralization and crystal morphology, Sediment. Geol., 426, 106044, https://doi.org/10.1016/j.sedgeo.2021.106044, 2021.

Retallack, G. J.: Ediacaran periglacial sedimentary structures, J. Palaeosci., 70, 5–30, https://doi.org/10.54991/jop.2021.8, 2021.

Retallack, G. J.: Early Ediacaran lichen from Death Valley, California, USA, J. Palaeosci., 71, 187–218, https://doi.org/10.54991/jop.2022.1841, 2022.

Roberts, J. A., Bennett, P. C., González, L. A., Macpherson, G. L., and Milliken, K. L.: Microbial precipitation of dolomite in methanogenic groundwater, Geology, 32, 277, https://doi.org/10.1130/G20246.2, 2004.

Roden, E. E., Kappler, A., Bauer, I., Jiang, J., Paul, A., Stoesser, R., Konishi, H., and Xu, H.: Extracellular electron transfer through microbial reduction of solid-phase humic substances, Nat. Geosci., 3, 417–421, https://doi.org/10.1038/ngeo870, 2010.

Rodriguez-Navarro, C., Jimenez-Lopez, C., Rodriguez-Navarro, A., Gonzalez-Muñoz, M. T., and Rodriguez-Gallego, M.: Bacterially mediated mineralization of vaterite, Geochim. Cosmochim. Ac., 71, 1197–1213, https://doi.org/10.1016/j.gca.2006.11.031, 2007.

Rogov, M., Ershova, V., Vereshchagin, O., Vasileva, K., Mikhailova, K., and Krylov, A.: Database of global glendonite and ikaite records throughout the Phanerozoic, Earth Syst. Sci. Data, 13, 343–356, https://doi.org/10.5194/essd-13-343-2021, 2021.

Rouillard, J., Van Zuilen, M., Pisapia, C., and Garcia-Ruiz, J. M.: An Alternative Approach for Assessing Biogenicity, Astrobiology, 21, 151–164, https://doi.org/10.1089/ast.2020.2282, 2021.

Salamuni, R., Marques Filho, P. L., and Sobanski, A. C.: Considerações sobre turbiditos da Formação Itararé (Carbonífero Superior), Rio Negro-PR e Mafra-SC, Boletim da Sociedade Brasileira de Geologia, 15, 1–19, 1966.

Salvany, J. M., García-Veigas, J., and Ortí, F.: Glauberite-halite association of the Zaragoza Gypsum Formation (Lower Miocene, Ebro Basin, NE Spain), Sedimentology, 54, 443–467, https://doi.org/10.1111/j.1365-3091.2006.00844.x, 2007.

Sánchez-Navas, A., de Cassia Oliveira-Barbosa, R., García-Casco, A., and Martín-Algarra, A.: Transformation of Andalusite to Kyanite in the Alpujarride Complex (Betic Cordillera, Southern Spain): Geologic Implications, J. Geol., 120, 557–574, https://doi.org/10.1086/666944, 2012.

Sanchez-Moral, S., Canaveras, J. C., Laiz, L., Saiz-Jimenez, C., Bedoya, J., and Luque, L.: Biomediated Precipitation of Calcium Carbonate Metastable Phases in Hypogean Environments: A Short Review, Geomicrobiol. J., 20, 491–500, https://doi.org/10.1080/713851131, 2003.

Santos, R. V., Dantas, E. L., de Oliveira, C. G., de Alvarenga, C. J. S., dos Anjos, C. W. D., Guimarães, E. M., and Oliveira, F. B.: Geochemical and thermal effects of a basic sill on black shales and limestones of the Permian Irati Formation, J. S. Am. Earth Sci., 28, 14–24, https://doi.org/10.1016/j.jsames.2008.12.002, 2009.

Sapota, T., Aldahan, A., and Al-Aasm, I. S.: Sedimentary facies and climate control on formation of vivianite and siderite microconcretions in sediments of Lake Baikal, Siberia, J. Paleolimnol., 36, 245–257, https://doi.org/10.1007/s10933-006-9005-x, 2006.

Saxby, J. D. and Stephenson, L. C.: Effect of an igneous intrusion on oil shale at Rundle (Australia), Chem. Geol., 63, 1–16, https://doi.org/10.1016/0009-2541(87)90068-4, 1987

Schemiko, D. C. B., Vesely, F. F., and Rodrigues, M. C. N. L.: Deep-water to fluvio-deltaic stratigraphic evolution of a deglaciated depocenter: The early Permian Rio do Sul and Rio Bonito formations, southern Brazil, J. S. Am. Earth Sci., 95, 102260, https://doi.org/10.1016/j.jsames.2019.102260, 2019.

Schiffbauer, J. D., Yin, L., Bodnar, R. J., Kaufman, A. J., Meng, F., Hu, J., Shen, B., Yuan, X., and Bao, H., Xiao, S.: Ultrastructural and Geochemical Characterization of Archean–Paleoproterozoic Graphite Particles: Implications for Recognizing Traces of Life in Highly Metamorphosed Rocks, Astrobiology, 7, 684–704, https://doi.org/10.1089/ast.2006.0098, 2007.

Schneider, R., Mühlmann, H., Tommasi, E., Medeiros, R. D., Daemon, R. F., and Nogueira, A. A.: Revisão estratigráfica da Bacia do Paraná, Congresso brasileiro de Geologia, 28, 41–65, 1974.

Schopf, J. W. and Kudryavtsev, A. B.: Biogenicity of Earth's earliest fossils: A resolution of the controversy, Gondwana Res., 22, 761–771, https://doi.org/10.1016/j.gr.2012.07.003, 2012.

Schopf, J. W., Kudryavtsev, A. B., Agresti, D. G., Wdowiak, T. J., and Czaja, A. D.: Laser–Raman imagery of Earth's earliest fossils, Nature, 416, 73–76, 2002.

Schubert, C. J., Nürnberg, D., Scheele, N., Pauer, F., and Kriews, M.: ^{13}C isotope depletion in ikaite crystals: evidence for methane release from the Siberian shelves, Geo-Mar. Lett., 17, 169–174, https://doi.org/10.1007/s003670050023, 1997.

Schultz, B., Thibault, N., and Huggett, J.: The minerals ikaite and its pseudomorph glendonite: Historical perspective and legacies of Douglas Shearman and Alec K. Smith, Proc. Geol. Assoc., https://doi.org/10.1016/j.pgeola.2022.02.003, 2022.

Sethmann, I. and Wörheide, G.: Structure and composition of calcareous sponge spicules: A review and comparison to structurally related biominerals, Micron, 39, 209–228, https://doi.org/10.1016/j.micron.2007.01.006, 2008.

Shearman, D. J., Mcgugan, A., Stein, C., and Smith, A. J.: Ikaite, $CaCO_3 \cdot 6\,H_2O$, precursor of the thinolites in the Quaternary tufas and tufa mounds of the Lahontan and Mono Lake Basins, western United States, Geol. Soc. Am. Bull., 101, 913–917, https://doi.org/10.1130/0016-7606(1989)101<0913:ICOPOT>2.3.CO;2, 1989.

Sibley, D. F., Nordeng, S. H., and Borkowski, M. L.: Dolomitization kinetics of hydrothermal bombs and natural settings, J. Sediment. Res., 64, 630–637, https://doi.org/10.1306/D4267E29-2B26-11D7-8648000102C1865D, 1994.

Silva, M. S.: Uso de medidas digitais em RGB em fitoclastos na caracterização da influência térmica das intrusivas ígneas (Grupo Serra Geral) nos siltitos da Formação Taciba, Itaiópolis, SC, Undergraduate geology monograph, Universidade Federal de Santa Catarina, Florianópolis, https://repositorio.ufsc.br/handle/123456789/218651 (last access: 26 January 2023), 2020.

Slater, G. F.: Biosignatures: Interpreting Evidence of the Origins and Diversity of Life, Geosci. Canada, 36, 170–178, 2009.

Sommer, V. P., Kuchle, J., and De Ros, L. F.: Seismic stratigraphic framework and seismic facies of the Aptian Pre-salt Barra Velha Formation in the Tupi Field, Santos Basin, Brazil, J. S. Am. Earth Sci., 118, 103947, https://doi.org/10.1016/j.jsames.2022.103947, 2022.

Souza, P. A.: Late Carboniferous palynostratigraphy of the Itararé Subgroup, northeastern Paraná Basin, Brazil, Rev. Palaeobot. Palynol., 138, 9–29, https://doi.org/10.1016/j.revpalbo.2005.09.004, 2006.

Spadafora, A., Perri, E., Mckenzie, J. A., and Vasconcelos, C.: Microbial biomineralization processes forming modern Ca:Mg carbonate stromatolites, Sedimentology, 57, 27–40, https://doi.org/10.1111/j.1365-3091.2009.01083.x, 2010.

Stockmann, G., Tollefsen, E., Skelton, A., Brüchert, V., Balic-Zunic, T., Langhof, J., Skogby, H., and Karlsson, A.: Control of a calcite inhibitor (phosphate) and temperature on ikaite precipitation in Ikka Fjord, southwest Greenland, Appl. Geochem., 89, 11–22, https://doi.org/10.1016/j.apgeochem.2017.11.005, 2018.

Suchý, V., Borecká, L., Pachnerová Brabcová, K., Havelcová, M., Svetlik, I., Machovič, V., Lapčák, L., and Ovšonková, Z. A.: Microbial signatures from speleothems: A petrographic and scanning electron microscopy study of coralloids from the Koněprusy Caves (the Bohemian Karst, Czech Republic), Sedimentology, 68, 1198–1226, https://doi.org/10.1111/sed.12826, 2021.

Teixeira, C. A. S., Sawakuchi, A. O., Bello, R. M. S., Nomura, S. F., Bertassoli, D. J., and Chamani, M. A. C.: Fluid inclusions in calcite filled opening fractures of the Serra Alta Formation reveal paleotemperatures and composition of diagenetic fluids percolating Permian shales of the Paraná Basin, J. S. Am. Earth Sci., 84, 242–254, https://doi.org/10.1016/j.jsames.2018.04.004, 2018.

Tisato, N., Torriani, S. F. F., Monteux, S., Sauro, F., De Waele, J., Tavagna, M. L., D'Angeli, I. M., Chailloux, D., Renda, M., Eglinton, T. I., and Bontognali, T. R. R.: Microbial mediation of complex subterranean mineral structures, Sci. Rep., 5, 15525, https://doi.org/10.1038/srep15525, 2015.

Toffolo, M. B.: The significance of aragonite in the interpretation of the microscopic archaeological record, Geoarchaeology, 36, 149–169, https://doi.org/10.1002/gea.21816, 2021.

Trampe, E. C. L., Larsen, J. E. N., Glaring, M. A., Stougaard, P., and Kühl, M.: In situ Dynamics of O_2, pH, Light, and Photosynthesis in Ikaite Tufa Columns (Ikka Fjord, Greenland) – A Unique Microbial Habitat, Front. Microbiol., 7, 128–143, https://doi.org/10.3389/fmicb.2016.00722, 2016.

Trichet, J., Défarge, C., Tribble, J., Tribble, G., and Sansone, F.: Christmas Island lagoonal lakes, models for the deposition of carbonate–evaporite–organic laminated sediments, Sediment. Geol., 140, 177–189, https://doi.org/10.1016/S0037-0738(00)00177-9, 2001.

Turner, E. C. and Jones, B.: Microscopic calcite dendrites in cold-water tufa: Implications for nucleation of micrite and cement, Sedimentology, 52, 1043–1066, https://doi.org/10.1111/j.1365-3091.2005.00741.x, 2005.

Uriz, M.-J., Turon, X., Becerro, M. A., and Agell, G.: Siliceous spicules and skeleton frameworks in sponges: Origin, diversity, ultrastructural patterns, and biological functions, Microsc. Res. Tech., 62, 279–299, https://doi.org/10.1002/jemt.10395, 2003.

Valdez Buso, V., Aquino, C. D., Paim, P. S. G., de Souza, P. A., Mori, A. L., Fallgatter, C., Milana, J. P., and Kneller, B.: Late Palaeozoic glacial cycles and subcycles in western Gondwana: Correlation of surface and subsurface data of the Paraná Basin, Brazil, Palaeogeogr. Palaeoclim. Palaeoecol., 531, 108435, https://doi.org/10.1016/j.palaeo.2017.09.004, 2019.

Valdez Buso, V., Milana, J. P., di Pasquo, M., Paim, P. S. G., Philipp, R. P., Aquino, C. D., Cagliari, J., Junior, F. C., and Kneller, B.: Timing of the Late Palaeozoic glaciation in western Gondwana: New ages and correlations from Paganzo and Paraná basins, Palaeogeogr. Palaeoclim. Palaeoecol., 544, 109624, https://doi.org/10.1016/j.palaeo.2020.109624, 2020.

Vasconcelos, C., McKenzie, J. A., Bernasconi, S., Grujic, D., and Tiens, A. J.: Microbial mediation as a possible mechanism for natural dolomite formation at low temperatures, Nature, 377, 220–222, https://doi.org/10.1038/377220a0, 1995.

Vasconcelos, C., Warthmann, R., McKenzie, J. A., Visscher, P. T., Bittermann, A. G., and van Lith, Y.: Lithifying microbial mats in Lagoa Vermelha, Brazil: Modern Precambrian relics?, Sediment. Geol., 185, 175–183, https://doi.org/10.1016/j.sedgeo.2005.12.022, 2006.

Verrecchia, E. P. and Verrecchia, K. E.: Needle-fiber Calcite: A Critical Review and a Proposed Classification, SEPM J. Sediment. Res., 64A, 650–664, https://doi.org/10.1306/D4267E33-2B26-11D7-8648000102C1865D, 1994.

Vesely, F. F. and Assine, M. L.: Deglaciation sequences in the Permo-Carboniferous Itararé Group, Paraná Basin, southern Brazil, J. S. Am. Earth Sci., 22, 156–168, https://doi.org/10.1016/j.jsames.2006.09.006, 2006.

Vesely, F. F., Delgado, D., Spisila, A. L., and Brumatti, M.: Divisão litoestratigráfica do das Grupo Itararé no Mapeamento da suscetibilidade vertentes naturais estado do Paraná translacionais em ante a ocorrência de escorregamentos um trecho da BR-376, através da análise, Bol. Parana. Geosci., 78, 3–23, 2021.

Vickers, M., Watkinson, M., Price, G. D., and Jerrett, R.: An improved model for the ikaite-glendonite transformation: evidence from the Lower Cretaceous of Spitsbergen, Svalbard, Nor. J. Geol., 98, 1–15, https://doi.org/10.17850/njg98-1-01, 2018.

Voigt, S., Oliver, K., and Small, B. J.: Potential Ice Crystal Marks From Pennsylvanian–Permian Equatorial Red-Beds of Northwest Colorado, U.S.A., Palaios, 36, 377–392, https://doi.org/10.2110/PALO.2021.024, 2021

Vuillemin, A., Wirth, R., Kemnitz, H., Schleicher, A. M., Friese, A., Bauer, K. W., Simister, R., Nomosatryo, S., Ordoñez, L., Ariztegui, D., Henny, C., Crowe, S. A., Benning, L. G., Kallmeyer, J., Russell, J. M., Bijaksana, S., Vogel, H., and The Towuti Drilling Project Science Team: Formation of diagenetic siderite in modern ferruginous sediments, Geology, 47, 540–544, https://doi.org/10.1130/G46100.1, 2019.

Wacey, D.: Establishing the Criteria for Early Life on Earth, Springer, 47–53, https://doi.org/10.1007/978-1-4020-9389-0_4, 2009.

Wacey, D.: Stromatolites in the ∼ 3400 Ma Strelley Pool Formation, Western Australia: Examining Biogenicity from the Macro- to the Nano-Scale, Astrobiology 10, 381–395, https://doi.org/10.1089/ast.2009.0423, 2010.

Wang, H., Ye, Y., Deng, Y., Liu, Y., Lyu, Y., Zhang, F., Wang, X., and Zhang, S.: Multi-Element Imaging of a 1.4 Ga Authigenic Siderite Crystal, Minerals, 11, 1395, https://doi.org/10.3390/min11121395, 2021.

Ward, W. C. and Halley, R. B.: Dolomitization in a Mixing Zone of Near-Seawater Composition, Late Pleistocene, Northeastern Yucatan Peninsula, SEPM J. Sediment. Res., 55, 407–420, https://doi.org/10.1306/212F86E8-2B24-11D7-8648000102C1865D, 1985.

Warren, J.: Dolomite: occurrence, evolution and economically important associations, Earth-Sci. Rev., 52, 1–81, https://doi.org/10.1016/S0012-8252(00)00022-2, 2000.

Warren, J. K.: Evaporites, brines and base metals: What is an evaporite? Defining the rock matrix, Aust. J. Earth Sci., 43, 115–132, https://doi.org/10.1080/08120099608728241, 1996.

Warren, J. K.: Evaporites through time: Tectonic, climatic and eustatic controls in marine and nonmarine deposits, Earth-Sci. Rev., 98, 217–268, https://doi.org/10.1016/j.earscirev.2009.11.004, 2010.

Warren, J. K.: Evaporites, Springer International Publishing, Cham, https://doi.org/10.1007/978-3-319-13512-0, 2016.

Weaver, C. E.: Shale-slate metamorphism in southern Appalachians, Elsevier, ISBN 0-444-42264-1, 1984.

Weaver, J. C. and Morse, D. E.: Molecular biology of demosponge axial filaments and their roles in biosilicification, Microsc. Res. Tech., 62, 356–367, https://doi.org/10.1002/jemt.10401, 2003.

Weiner, S.: Biomineralization: A structural perspective, J. Struct. Biol., 163, 229–234, https://doi.org/10.1016/j.jsb.2008.02.001, 2008.

Weiner, S. and Dove, P.: An Overview of Biomineralization Processes and the Problem of the Vital Effect, Rev. Mineral. Geochem., 54, 1–29, https://doi.org/10.2113/0540001, 2003.

Weinschütz, L. C. and de Castro, J. C.: Seqüências deposicionais da Formação Taciba (Grupo Itararé, Neocarbonífero a Eopermiano) na região de Mafra (SC), Bacia do Paraná, Brazil. J. Geol., 36, 243–252, 2006.

Westall, F.: Morphological Biosignatures in Early Terrestrial and Extraterrestrial Materials, Space Sci. Rev., 135, 95–114, https://doi.org/10.1007/s11214-008-9354-z, 2008.

Whitney, K. D.: Systems of Biomineralization in the Fungi, in: Origin, Evolution, and Modern Aspects of Biomineralization in Plants and Animals, Springer US, Boston, MA, 433–441, https://doi.org/10.1007/978-1-4757-6114-6_34, 1989.

Wilson, M. J., Jones, D., and Russell, J. D.: Glushinskite, a naturally occurring magnesium oxalate, Mineral. Mag., 43, 837–840, https://doi.org/10.1180/minmag.1980.043.331.02, 1980.

Wolf, K. H.: Gradational sedimentary products of calcareous algae, Sedimentology, 5, 1–37, https://doi.org/10.1111/j.1365-3091.1965.tb01556.x, 1965.

Worden, R. H. and Burley, S. D.: Sandstone Diagenesis: The Evolution of Sand to Stone, in: Sandstone Dia-

genesis, Blackwell Publishing Ltd., Oxford, UK, 1–44, https://doi.org/10.1002/9781444304459.ch, 2009.

Wright, D. T. and Wacey, D.: Sedimentary dolomite: a reality check, Geol. Soc. Lond. Spec. Publ., 235, 65–74, https://doi.org/10.1144/GSL.SP.2004.235.01.03, 2004.

Wright, D. T. and Wacey, D.: Precipitation of dolomite using sulphate-reducing bacteria from the Coorong Region, South Australia: significance and implications, Sedimentology, 52, 987–1008, https://doi.org/10.1111/j.1365-3091.2005.00732.x, 2005.

Wright, V. P. and Barnett, A. J.: An abiotic model for the development of textures in some South Atlantic early Cretaceous lacustrine carbonates, Geol. Soc. Spec. Publ., 418, 209–219, https://doi.org/10.1144/SP418.3, 2015.

Xia, C., Ye, B., Jiang, J., and Hou, Z.: Review of natural origin, distribution, and long-term conservation of CO_2 in sedimentary basins of China, Earth-Sci. Rev., 226, 103953, https://doi.org/10.1016/j.earscirev.2022.103953, 2022.

Xu, F., You, X., Li, Q., and Liu, Y.: Can primary ferroan dolomite and ankerite be precipitated? Its implications for formation of submarine methane-derived authigenic carbonate (MDAC) chimney, Minerals, 9, 413, https://doi.org/10.3390/min9070413, 2019.

Zalán, P. V., Conceição, J. J., Astolfi, M. M., Tiriba Appi, V., Wolff, S., and Santos Vieira, I.: Estilos estruturais relacionados a intrusões magmáticas básicas em rochas sedimentares, Boletim Técnico da Petrobrás, 4, 221–230, 1985.

Zekri, A. Y., Shedid, S. A., and Almehaideb, R. A.: Investigation of supercritical carbon dioxide, asphaltenic crude oil, and formation brine interactions in carbonate formations, J. Petrol. Sci. Eng., 69, 63–70, https://doi.org/10.1016/j.petrol.2009.05.009, 2009.

Zhang, Y., Sun, H., Stowell, H. H., Zayernouri, M., and Hansen, S. E.: A review of applications of fractional calculus in Earth system dynamics, Chaos Solit. Fract., 102, 29–46, https://doi.org/10.1016/j.chaos.2017.03.051, 2017.

Zhou, X., Lu, Z., Rickaby, R. E. M., Domack, E. W., Wellner, J. S., and Kennedy, H. A.: Ikaite Abundance Controlled by Porewater Phosphorus Level: Potential Links to Dust and Productivity, J. Geol., 123, 269–281, https://doi.org/10.1086/681918, 2015.

Zhu, L., Zhao, Q., Zheng, X., and Xie, Y.: Formation of star-shaped calcite crystals with Mg^{2+} inorganic mineralizer without organic template, J. Solid State Chem., 179, 1247–1252, https://doi.org/10.1016/j.jssc.2006.01.036, 2006.